Theoretical Notes
Note 227

DNA 3370T

THE EFFECT OF GROUND REFLECTION ON OBSERVED EMP WAVEFORMS

TN 223

Michael A. Messier

Mission Research Corporation
735 State Street
Santa Barbara, California 93101

11 September 1974 July 1975

Topical Report

CONTRACT No. DNA 001-73-C-0118

APPROVED FOR PUBLIC RELEASE;
DISTRIBUTION UNLIMITED.

THIS WORK SPONSORED BY THE DEFENSE NUCLEAR AGENCY
UNDER SUBTASK R99QAXEA094-32.

Prepared for

Director
DEFENSE NUCLEAR AGENCY
Washington, D. C. 20305

PREFACE

The effect of ground reflections on EMP waveforms is considered, with the incident pulse treated as a plane wave and the ground as a homogeneous, isotropic conducting dielectric. Fresnel's equations are introduced and the reflection geometry is approximated for a spherical earth. General techniques for calculating the reflected and total signal are discussed and, where available, currently existing computer codes are noted. Commonly used approximations are described and compared with numerical calculations and with a new approximation which should prove quite useful. Emphasis is placed on the reflection of high altitude burst signals and an appendix is included which discusses their polarity. An approximation is provided which allows an estimation of this polarity without the necessity of making an EMP calculation. Sample calculations are provided which show the effect of a "typical" range of ground parameters.

TABLE OF CONTENTS

LIST OF FIGURES

SECTION I
INTRODUCTION

Radiated field time waveforms usually represent the direct field, which, in the case of a medium or high-altitude burst, would be seen by an observer in the absence of a reflecting ground. In this report, the effect of ground reflections will be considered from the limited, but useful, point of view that the ground is a plane surface reflecting plane waves. After a somewhat general outline of theory and methods, the discussion will be directed to the problem of the high-altitude magnetic turning signal.

The purpose of this report is threefold: (1) to review the subject of reflections, indicating currently available codes and techniques, (2) to point out some misconceptions about the high-altitude burst signal, which are causing some people to handle the problem of reflections incorrectly, and (3) to provide and evaluate some useful approximations which can be used to estimate the reflected signal.

The problem of reflections need only be considered for systems on the ground or close enough to it to allow the reflected signal to interfere with that propagated directly from the burst. The effects on the signal seen by a surface observer are quite pronounced and, in general, involve a decrease in the horizontal electric field and vertical magnetic field and an increase in the vertical electric field and horizontal magnetic field. It is therefore quite important to know the polarization of the incident field. In the case of the high-altitude signal, many people have assumed the wrong polarity.

The following section will be a general discussion of plane wave reflection as applied to EMP problems. This will include the

problem geometry, Fresnel's equations, various calculational techniques (exact and approximate), and estimations of "typical" soil electrical properties. Section 3 discusses pulse penetration into the ground. The information provided in Section 2 will be used in Section 4 where several sample problems are considered with emphasis placed on the high-altitude burst problem. Appendix A shows the signal polarity of a typical high-altitude burst.

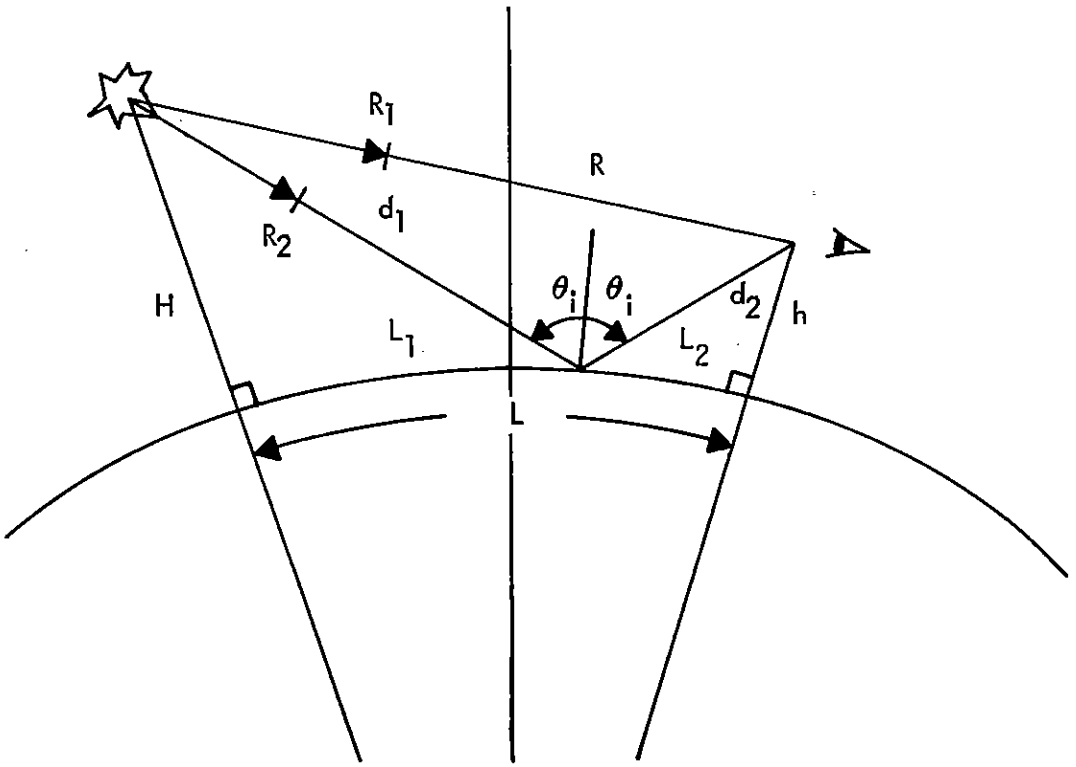

Figure 1. General reflection problem geometry.

SECTION II
PLANE WAVE REFLECTION - THEORY AND CALCULATIONAL TECHNIQUES

In this sub-section, the general problem of the reflection of plane waves off of the earth will be discussed, with emphasis on the types of problems encountered in the study of EMP environments. The geometry of the problem will first be discussed, followed by the presentation of Fresnel's equations. Having seen the part that the quantities conductivity, dielectric constant, and magnetic permeability play in the determination of reflection properties, the range of values found in natural soils and sea water, will be displayed. Currently existing calculational techniques (Fourier transform and convolution) will then be discussed. The existence of computer codes will be disclosed where appropriate. Finally, some useful approximation techniques will be shown.

2.1 PROBLEM GEOMETRY AND FRESNEL'S EQUATIONS

The general EMP reflection problem is that shown in Figure 1. A spherical wave propagates radially outward from the direction of the burst point. Some of the wave reaches an off-the-surface observer directly while another portion of the wavefront reflects off of the earth and arrives at the observer after some delay time, t_D, relative to the arrival of the direct wave. An observer at the surface sees both signals simultaneously. For purposes of this discussion ionospheric and multiple reflections will be ignored. It also will be assumed that the reflecting surface is smooth, the propagating media are isotropic and that there is no refraction except at the air/ground interface. If distances are large enough to allow the spherical

wavefront to be approximated locally by plane wavefronts with appropriate geometric attenuation, the problem reduces to that shown in Figures 2 and 3, where the incident electric field has been decomposed into components normal to and parallel to the plane of incidence. Since most common heights-of-burst (H) and interesting observer altitudes (h) are much less than the radius of the earth (R_e), the following approximations may be used to calculate the parameters necessary for determining the reflection coefficient and geometric attenuation (assuming that H, h, and L, the surface distance between burst point and observer, are initially known):

$$L_1 \simeq L \left[1 + \frac{h}{H} \frac{\left(1 + \frac{H}{R_e}\right)}{\left(1 + \frac{h}{R_e}\right)} \right]^{-1} \tag{2.1}$$

$$\tan \theta_i \simeq \frac{L_1}{H} \left\{ \frac{1 - \frac{1}{6}\left(\frac{L_1}{R_e}\right)^2}{1 - \frac{1}{2}\frac{{L_1}^2}{HR_e}\left[1 + 2\left(\frac{H}{L_1}\right)^2\right]} \right\} \tag{2.2}$$

$${d_1}^2 \simeq H^2 + {L_1}^2 \left(1 + \frac{H}{R_e}\right) \tag{2.3}$$

$$R^2 \simeq (H - h)^2 + L^2 \left(1 + \frac{H + h}{R_e}\right) \tag{2.4}$$

$$\frac{L_2}{L_1} \simeq \frac{h}{H} \frac{\left(1 + \frac{H}{R_e}\right)}{\left(1 + \frac{h}{R_e}\right)} \tag{2.5}$$

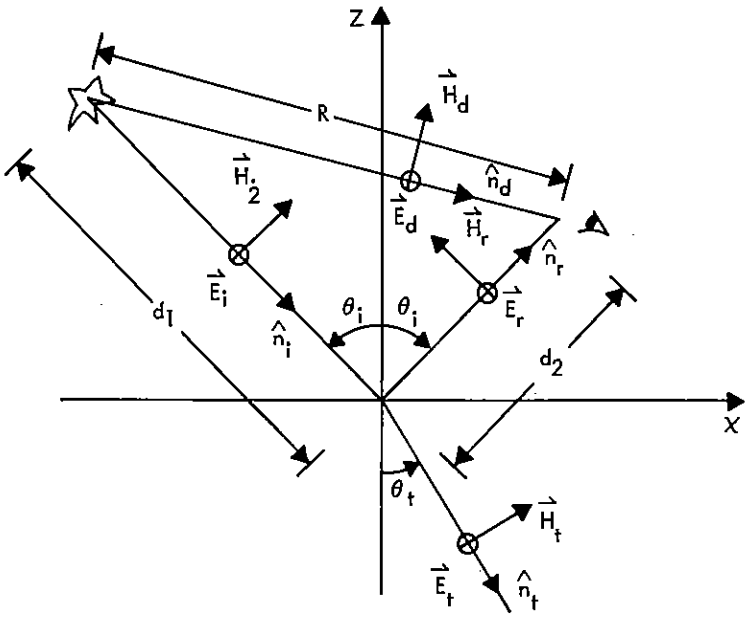

Figure 2. Simplified reflection problem. Electric field normal to plane of incidence.

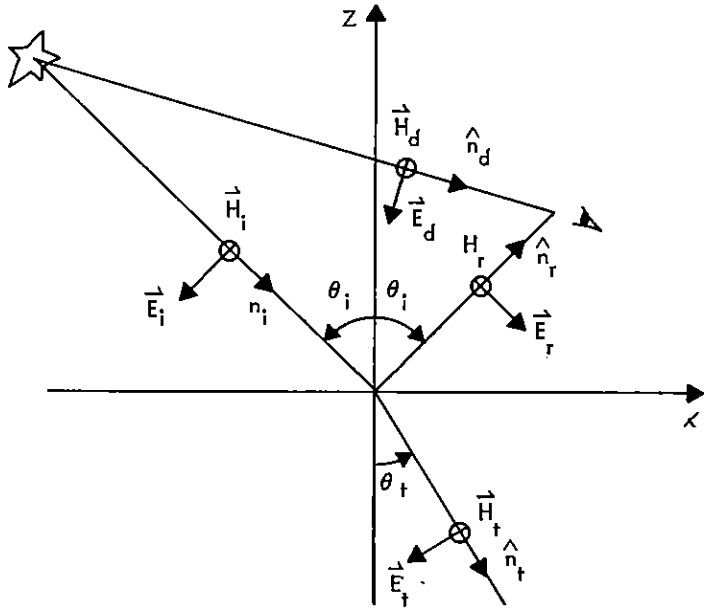

Figure 3. Simplified reflection problem. Electric field parallel to plane of incidence.

$$\frac{d_2}{d_1} \simeq \frac{h}{H} \frac{\left(1 - \frac{1}{2} \frac{L_2}{R_e}\right)}{\left(1 - \frac{1}{2} \frac{L_1}{R_e}\right)} \tag{2.6}$$

When the distances are small enough to allow a plane-earth approximation, the equations reduce to:

$$L_1 \simeq \frac{1}{1 + \frac{h}{H}} \tag{2.7}$$

$$\tan\theta_i \simeq \frac{L}{H + h} \tag{2.8}$$

$$R^2 \simeq (H - h)^2 + L^2 \tag{2.9}$$

$$d^2 \equiv (d_1 + d_2)^2 \simeq (H + h)^2 + L^2 \tag{2.10}$$

$$\frac{d_2}{d_1} \simeq \frac{L_2}{L_1} \simeq \frac{h}{H} \tag{2.11}$$

The delay between the directly propagated and reflected pulses is

$$t_D = \frac{1}{c} (d - R) \tag{2.12}$$

where c is the speed of light in air. The code which calculates the pulse which the observer sees directly and the pulse which is to be reflected off of the earth, may only carry the calculation out to some distance where one can consider the pulses to be freely propagating. The field seen by the observer can be calculated by appropriately scaling the direct and reflected pulses. If the direct pulse is known at the range R_1, it must be scaled by the factor

$$S_d = \frac{R_1}{R} , \tag{2.13}$$

in order to calculate that seen by the observer. Similarly, if the reflected pulse is calculated from one which is known at the distance R_2 (see Figure 1), it must be scaled by the factor

$$S_r = \frac{R_2}{d} \tag{2.14}$$

In order to calculate the reflected pulse, the incident pulse can be Fourier transformed and the reflection coefficient can be calculated for pure frequencies. The reflected pulse would then be found by an inverse transform. Alternatively, the frequency dependent reflection coefficient can be inverse transformed and convoluted with the incident waveform or its time derivative. The frequency dependent reflection coefficients are given by Fresnel's equations, which can be found in any elementary EM text. Using the convention shown in Figures 2 and 3, and assuming that the incident and reflected waves propagate in free space, the reflection coefficients are

$$r_N \equiv \left(\frac{E_{or}}{E_{oi}}\right)_N = \frac{1 - \frac{n}{\mu_r}\frac{\cos\theta_t}{\cos\theta_i}}{1 + \frac{n}{\mu_r}\frac{\cos\theta_t}{\cos\theta_i}} \tag{2.15}$$

For the case of the electric field being normal to the plane of incidence, and

$$r_p \equiv \left(\frac{E_{or}}{E_{oi}}\right)_p = \frac{1 - \frac{\mu_r}{n}\frac{\cos\theta_t}{\cos\theta_i}}{1 + \frac{\mu_r}{n}\frac{\cos\theta_t}{\cos\theta_i}} \tag{2.16}$$

for the case of the electric field being parallel to the plane of incidence. Here, the complex index of refraction of the reflecting medium is given by

$$n^2 = \varepsilon_r \mu_r \left(1 - i\frac{\sigma}{\varepsilon\omega}\right) , \tag{2.17}$$

where σ is the conductivity of the medium, ε_r is the dielectric constant, μ_r is the relative permeability, and ω is the signal frequency (radians/sec). The permittivity of the medium is given by $\varepsilon = \varepsilon_r \varepsilon_o$, where $\varepsilon_o = 8.854 \times 10^{-12}$ Farad/m. The permeability of the medium is given by $\mu = \mu_r \mu_o$, where $\mu_o = 4\pi \times 10^{-7}$ Henry/m. The transmission angle, θ_t, is given by Snell's law, in $\sin \theta_t = \sin \theta_i$. The wave convention assumed here is

$$E = E_o \exp\left[-i\left(\omega t + \frac{n}{\lambda_o} \hat{n} \cdot \vec{r}\right)\right] \tag{2.18}$$

for a wave traveling in the $+r$ direction. The wave number, k, is given by

$$k = \frac{n}{\lambda_o} , \tag{2.19}$$

where λ_o is the free space wavelength divided by 2π. The wave impedence is

$$Z = \frac{\omega\mu}{k} = \frac{\mu_r}{n} Z_o , \tag{2.20}$$

where the impedence of free space is

$$Z_o = \left(\frac{\mu_o}{\varepsilon_o}\right)^{1/2} \simeq 376.7 \text{ ohms} \tag{2.21}$$

The transmission functions, which give the signal propagating into the ground are

$$t_N \equiv \left(\frac{E_{ot}}{E_{oi}}\right)_N = \frac{2}{1 + \frac{n}{\mu_r} \frac{\cos\theta_t}{\cos\theta_i}} , \tag{2.22}$$

when the electric field is normal to the plane of incidence, and

$$t_p \equiv \left(\frac{E_{ot}}{E_{oi}}\right)_p = \frac{2}{\frac{n}{\mu_r} + \frac{\cos\theta_t}{\cos\theta_i}} , \qquad (2.23)$$

when the electric field is parallel to the plane of incidence.

The waveform actually seen by an observer is the vector sum of the direct signal and the reflected signal, each multiplied by the appropriate scale factor. The total signal can be calculated either in the time domain, by adding the reflected signal to the direct signal with the proper delay, or in the frequency domain, by adding the reflected signal to the direct signal with the proper phase shift. An interesting and simple case is that of a point observer on the ground. In this case, the incident pulse is the direct signal so that the waveforms and scale factors are equal and the delay or phase shift is zero. In the case where the electric field is normal to the plane of incidence, the incident and reflected field vectors are parallel and the total field is given simply by

$$\hat{E}_T(w) = \hat{E}_i(w)\left[1 + r_N\left(\omega, \theta_i\right)\right] = \hat{E}_i t_N\left(\omega, \theta_i\right) \qquad (2.24)$$

in the frequency domain. A caret over a quantity denotes the Fourier transformed quantity. The transfer function for the total field normal to the plane of incidence is:

$$T_N\left(\omega, \theta_i\right) \equiv 1 + r_N\left(\omega, \theta_i\right) = t_N\left(\omega, \theta_i\right) \qquad (2.25)$$

In the case of the electric field being parallel to the plane of incidence, we must deal with the addition of two vector components. At the risk of unnecessarily complicating matters, the transfer function for the total signal will be developed in two coordinate systems. The first system

will consider the components in the vertical (z) and horizontal (x) directions. This system facilitates coupling calculations. The second system will be parallel to the incident field component (θ) and the radial direction (r). The system is described in Figure 4. The utility of this system is in comparing with the field that would be predicted without including the presence of the earth. Then, there would be no r component, all the field being in the θ component (and in the ϕ or y component which was dealt with above). By simple trigonometry, one can see that the transfer function to the z component is

$$T_{PZ}(\omega, \theta_i) = -\left[1 + r_p(\omega, \theta_i)\right] \sin\theta_i \tag{2.26}$$

while that to the x component is

$$T_{PX}(\omega, \theta_i) = -\left[1 - r_p(\omega, \theta_i)\right] \cos\theta_i \tag{2.27}$$

Similarly, the transfer function which gives the θ component (parallel to incoming field) is

$$T_{P\theta}(\omega, \theta_i) = 1 - r_p(\omega, \theta_i) \cos(2\theta_i) \tag{2.28}$$

and that which gives the radial component in the direction away from the burst is

$$T_{PR}(\omega, \theta_i) = r_p \sin(2\theta_i) \tag{2.29}$$

These transfer functions, times the Fourier transform of the proper component of the incident pulse, give the transform of the orthogonal components of the pulse at the ground. In many instances, the amplitude spectrum is enough for certain estimations of coupling or the Fourier transform can be used directly as an input to a coupling code. In other cases, an inverse transform or convolution must be used because an incident time waveform is required.

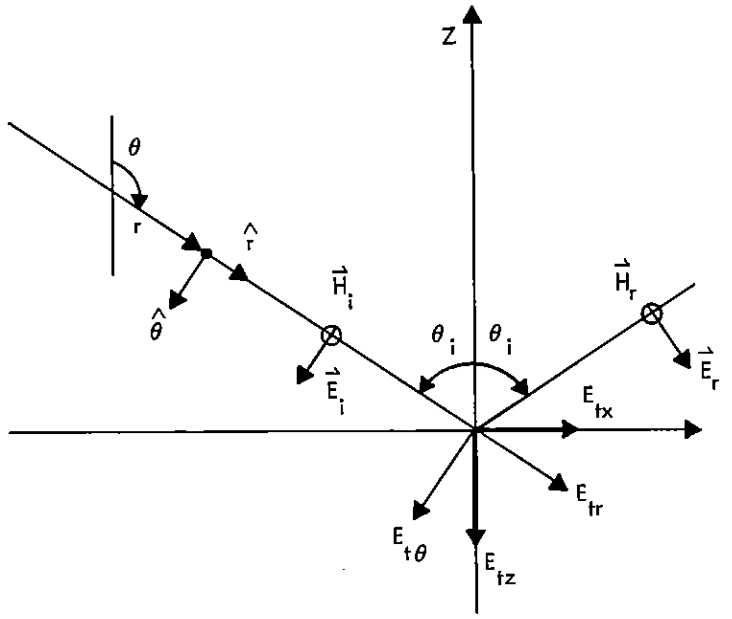

Figure 4. Two coordinate systems for calculating the total electric field at the surface.

These transfer functions are for "point" observers. Most systems known to this author have a finite size and can only be approximated by point observers under certain circumstances. An observer is essentially a point when its dimensions are much less than a wavelength, in which case there is no significant phase change in the observed signal over its surface. Real objects couple most strongly to wavelengths on the same order as the object dimensions. Therefore, it follows that a finite sized object couples best to combined direct and reflected fields which probably add up with very different relative phases over the surface of the body and one cannot simply integrate the total field seen by a single point observer. This fact will, of course, be ignored.

During the remainder of this section only the electric field reflection coefficients will be discussed. In free space, the magnetic

field is related to the electric field by

$$| \vec{E} | = Z_o | \vec{H} |$$

and the magnetic induction is related by

$$| \vec{E} | = c | \vec{B} |$$

where c and Z_o have been previously defined as the speed of light and the impedance of free space. Therefore, using the electric field reflection coefficient, the vector convention described by Figures 2 and 3, and the above relation for the vector magnitudes, one can easily determine the reflected and total magnetic field quantities.

2.2 Typical Soil Parameters

In order to use Fresnel's equations, we must be able to characterize the earth, at the point of reflection, in terms of a dielectric constant, conductivity, and magnetic permeability. As one might expect, the subject is quite complicated and could not possibly be treated here in the detail it deserves. The objective of this section will be limited to giving the reader an idea of the range of values that the parameters can assume. It will be seen that, for naturally occuring soils, the dielectric constant and conductivity are essentially a function of soil water content and signal frequency, not of mineral type. The magnetic permeability can be considered to be that of free space, except in ores with high iron content.

There have been earth impedance measurements made at specific sites of interest, e.g. the Malmstrom Minuteman site in Montana (unpublished, performed by the United States Geological Survey for the Air Force Weapons Laboratory), and sections of Wisconson and Michigan (Reference 1). The most widely used study, however, is a general one

published by Scott on the electrical and magnetic properties of rock and soil (Reference 2). In this study, the conductivity and dielectric constant of several types or soil and rock were determined as a function of water content and frequency (10^2Hz - 10^6Hz). The magnetic permeability is known to be essentially constant over the range of parameters considered. It was found that one could usefully describe the conductivity and dielectric constant as functions of frequency and water content alone. A set of curve-fits was developed which became known as "Scott's Universal Curves". Despite the awe-inspiring title, Scott's curves are only intended to be a means of estimating the parameters of normal types of rock and soil between 100 Hz and 1 MHz when better information is not available. Usually, better information is not available. Even less is available above 1 MHz, which is the region of most interest for magnetic dipole signals and is above the region of validity for Scott's curves.

Scott's curve-fit for conductivity is

$$K = -0.604 + 1.640\,W - 0.062\,F + 0.062\,W^2 - 0.070\,FW + 0.021\,F^2 \qquad (2.30)$$

and that for dielectric constant is

$$D = 4.905 + 1.308\,W - 0.971\,F + 0.111\,W^2 - 0.168\,FW + 0.059\,F^2 \qquad (2.31)$$

where

$K = \log_{10}$ of conductivity (millimho/m)
$D = \log_{10}$ of dielectric constant ($\varepsilon/\varepsilon_0$)
$W = \log_{10}$ of water content (percent by volume)
$F = \log_{10}$ of frequency (Hz)

Sample curves are plotted in Figures 5 and 6. The curves are extrapolated out to 100 MHz and compared with other measurements. (References

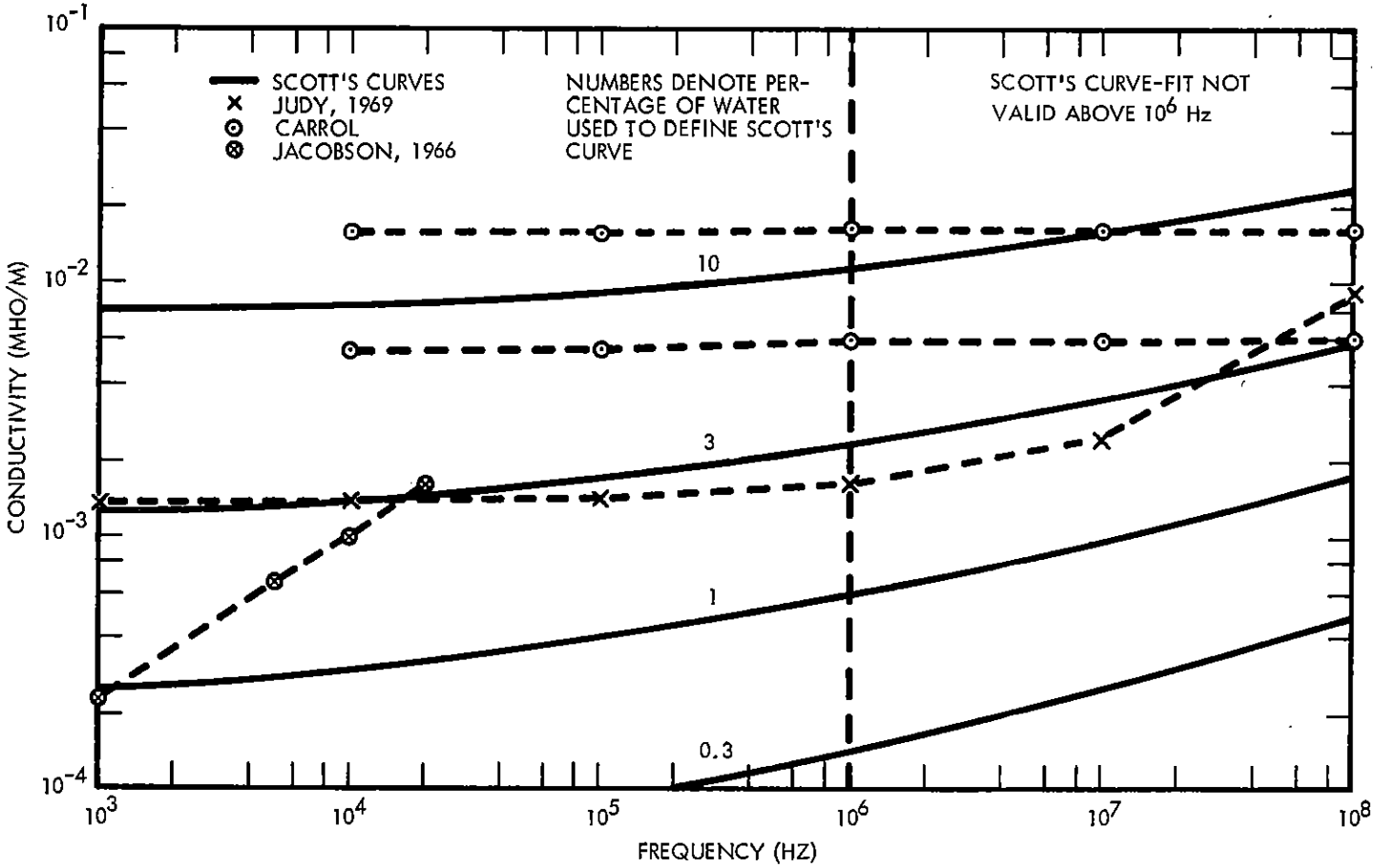

Figure 5. Comparison of conductivity predicted by Scott's Universal Curves and selected data.

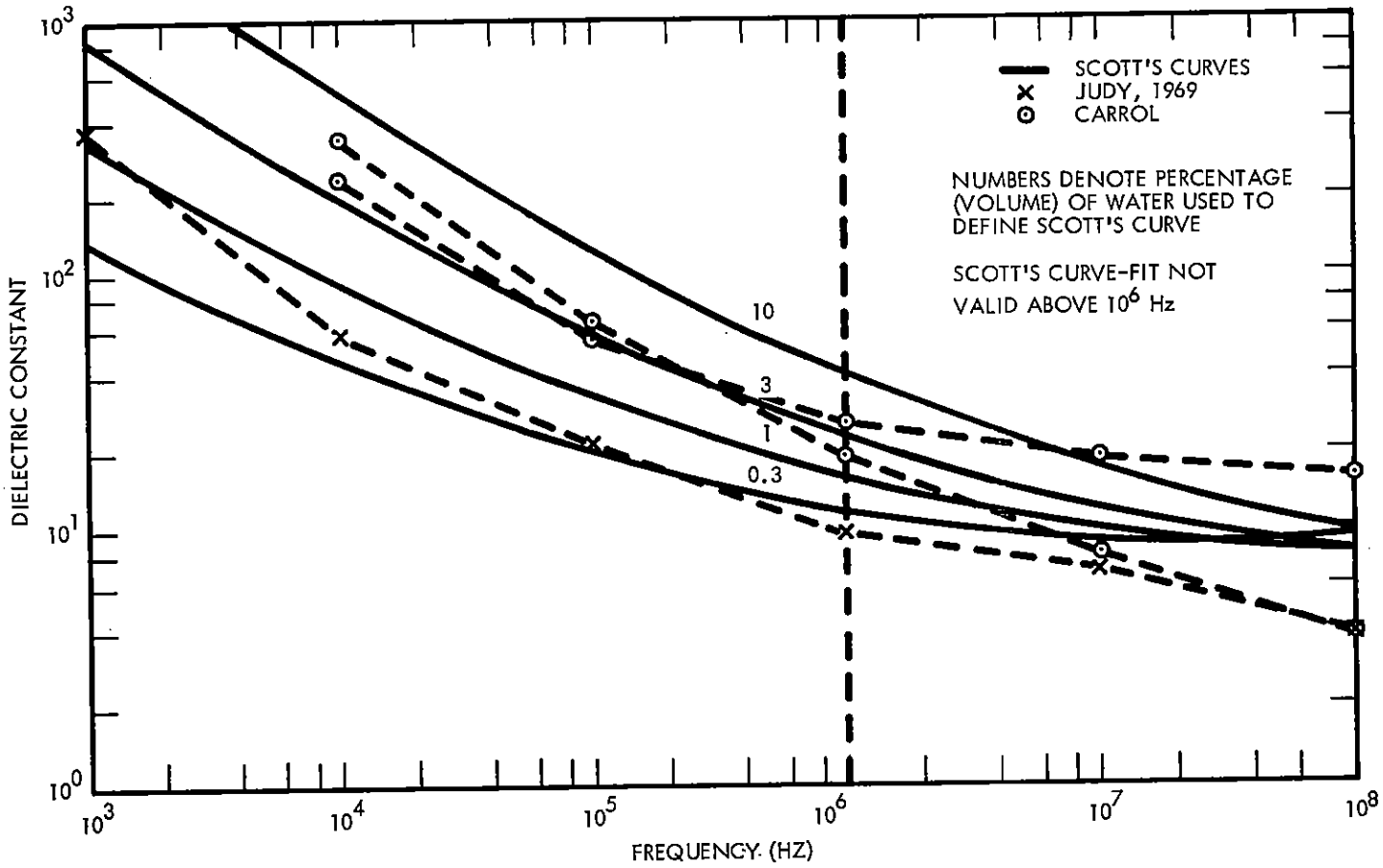

Figure 6. Comparison of dielectric constant predicted by Scott's Universal Curves and selected data.

3 and 4). The measurements made by Carrol were on samples taken at a Minuteman site and were graphically extrapolated above 10^6 Hz. The measurements made by Judy (Reference 3) were to test a new technique which had been developed; only one data sample was shown in the report.

Scott's curves can probably be extrapolated out to 10 MHz with reasonable success. The dielectric constant fit will start to turn up for some high frequency because of its parabolic nature.

Judy's data, in which those authors expressed sufficient confidence, show two significant features: (1) the conductivity curve rises dramatically at ~100 MHz and (2) the dielectric constant also rises quite noticeably for frequencies below 10 KHz. At 100 MHz, the dielectric constant begins to decrease at a faster rate with frequency. The behavior at high frequencies should be of immediate concern because all surface burst codes and most operational reflection codes assume constant conductivity and dielectric constant. This did not seem to be a bad approximation for conductivity, which varies very little with frequency below 10 MHz. It may turn out to be a very bad approximation all around.

Longmire (In Reference 5) has developed a curve-fit procedure based on a model of the earth as an RC network. This model seems plausible in that with many fissures containing water, one would expect to find ionic conduction accounting for the resistors in the equivalent circuit. A fissure which terminates would be capacitively coupled to nearby Fissures. One would not expect inductive coupling without helical current paths. A model of this nature shows the relation between the frequency dependence of dielectric constant and conductivity and, in particular, indicates that an increase in conductivity, with increase in frequency, should be accompanied by a decrease in dielectric constant. Judy's data is consistent with this model in that the anomalous rise in conductivity with frequency near 100 MHz is accompanied

by approximately the same decrease in dielectric constant as predicted by theory.

One type of variation that is ignored here is the variation of the earth's electrical parameters with depth. This type of variation depends very much upon geographical location and could make a significant difference in the reflection of frequencies whose wavelength or skin depth is of the same order as the depth of variation (or greater). The reflection coefficient for multi-slab materials can be calculated if necessary.

2.3 Fourier Transform Method

The most straight-forward method of obtaining the reflected signal in the time domain is to Fourier (or Laplace) transform the incident waveform, multiplying by the frequency dependent reflection coefficient, and inverse transform the product. The total signal is found by adding the direct and reflected time waveforms vectorially and accounting for the geometric attenuation and delay of the reflected pulse. If one can allow the shape of the incident pulse to be held constant, only a single transform will be required. The calculation of the reflection coefficient takes a negligible amount of computer time. An inverse transform must be done for each change in the reflection coefficient, e.g., changes in incident angle or variation of electrical parameters with frequency. This is one fact that warrants consideration when comparing with convolution methods. The subject of Fourier transformations is too complicated and general to be considered here. However, there are some specific problems involved with this type of operation. Both the forward and inverse transforms must be performed very carefully with a sufficiently large time and frequency point density. If an analytical time waveform cannot be used, the digitized waveform should be quite smooth. A spline-fit type of

transform can be helpful. The fact that a given inverse transform computer code can return the original time waveform is no indication that it will return an intelligible waveform after the transform has been operated upon by a transfer function. Experience has shown that the success of the inverse transform depends a great deal upon how the transfer function is treated. A single function over the entire frequency span works best. The discontinuities present in a multipiece fit, such as might be used in representing the conductivity or dielectric constant, tend to cause gliches in the time waveform. The phase convention used in deriving the transfer function must be the same as was used in defining the inverse transform. The sum of the transfer function phase and the incident signal phase should be set equal to zero at the low end of the frequency range so that the phase at least starts out in a well-behaved manner during the integration. This normalization must maintain the phase convention.

There is at least one operating reflection code based upon the Fourier transform principle. It is called PROGRAM RR and was written by John Wood of Science Applications, Inc. under contract to the Air Force Weapons Laboratory. Some results from this code are presented in Section 4.3 for observers both above and on the surface. The geometry and output of this code was modified for presentation in this report.

2.4 Convolution Techniques

The alternative to the Fourier or Laplace transform method is the convolution method. If one knows the response of the reflecting medium to an impulse, or delta, function and if the incident pulse is zero for all times less than zero, the reflected pulse is given by

$$E_r(t,\theta_i) = \int_0^t E_i(\tau)\ Q(t-\tau,\theta_i)\ d\tau \qquad (2.32)$$

where E_r is the reflected waveform, E_i is the incident waveform, and Q is the impulse response function. Given the medium's response to a step function, the reflected pulse is found by

$$E_r(t,\theta_i) = \int_0^t \dot{E}_i(\tau)\ S(t-\tau,\theta_i)\ d\tau \qquad (2.33)$$

where S is the step function response. Note that the time derivative of the incident pulse is convoluted with the step function response.

In the frequency domain, the impulse response is given by Fresnel's equations. It is convenient to discuss the problem in terms of Laplace transforms by making the substitution $s = i\omega$ in the frequency domain equations. The step function response is found by dividing the impulse response by s. An inverse Laplace transform must be made in order to obtain the time domain response functions. This is facilitated by using the step function response, since the s^{-1} factor improves the convergence of the integral at high frequencies. In the time domain, the two responses are related through

$$Q(t) = \frac{d}{dt}\ S(t) \qquad (2.34)$$

In general, an analytic inverse transform does not exist and one must be performed numerically for each angle of incidence and set of electrical parameters. A useful approximation does exist for the case of large refractive index and frequency independent electrical parameters. This allows one to find analytical response functions in the time domain without a time consuming inverse transform. Approximate methods are described in Section 2.5. Even

with an analytical response function, the convolution method is quite expensive, since an integral from 0 to t must be performed for each t of interest.

Previous to the development of the Fourier transform code mentioned in the last section, AFWL used a convolution type of code based upon the work of Baum (Reference 6). The code, called PROGRAM REFLECT (Reference 7), still exists and might be modified so as to be as useful as its successor, PROGRAM RR, through the use of analytical approximations for the step function response, instead of the numerical inverse transform method now used to calculate the response function. The basic problem with the full numerical calculation is the fact that one convolutes the time derivative of a digitized waveform, which can be quite noisy, with a response function calculated by a numerical inverse transform, which can be just as noisy. After interpolating, multiplying, and integrating, the resulting waveform cannot be guaranteed to resemble reality. However, immense improvement occurs if either the incident waveform or the response function is analytic so that one source of noise and the need for numerical interpolation is eliminated. The use of an analytical impulse response function, so that the time derivative of digitized incident waveform is not needed, will further improve the results.

High speed convolution programs, like high speed Fourier transform programs, can be written if constant time step size is used. This is not generally practical in EMP work.

2.5 Some Useful Approximations

When one wants to estimate the effect of ground reflections on an occasional high altitude burst pulse, it seems a little impractical to

build a transform or convolution code or spend time getting someone else's working on your machine. In this section, some methods for making estimates of reflection effects in both the frequency and time domain are shown.

2.5.1 Dielectric Approximation

For frequencies such that the ratio $\sigma/\varepsilon\omega$ is much less than unity, the index of refraction is given simply by

$$n \simeq \sqrt{\varepsilon_r} \tag{2.35}$$

If over these high frequencies, the dielectric coefficient, ε_r, can be considered constant, than the index of refraction and reflection coefficient will also be constant with respect to frequency. With some relatively simple waveform, such as the magnetic dipole signal, high frequencies can be associated with early times, so that if the ground conductivity is low enough (and dielectric coefficient large enough so that relaxation time

$$\tau_r \equiv \varepsilon/\sigma \tag{2.36}$$

is large enough), the reflection coefficient can be considered constant at early times. The reflected pulse is then just the incident pulse times a constant. The total signal at an arbitrary observer is the vector sum of the directly propagated pulse and the reflected pulse with appropriate consideration given to geometric attenuation and delay.

Rewriting equations (2.15) and (2.16) (letting $\mu_r = 1$), the reflection coefficients for the electric field normal and parallel to the plane of incidence are

$$r_N = \frac{1 - \sqrt{\varepsilon_r}\ \dfrac{\cos\theta_t}{\cos\theta_i}}{1 + \sqrt{\varepsilon_r}\ \dfrac{\cos\theta_t}{\cos\theta_i}} \tag{2.37}$$

and

$$r_P = \frac{1 - \dfrac{1}{\sqrt{\varepsilon_r}}\ \dfrac{\cos\theta_t}{\cos\theta_i}}{1 + \dfrac{1}{\sqrt{\varepsilon_r}}\ \dfrac{\cos\theta_t}{\cos\theta_i}} \tag{2.38}$$

respectively. Snell's law gives

$$\sin\theta_t = \frac{\sin\theta_i}{\sqrt{\varepsilon_r}} \tag{2.39}$$

The sign conventions are illustrated in Figures 2 and 3. If the incident pulse is given by $E_i(t)$, the reflected pulse at the point of reflection is

$$E_r(t) = r\, E_i(t) \tag{2.40}$$

where r is either r_N or r_P, depending upon the polarity of the incident pulse. A pulse with arbitrary polarity can be decomposed into components which are normal and parallel to the plane of incidence. If the angular distance between the observer and the reflection point is small, as measured at the burst, the pulse propagated directly to the observer will have the same time waveform, in this approximation, as the reflected pulse. The total signal is then

$$\vec{E}_T(t) = R_o \left[E_o(t)\ \frac{\hat{e}_d}{R} + rE_o(t - t_d)U(t - t_d)\ \frac{\hat{e}_r}{d} \right] \tag{2.41}$$

where $\hat{e}_d$ and $\hat{e}_r$ are unit polarization vectors, $U(t-t_d)$ is the unit step function, t_d is the delay of the reflected pulse relative to the direct pulse ($t_d = 1/c\ (d-R)$), R is the radial distance from burst to observer, d is the path length for the reflected pulse, and $E_O(t)$, is the pulse time waveform known at a distance R_O from the burst point. The expression is simpler for a surface observer, since d=R and $t_d = 0$. For the case of the incident electric field being normal to the plane of incidence, the reflected signal is parallel and the total signal is

$$E_T(t) = T_N \frac{R_O}{R} E_O(t) \tag{2.42}$$

where

$$T_N = 1 + r_N \tag{2.43}$$

When the electric field is parallel to the plane of incidence, the vertical component of the total electric field is given by

$$E_{TZ}(t) = T_{PZ} \frac{R_O}{R} E_O(t) \tag{2.44}$$

and the horizontal (X) component is

$$E_{TX}(t) = T_{PX} \frac{R_O}{R} E_O(t) \tag{2.45}$$

where

$$T_{PZ} = -(1 + r_p) \sin\theta_i \tag{2.46}$$

and

$$T_{PX} = -(1 - r_p) \cos\theta_i \tag{2.47}$$

The Fourier spectrum seen by an off-the-ground observer will be the same as the single pulse spectrum, except that oscillations corresponding to the pulse delay time will be superimposed. If a time waveform is of the form

$$E(t) = E_o(t) + aE_o(t - t_d)U(t - t_d) \tag{2.48}$$

its Fourier transform will be of the form

$$\hat{E}(\omega) = \hat{E}_o(\omega)\left(1 + a\, e^{-i\omega t_d}\right) \tag{2.49}$$

which has the amplitude

$$|\hat{E}(\omega)| = |\hat{E}_o(\omega)|\left(1 + a^2 + 2a\cos\omega t_d\right)^{1/2} \tag{2.50}$$

The effect of adding two pulses is to redistribute the energy contained in the pulses such that frequencies equal to n/t_d, where n is an even integer, get a maximum amount of energy (or minimum if a is negative) while those corresponding to odd n have the energy minimized.

The dielectric approximation is currently being used by Tal Wyatt at Harry Diamond Laboratory.

2.5.2 Perfect Conductor Approximation

At the opposite extreme from the dielectric approximation is the perfect conductor approximation, which is good to first order when $\sigma/\varepsilon\omega$ is much greater than unity. In this approximation,

$$r_N \simeq -1 \tag{2.51}$$

$$r_p \simeq 1 \tag{2.52}$$

so that the low frequencies are totally reflected. In this approximation, all electric fields parallel to the surface are shorted out there so that the total field is only in the vertical direction. Obviously, this approximation is not very useful when one needs to know the horizontal component of the field for coupling electric fields into ground systems. The horizontal magnetic field is finite, however, and this might be used for coupling into vertical loops. In the time domain, the infinite conductor approximation may not be considered valid when the relative change in the field is large over a relaxation period,

$$\tau_r = \varepsilon/\sigma.$$

Fortunately, it is possible to use an approximation for large values of refractive index which is normally valid over all frequencies. A step function response can then be found in the time domain, assuming that the conductivity and dielectric coefficient can be considered constant in their effect on the reflection coefficient.

2.5.3 Large Refractive Index Approximation

An approximation which is almost always valid in real problems, except in the case of grazing incidence with the E-vector parallel to the plane of incidence, is that in which the magnitude of the index of refraction is assumed to be much greater than unity. This is true at high frequencies for $\sqrt{\varepsilon_r} >> 1$, and even more true at low frequencies because $\sigma/\varepsilon\omega >> 1$. In this discussion, we will replace the frequency with the Laplace transform variable

$$s \equiv i\omega \tag{2.53}$$

so that certain transformations may be made more easily. Then the index of refraction is

$$n = \left(\varepsilon_r\right)^{1/2} \left(1 + \frac{\sigma}{\varepsilon s}\right)^{1/2} \tag{2.54}$$

In the case that $n \gg 1$, the transmission angle cosine ($\cos\theta_t$) will be very nearly unity. This is true for even $\theta_i = 90°$, to within 13% when $|n|$ is as low as 2. It is a much better approximation for smaller angles and more common $|n|$. Using these approximations and a single term of a binomial expansion, the reflection coefficients become

$$r_N \simeq -\left(1 - 2 \frac{\cos\theta_i}{n}\right) \tag{2.55}$$

and, for $n \cos\theta_i \gg 1$,

$$r_p \simeq 1 - \frac{2}{n \cos\theta_i} \tag{2.56}$$

Assuming constant σ and ε, the frequency domain step function responses, $\tilde{S}_N$ and $\tilde{S}_p$ are found by dividing by s and the time domain responses can be determined by an inverse Laplace transform to be (Abramowitz, 1964)

$$S_N \simeq -\left[1 - \frac{2 \cos\theta_i}{\sqrt{\varepsilon_r}} F\left(\frac{1}{2} t_r\right)\right] U\left(\frac{1}{2} t_r\right) \tag{2.57}$$

$$S_p \simeq \left[1 - \frac{2}{\sqrt{\varepsilon_r} \cos\theta_i} F\left(\frac{1}{2} t_r\right)\right] U\left(\frac{1}{2} t_r\right) \tag{2.58}$$

where

$$t_r \equiv \frac{\sigma}{\varepsilon} t$$

$$F(\chi) \equiv e^{-\chi} I_o(\chi)$$

$I_o(\chi)$ is the modified Bessel function

$U(t_r)$ is the unit step function

Taking the time derivative, one obtains the impulse response functions,

$$Q_N = -\frac{\sigma}{2\varepsilon}\left\{ \delta\left(\frac{1}{2}t_r\right)\left[1 - \frac{2\cos\theta_i}{\sqrt{\varepsilon_r}} F\left(\frac{1}{2}t_r\right)\right] - U\left(\frac{1}{2}t_r\right)\frac{2\cos\theta_i}{\sqrt{\varepsilon_r}} F^1\left(\frac{1}{2}t_r\right)\right\} \quad (2.59)$$

$$Q_p = \frac{\sigma}{2\varepsilon}\left\{ \delta\left(\frac{1}{2}t_r\right)\left[1 - \frac{2F\left(\frac{1}{2}t_r\right)}{\sqrt{\varepsilon_r}\cos\theta_i}\right] - U\left(\frac{1}{2}t_r\right)\frac{2F^1\left(\frac{1}{2}t_r\right)}{\sqrt{\varepsilon_r}\cos\theta_i}\right\} \quad (2.60)$$

where

$$F^1(\chi) = -e^{-\chi}\left[I_o(\chi) - I_1(\chi)\right]$$

$\delta(t_r)$ is the impulse function

Figure 7 shows the functions $F(\chi)$ and $F^1(\chi)$. In the limit of large χ,

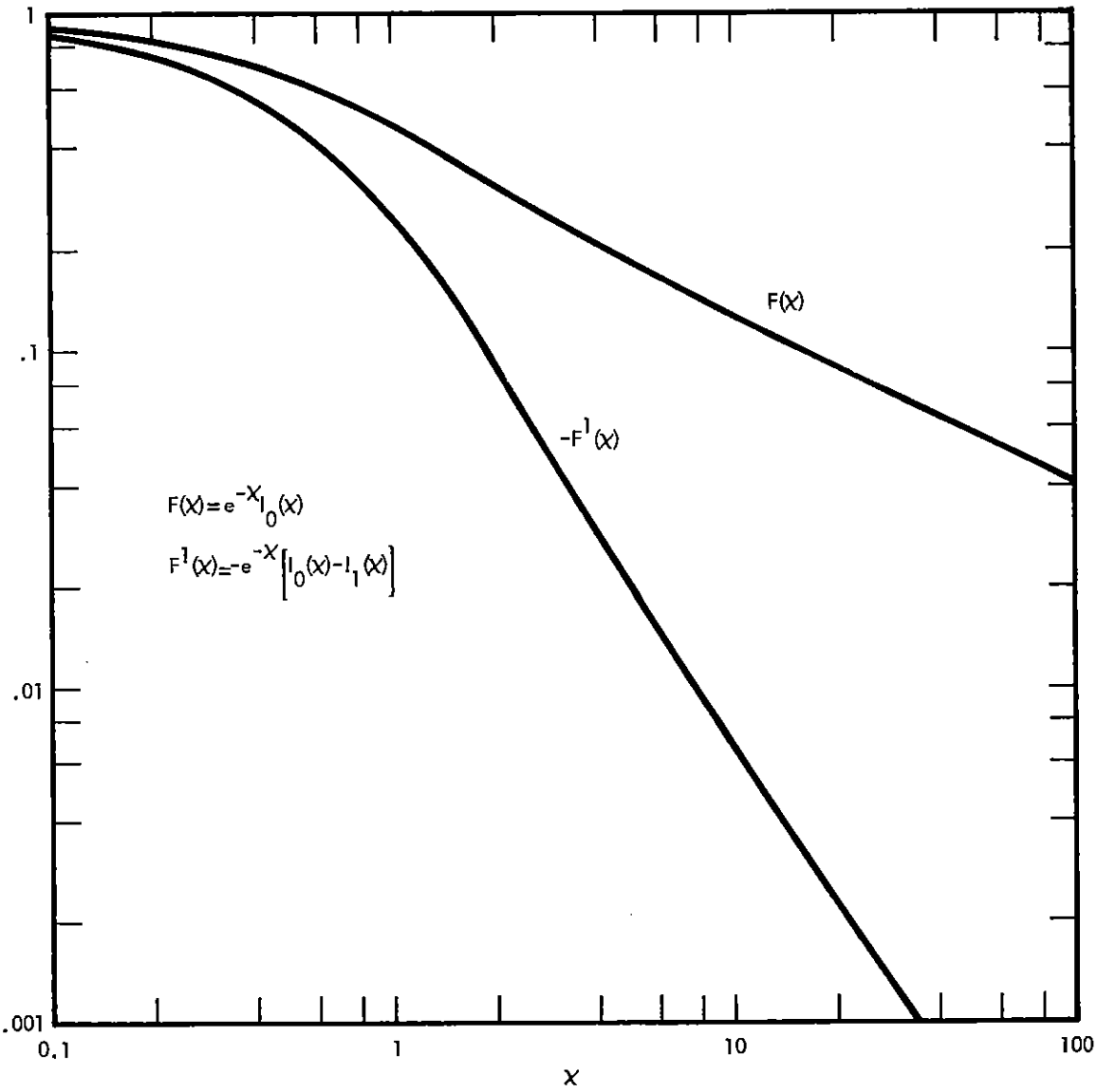

Figure 7. Plot of the functions F(x) and F'(x), which are used in the calculation of the step and impulse response functions.

$$F(\chi) \simeq \frac{1}{\sqrt{2\,\pi\,\chi}} \tag{2.61}$$

$$F^{1}(\chi) \simeq -\frac{1}{2\sqrt{2\pi}\,\chi^{3/2}} \tag{2.62}$$

For $\chi << \sqrt{3}$,

$$F(\chi) \simeq e^{-\chi} \tag{2.63}$$

$$F^{1}(\chi) \simeq -e^{-\chi}\left(1 - \frac{1}{2}\chi\right) \tag{2.64}$$

As a check on the calculation, one can see that at late times, the response functions are independent of ε_r and, at very early times, independent of σ. This agrees with the low and high frequency behavior, respectively.

For the special case of a surface observer, the total field transfer functions are approximately

$$T_N \simeq \frac{2}{n}\cos\theta_i \tag{2.65}$$

when the electric field is normal to the plane of incidence and

$$T_{PX} \simeq -\frac{2}{n} \tag{2.66}$$

$$T_{PZ} \simeq -2\sin\theta_i\left(1 - \frac{1}{n\cos\theta_i}\right) \tag{2.67}$$

for the horizontal and vertical components when the electric field is parallel to the plane of incidence. It is interesting to note that the horizontal component of the total field is independent of incident angle when the electric field is parallel to the plane of incidence (and $n\cos\theta_i >> 1$). The corresponding time domain step function

responses are

$$ST_N = \frac{2\cos\theta_i}{\sqrt{\varepsilon_r}} \; F\left(\frac{1}{2}t_r\right) \; U\left(\frac{1}{2}t_r\right) \tag{2.68}$$

$$ST_{PX} = -\frac{2}{\sqrt{\varepsilon_r}} \; F\left(\frac{1}{2}t_r\right) \; U\left(\frac{1}{2}t_r\right) \tag{2.69}$$

$$ST_{PZ} = -2\sin\theta_i \left[1 - \frac{F\left(\frac{1}{2}t_r\right)}{\sqrt{\varepsilon_r}\cos\theta_i}\right] U\left(\frac{1}{2}t_r\right) \tag{2.70}$$

Finally, the impulse response functions are

$$QT_N = \frac{\cos\theta_i}{\sqrt{\varepsilon_r}} \left(\frac{\sigma}{\varepsilon}\right)\left[F\left(\frac{1}{2}t_r\right)\delta\left(\frac{1}{2}t_r\right) + F^1\left(\frac{1}{2}t_r\right)U\left(\frac{1}{2}t_r\right)\right] \tag{2.71}$$

$$QT_{PX} = -\frac{1}{\sqrt{\varepsilon}}\left(\frac{\sigma}{\varepsilon}\right)\left[F\left(\frac{1}{2}t_r\right)\delta\left(\frac{1}{2}t_r\right) + F^1\left(\frac{1}{2}t_r\right)U\left(\frac{1}{2}t_r\right)\right] \tag{2.72}$$

$$QT_{PZ} = -\left(\frac{\sigma}{\varepsilon}\right)\sin\theta_i \left\{\left[1 - \frac{F\left(\frac{1}{2}t_r\right)}{\sqrt{\varepsilon_r}\cos\theta_i}\right]\delta\left(\frac{1}{2}t_r\right) - \frac{F^1\left(\frac{1}{2}t_r\right)}{\sqrt{\varepsilon_r}\cos\theta_i} U\left(\frac{1}{2}t_r\right)\right\} \tag{2.73}$$

As previously mentioned, the convolution integral can assume two forms, involving either the step function response or the impulse function response (see Reference 8):

$$E_r(t) = \int_0^t \dot{E}_i(\tau)\, S(t - \tau)\, d\tau \tag{2.74}$$

$$E_r(t) = \int_0^t E_i(\tau)\, Q(t - \tau)\, d\tau \tag{2.75}$$

If the incident pulse is either very fast or very slow compared to the response functions, the convolution integrals can be approximated by algebraic expressions which, at least, provide a first order correction to the assumption of frequency independent refractive index.

Consider first, the case where $E(t)$ is rapidly changing compared to the response functions, such that the major contribution to the convolution integral comes from a limited region of time determined entirely by the electric field waveform. This situation is emphasized by the form of the convolution integral in which $\dot{E}_i(t)$ and $S(t)$ are used (Equation (2.74)). If E_i has only one significant peak determining the evaluation of the convolution, then it can be approximated by

$$E_r(t) \simeq \bar{S}\, E_i(t) \tag{2.76}$$

where $\bar{S}$ is the mean value of $S(t-\tau)$ over the period of time that $E_i(\tau)$ is significant. If $E_i(t)$ has multiple peaks, the convolution can be represented by a summation of the form

$$E_r(t) = \bar{S}_N\, E_i(t) + \sum_{n=1}^{N-1} \left(\bar{S}_{n-1} - \bar{S}_n\right)\, E_i\left(t_n\right) \tag{2.77}$$

where the $\bar{S}_n$ are representative values of $S(t-\tau)$ near the times when the largest contributions to the integral are being made. Figure 8 is a qualitative example of a double pulsed waveform being convoluted with a response function which asymptotically approaches unity. The time, t, to which the convolution is being performed, is in the decaying

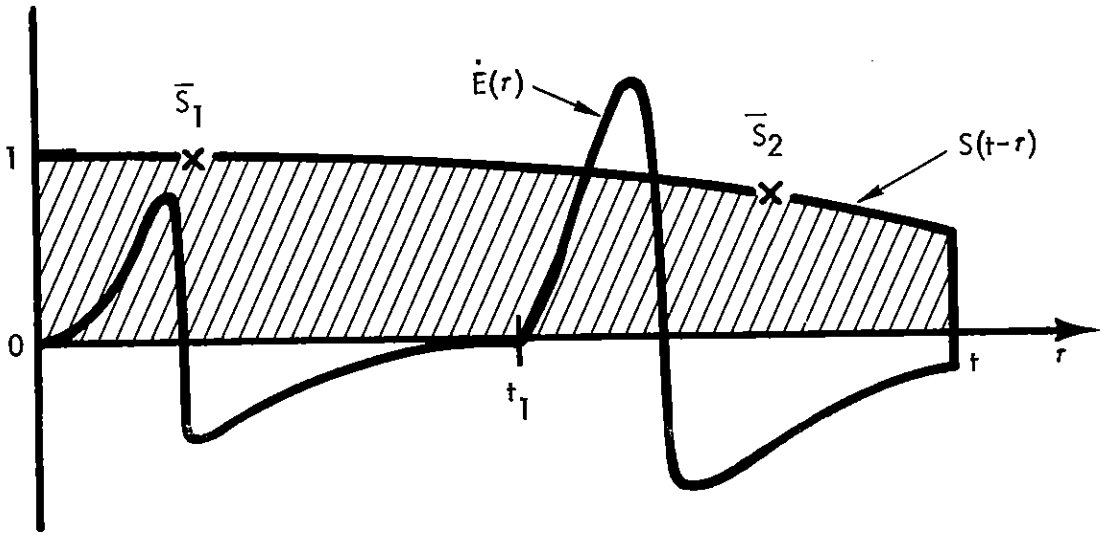

Figure 8. Qualitative example of how the parameters used in the convolution approximation (fast E-field) are chosen.

part of the second pulse. If a single pulse is being considered, a first order approximation for $\bar{S}$ could be $S(t)$.

A similar approximation can be found when $E_i(t)$ varies much more slowly than the response functions. In this case, we use the second form of the convolution in order to emphasize the slowness of $E_i(t)$ and the relative speed of variation of $S(t)$ by using the impulse response function (Equation (2.75)). In this case, we use a mean value of $E_i(\tau)$ and integrate the impulse response function to obtain the step function response:

$$E_r(t) \simeq \bar{E}_i \, S(t) \tag{2.78}$$

The reflection coefficients yield step function responses which asymptotically approach unity so that they eventually look constant compared to any waveform. The transfer functions for the horizontal components

of the total surface field asymptotically approach zero at late times. As a first order approximation, $E_i(t)$ can sometimes be used for $\bar{E}_i$. Thus Equations 2.76 and 2.68 both yield $E_r(t)^2\, E_i(t)\, S(t)$ as a first order approximation. This approximation is tested in Section IV.

The accuracy of the approximations for the step function responses can be estimated by comparison with the response functions calculated by Baum using a numerical inverse transformation (Reference 6).

2.5.4 The Constant Electrical Parameter Approximation

It is often quite convenient to make the assumption that σ and ε are independent of frequency. Comparisons between calculations which use this assumption and those which use Scott's curves with some type of extrapolation (Section 4), indicate that the frequency dependence of the reflection coefficients is quite small despite the fact that the ε can vary several orders of magnitude over an interesting frequency range. It is important to know whether this is a general property of the reflection coefficient or whether it is more a property of Scott's curves. Beginning with the equation for the index of refraction,

$$n = \sqrt{\varepsilon_r}\left(1 - i\,\frac{\sigma}{\varepsilon\omega}\right)^{1/2} \tag{2.79}$$

we see that at high frequencies,

$$n \simeq \sqrt{\varepsilon_r} \tag{2.80}$$

i.e., the refractive index depends upon the square root of the dielectric coefficient. At low frequencies,

$$|\,n\,| \simeq \sqrt{\frac{\sigma}{\varepsilon_0\omega}} \tag{2.81}$$

i.e., the magnitude of the refractive index depends upon the square root of the ratio of conductivity to frequency. Scott's curve-fits indicate that at low frequencies, the conductivity varies very slowly with frequency and is essentially constant. Hence, a constant conductivity approximation is quite valid and, since Scott's fits should be reasonably accurate at the low frequencies of interest to EMP work, one does not expect this situation to change drastically. Judy's data (Section 17.8.2.2) indicates a large increase in conductivity above 10 MHz, but at those frequencies the refractive index is no longer sensitive to changes in σ. At those frequencies, n is determined by $\sqrt{\varepsilon_r}$. Judy's data and Longmire's theory indicate that this increase in $\sqrt{\varepsilon_\sigma}$ is accompanied by a decrease in conductivity. The frequency dependent calculations have extrapolated Scott's curves (which are not valid above 1 MHz) in such a way that the curves, which approach a minimum because of their parabolic nature, are forced to remain constant at their minimum value. Therefore, it is this artificial device which made the constant ε approximation look good. If Judy's data is a reasonable representation of the behaviour of ε above 10 MHz, ε might be expected to vary as $\omega^{-1/3}$ or $\omega^{-1/2}$. The refractive index would then vary as $\omega^{-1/6}$ or $\omega^{-1/4}$ at high frequencies and still be considered constant.

At intermediate frequencies, where $\frac{\sigma}{\varepsilon\omega} \sim 1$, the magnitude of n is dominated mostly by $\sqrt{\varepsilon_r}$, which varies roughly as $\omega^{-1/4}$. It can be concluded, then, that the approximation of constant σ and ε will be good, even with foreseeable changes in the dependence of ground parameters. The constant values should be chosen at an appropriate low frequency and ε should be chosen at an appropriate high frequency. These conclusions are not necessarily true for "abnormal" media such as saturated and leached earth or sea water.

SECTION III
PULSE PENETRATION INTO THE GROUND

In this section, the nature of the pulse which penetrates into the ground, when a signal reflects off of the surface, will be briefly discussed. The general subject of wave and pulse propagation in dissipative media has been thoroughly explored (see, for example, Malik, Reference 9) as a one dimensional problem involving homogeneous media. For the purposes of this discussion, the problem will also be viewed as one dimensional in nature, and the ground will be approximated as a single homogeneous material.

The wave that initially penetrates the surface is given the two Fresnel equations for the transmitted component. In the reflection process, the low frequency components are removed from the transmitted electric pulse because the surface appears to be a good conductor. The behaviour of the magnetic field is somewhat different, however, as is demonstrated by the fact that at the surface of a perfect conductor, the horizontal component of an incident magnetic field is doubled, while the horizontal component of an electric field goes to zero. Then, because the tangential components of $\vec{E}$ and $\vec{H}$ are continuous across the interface and because the transmitted field is nearly horizontal in the case of a medium with large $|n|$, one immediately sees that the low frequency magnetic field will not be attenuated in the same manner as the electric field.

Using equations (2.22) and (2.23) and the large index of refraction approximation discussed in Section 2.5, the electric field

transmission coefficients are approximately

$$t_N \simeq \frac{2}{n} \cos\theta_i \tag{3.1}$$

when $\vec{E}$ is normal to the plane of incidence, and

$$t_P \simeq \frac{2}{n} \tag{3.2}$$

when $\vec{E}$ is parallel to the plane of incidence and $n \cos\theta_i >> 1$. In this approximation the penetrating plane waves are parallel to the surface. The relative magnetic permeability (μ_r) is assumed to be unity. The magnetic field is related to the electric field by

$$| \vec{H} | = \frac{1}{Z} | \vec{E} | = \frac{n}{Z_0} | \vec{E} | \tag{3.3}$$

so that the magnetic fields which penetrate the surface are approximately independent of n. Here, Z is the wave impedance and Z_0 is the impedence of free space (~ 377 ohm).

After penetrating the surface, the waves propagate as plane waves with the spatial dependence

$$F_t(\ell) = F_{to} \exp(-ik\ell) \tag{3.4}$$

where F_t is either the electric or magnetic field, F_{to} is the field amplitude at the surface, $k = n/\lambda\!\!\!^{-}_0$ is the wave number, $\lambda\!\!\!^{-}_0$ is the free space wavelength divided by 2π, ℓ is the distance along the downward ray ($-z$ in the large n approximation), and n is the index of refraction. The real and imaginary parts of $n = n_r - i\, n_i$ are given by

$$n_r = \sqrt{\frac{\varepsilon_r}{2}} \left[\sqrt{1 + \left(\frac{\sigma}{\varepsilon\omega}\right)^2} + 1 \right]^{1/2} \tag{3.5}$$

$$n_i = \sqrt{\frac{\varepsilon_r}{2}} \left[\sqrt{1 + \left(\frac{\sigma}{\varepsilon\omega}\right)^2} - 1 \right]^{1/2} \qquad (3.6)$$

The imaginary part of k, which determines the attenuation with distance, is fairly constant for $\frac{\sigma}{\varepsilon\omega} \lesssim 1$, i.e., for high frequencies, and has the value

$$k_i \simeq \frac{Z_0\, \sigma}{2\sqrt{\varepsilon_r}}, \qquad \frac{\sigma}{\varepsilon\omega} \lesssim 1 \qquad (3.7)$$

For continually decreasing frequencies, the real and imaginary parts become equal to each other and decrease as

$$k_i \simeq 1/\delta(\omega), \quad \frac{\sigma}{\varepsilon\omega} >> 1 \qquad (3.8)$$

where the skin depth is given by

$$\delta(\omega) \equiv \sqrt{\frac{2}{\mu_0 \sigma\, \omega}} \qquad (3.9)$$

Thus, after initial penetration, the ground acts as a low pass filter, with the high frequencies being increasingly attenuated with increasing depth. The low frequencies roll off as $\exp(-a\sqrt{\omega})$, with "a" a constant.

We now combine the transmission and attenuation coefficients in order to relate the field incident at the surface with the fields seen at some distance Z in the ground, using the "large n" approximations. For purposes of penetration study, z will be measured with the positive direction downward. We will use the incident electric field as the initial condition. The electric field components at the depth z are then

$$\hat{E}_{tN}(\omega,z) \simeq 2\cos\theta_i \frac{\exp\left(-i\frac{n}{\lambda_0}z\right)}{n} \hat{E}_{iN}(\omega,0) \qquad (3.10)$$

$$\hat{E}_{tP}(\omega,z) \simeq 2\frac{\exp\left(-i\frac{n}{\lambda_0}z\right)}{n} \hat{E}_{iP}(\omega,0). \qquad (3.11)$$

For easy reference, we rewrite n

$$n = \sqrt{\varepsilon_r}\left(1 - i\frac{\sigma}{\varepsilon\omega}\right)^{1/2} \qquad (3.12)$$

The magnetic field corresponding to $\hat{E}_{tN}$ is

$$\hat{H}_{tN}(\omega,z) \simeq \frac{2}{Z_0}\cos\theta_i \exp\left(-i\frac{n}{\lambda_0}z\right) \hat{E}_{iN}(\omega,0) \qquad (3.13)$$

and that corresponding to $\hat{E}_{tP}$ is

$$\hat{H}_{tP}(\omega,z) = \frac{2}{Z_0}\exp\left(-i\frac{n}{\lambda_0}z\right) \hat{E}_{iP}(\omega,0) \qquad (3.14)$$

For high frequencies, $\frac{\sigma}{\varepsilon\omega} << 1$, the field magnitudes are approximately

$$|\hat{E}_{tN}(\omega,z)| \simeq -\frac{2}{\sqrt{\varepsilon_r}}\cos\theta_i \exp\left(-\frac{Z_0\sigma}{2\sqrt{\varepsilon_r}}z\right) |\hat{E}_{iN}(\omega,0)| \qquad (3.15)$$

$$|\hat{E}_{tP}(\omega,z)| \simeq \frac{2}{\sqrt{\varepsilon_r}}\exp\left(-\frac{Z_0\sigma}{2\sqrt{\varepsilon_r}}z\right) |\hat{E}_{iP}(\omega,0)| \qquad (3.16)$$

$$|\hat{H}_{tN}(\omega,z)| \simeq \frac{2}{Z_o}\cos\theta_i \exp\left(\frac{Z_0\,\sigma}{2\sqrt{\epsilon_r}}\, z\right)|\hat{E}_{iN}(\omega,o)| \qquad (3.17)$$

$$|\hat{H}_{tP}(\omega,z)| \simeq \frac{2}{Z_o}\exp\left(-\frac{Z_0\sigma}{2\sqrt{\epsilon_r}}\, z\right)|\hat{E}_{iP}(\omega,o)| \qquad (3.18)$$

For low frequencies, $\frac{\sigma}{\epsilon\omega} >> 1$, they are

$$|\hat{E}_{tN}(\omega,z)| \simeq 2\left(\frac{\epsilon_0\omega}{\sigma}\right)\cos\theta_i \exp\left(-\sqrt{\frac{\mu\sigma\omega}{2}}\, z\right)|\hat{E}_{iN}(\omega,0)| \qquad (3.19)$$

$$|\hat{E}_{tP}(\omega,z)| \simeq 2\left(\frac{\epsilon_0\omega}{\sigma}\right)\exp\left(-\sqrt{\frac{\mu\sigma\omega}{2}}\, z\right)|\hat{E}_{iP}(\omega,0)| \qquad (3.20)$$

$$|\hat{H}_{tN}(\omega,z)| \simeq \frac{2}{Z_o}\cos\theta_i \exp\left(-\sqrt{\frac{\mu\sigma\omega}{2}}\, z\right)|\hat{E}_{iP}(\omega,0)| \qquad (3.21)$$

$$|\hat{H}_{tP}(\omega,z)| \simeq \frac{2}{Z_o}\exp\left(-\sqrt{\frac{\mu\sigma\omega}{2}}\, z\right)|\hat{E}_{iP}(\omega,0)| \qquad (3.22)$$

In the time domain, which will not be discussed in detail here (see Reference 10) , the filtering action of the conducting medium causes the propagating pulse to become drawn out in space and time, falling off exponentially with what is sometimes referred to as the "residue" signal. This behavior is characteristic of the diffusion equation, which describes the low frequency problem.

Impulse and step function responses have been calculated for constant σ and ϵ by Malik, (Reference 8). These do not include

the reflection portion of the total transfer function, but assume the field to be defined at the upper boundary. Such response functions can be used directly with the magnetic field in the large n approximation since the transmitted electric field is related to the incident electric field by a constant.

In the case of a surface burst, which has been ignored, the fields in the ground are usually calculated as part of the normal numerical calculation. The lower boundary is normally on the order of 100 meters. For deep penetration studies, one can do a diffusion calculation rather simply in the frequency domain or use a transform or convolution technique to calculate the time domain. A deep penetration code (Reference 11) is available at Mission Research Corporation. Examples of electric and magnetic field transfer functions for penetration to several depths are shown in Section IV.

SECTION IV
SAMPLE CALCULATIONS

In this section, selected calculations are made in order to illustrate the use of the equations and approximations presented in previous sections and to give the reader a "feel" for the effects being discussed. In 4.1 the reflection coefficients and surface observer transfer functions will be discussed in terms of their frequency dependence for "typical" soil parameters. Most calculations will assume constant conductivity and dielectric coefficient, but one comparison with an extrapolated Scott's curve-fit will be made. The polarization data used in this section is taken from Appendix A. There, formulas are introduced which allow one to estimate the fraction of the total field oriented parallel and normal to the plane of incidence, given the observer position with respect to the burst and the geomagnetic field. In section 4.2, time domain calculations are shown for various observers and a 100 km altitude burst. Then results from using approximational techniques and machine calculations are compared.

4.1 Frequency Domain Calculations

In this section, examples are given using the complex reflection coefficients for several values of conductivity (σ) and dielectric coefficient (ε_r) which bracket the most likely values to be encountered in realistic situations. In all but one example, constant values of σ and ε_r are used. This is justified (1) because of the analysis of the constant parameter approximation given in

Section 2.5, (2) by the comparison with an extrapolated Scott's curve-fit show later in this section, (3) because the high frequency behavior of σ and $\varepsilon_{r_\perp}$ is not well known, and (4) the average application of reflection techniques to actual systems analysis probably will not be sophisticated enough to allow a representation of frequency dependent electrical parameters.

In each case, the amplitude and phase of the two complex reflection coefficients, r_N and r_p will be shown. The coefficient r_N describes the reflection of the electric field component normal to the plane of incidence while r_p describes the reflection of the electric field component parallel to the plane of incidence. The coefficients are shown as a function of frequency for various angles of incidence (0°, 30°, 60°, 80°, 85°, 87°, and 89.9°). The coordinate systems and geometry are described in Section 2. In general, the phase of r_N is near π and that of r_p is very small, so that they are essentially real quantities given by the amplitude times -1 or +1 respectively. The exception to this is r_p for near grazing incident angles (~ 90°). In this case, the phase is small for low frequencies, but passes through $\pi/2$ (dashed line in Figures) and asymptotically approaches π for increasing frequency. Thus, the real part of r_p changes sign as a function of frequency for fixed angle of incidence. In the case of a pure dielectric, where the frequency dependence can be ignored, the angle of incidence at which r_p changes sign is known as the Brewster angle and devices utilizing this property are used to polarize light. The property will also be important in one aspect of the ionospherically propagated satellite environment. It has been suggested that the worst case environment might be that due to a grazingly reflected signal with vertical polarity, combining with a nearly parallel pulse that does not reflect. It was proposed that this would effectively double the available field strength, as would be the case for low frequencies. However, because of the Brewster phenomenon, what really would happen would be the partial cancellation of the high frequency components of the pulse and a reduction of the threat.

Two sets of electrical parameters were chosen to represent the expected variation of soil reflection properties: $\sigma = 1.15 \times 10^{-2}$ mho/m, $\varepsilon_r = 41.1$ and $\sigma = 6.03 \times 10^{-4}$ mho/m, $\varepsilon_r = 16.0$. These values are predicted by Scott's curves at 1 MHz for water contents of 10 percent and one percent by volume. It was desirable to choose values which enable a direct comparison with the reflection coefficients predicted through Scott's curves and 1 MHz is the highest frequency at which they are valid. Values of conductivity near 10^{-2} mho/m and 10^{-3} mho/m are desirable since typical values of conductivity lie within this range and constant values within this range are commonly used as representative values in surface burst codes.

Scott's curve-fit for 10 percent water content is used to calculate reflection coefficients which can be compared to the 1.15×10^{-2} mho/m calculation in order to indicate the errors involved in assuming constant electrical parameters. The results are inconclusive however, because Scott's curves are not valid above 1 MHz (see Section 2.2). They were extrapolated by simply continuing the conductivity function (increasing with frequency) and by allowing the dielectric coefficient function to reach its minimum and preserving the minimum value for all higher frequencies.

In addition to the typical soil parameters, the reflection coefficients for seawater are calculated using $\sigma = 5$ mho/m and $\varepsilon_r = 81$.

After the reflection coefficients are shown, the transfer functions for the total field seen by a point surface observer are illustrated for the representative soil parameters. These are easy to calculate since no delay time is involved. When a finite delay exists between the arrival of the direct and reflected pulses oscillations appear in the spectrum such as described under the dielectric approximation in Section 2.5. These oscillations correspond to a redistribution of energy such that it is concentrated in frequencies equal to even

multiples of $1/t_d$, where t_d is the delay of the reflected pulse relative to the incident pulse. Total field transfer functions can be rather simply calculated when the reflection coefficient is a constant, e.g., in the dielectric and perfect conductor approximations. Otherwise, it is easier to work in the time domain.

Figures 9 and 10 show r_N, Figures 11 and 12 show r_p for $\sigma=1.15\text{x}10^{-2}$ mho/m. Figures 13 through 16 show the same for Scott's 10 percent water content curves. Note that there is less variation with frequency at high frequencies in the case of constant parameters. The discrepancy is not large except in the case of r_p with large incident angle. Figures 17 through 20 show the reflection coefficients for $\sigma=6.03\text{x}10^{-4}$ mho/m. Note the large high frequency region in which the ground appears to be a dielectric. Figures 21 and 22 show r_p for seawater. The other reflection coefficient, r_N, is not shown since it is so close to -1. An idea of how close can be gained from Figure 29, a graph of the magnitude of the surface observer transfer function, T_N, where $T_N = r_N + 1$.

An especially interesting observer for which one might want to know the total field, is an observer at the surface. Such observers might be cables, hardened UHF antennas and circumvention or warning detectors. Using the equations in Section 2.1, the electric field transfer functions T_N, T_{PX}, and T_{PZ} were calculated for the cases $\sigma=1.15\text{x}10^{-2}$ mho/m, $\varepsilon_r=41.1$ and $\sigma=6.03\text{x}10^{-4}$ mho/m, $\varepsilon_r=16.0$. The amplitudes of these quantities are shown in Figures 23 through 28. The phases are not shown since they were very small in the case of T_N and close to π in the cases of T_{PX} and T_{PZ}. Thus, the real parts of the transfer functions (which is really what one is interested in) can be approximated by $|T_N|$ and $-|T_{PX}|$, $-|T_{PZ}|$. The reference coordinate systems are shown in Figures 1.2a and 1.2b. Figure 29 shows $|T_N|$ for seawater.

It would have been desirable to show the transfer functions for the magnetic field also, but space is limited. However, as a general rule, the magnetic field components add constructively where the electric fields add destructively and vis versa. The relation between the magnetic and electric fields is shown in the last paragraph of Section 2. The reflection coefficient for the component of the magnetic field normal to the plane of incidence is r_p and that for the parallel component is r_N. However, the vector addition to find the total field is different, as shown in Figures 2 and 3, so that for example, the horizontal components add constructively at the surface instead of partially cancelling.

Finally, in Figures 30 and 31, the transfer function for fields penetrating into the ground are shown. The angle of incidence chosen for this example is 0° so that all electric and magnetic field components are tangent to the surface. The 1.15×10^{-2} mho/m ground conductivity was used. In the case of the electric field, the reflection of the field at the surface (which filters out low frequencies) has more influence on the spectrum which penetrates to several meters than does the attenuation caused by propagating through the conducting soil. The attenuation has the most effect with high frequencies. When penetrating to depths on the order of tens of meters or more, both the high and low frequencies are severly attenuated, leaving a band of frequencies in the megahertz region. Time waveforms have not been calculated, but one could probably expect it to be a slowly rising pulse, decaying into a megahertz and lower type of oscillation. Figure 31 shows the magnetic field transfer function for the same problem. The transmission coefficient causes a very slight loss of the high frequency content (relative to the low frequency content, all are almost doubled). For all practical purposes, however, one can simply double the spectrum of the incident field and consider only attenuation when calculating the spectrum of the penetrating pulse. At depths of tens of meters, the high frequencies

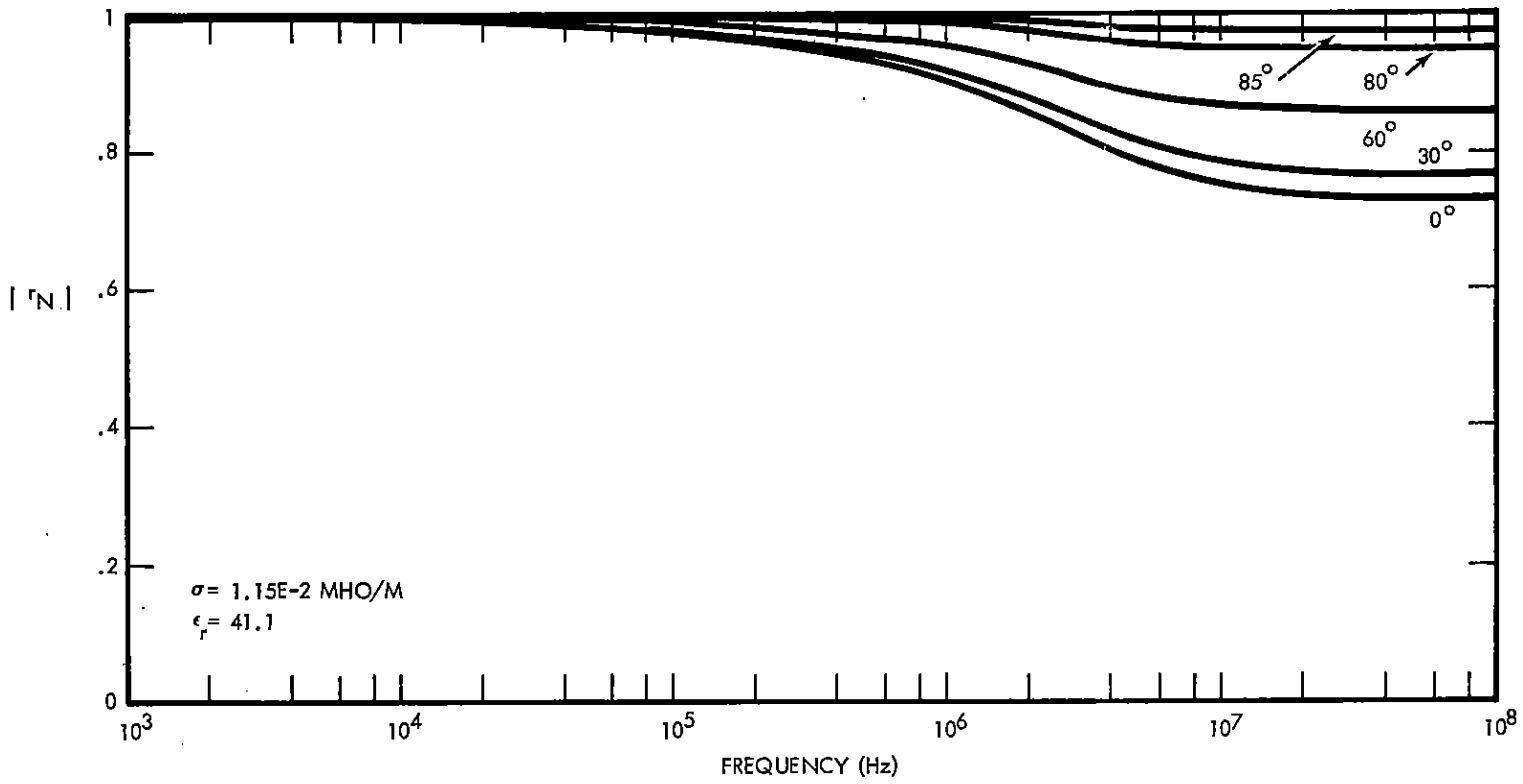

Figure 9. Amplitude of reflection coefficient for electric field component normal to plane of incidence (constant electrical parameters). Curves are for various incident angles.

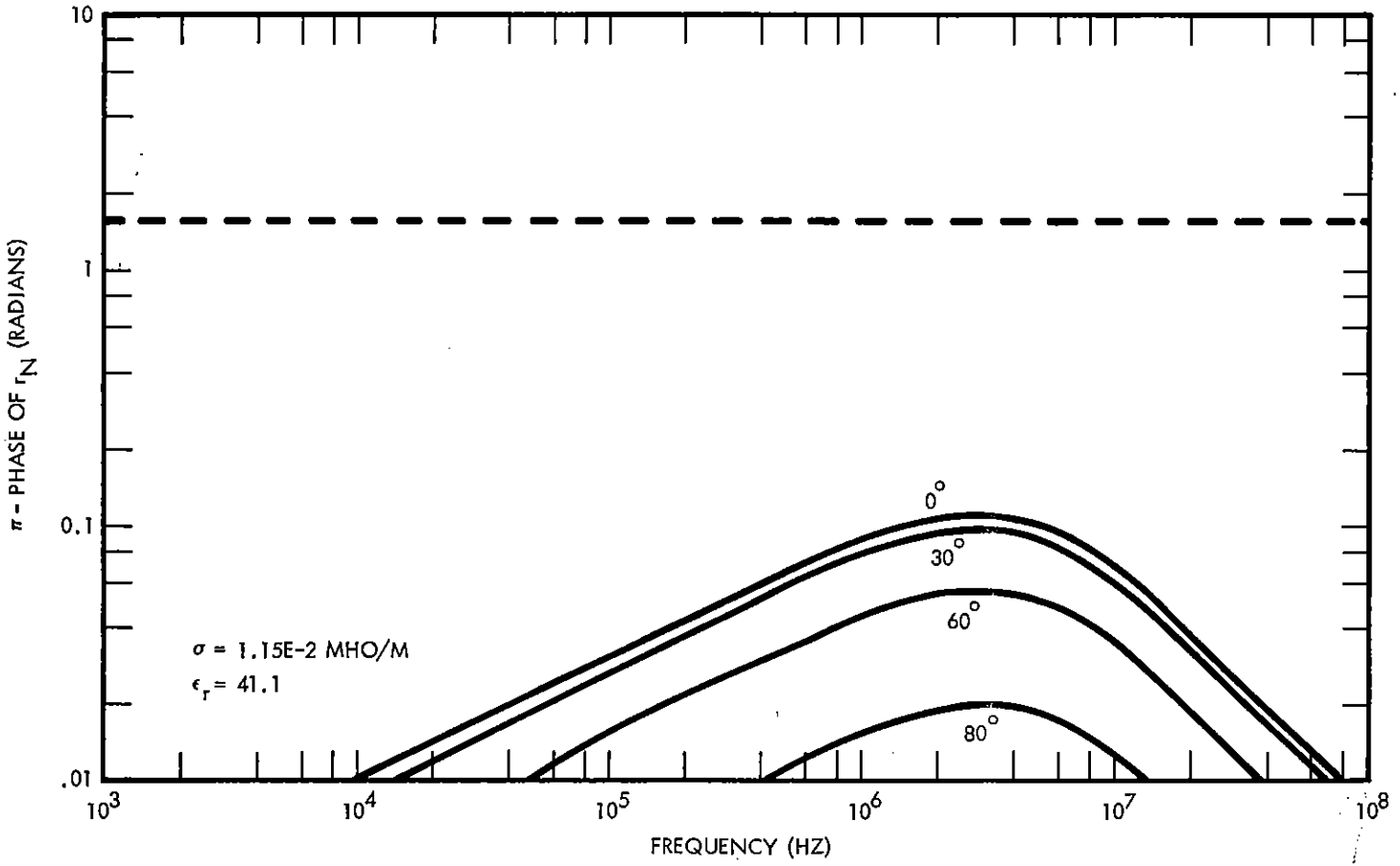

Figure 10. Phase of reflection coefficient for electric field component normal to plane of incidence (constant electrical parameters). Curves are for various incident angles.

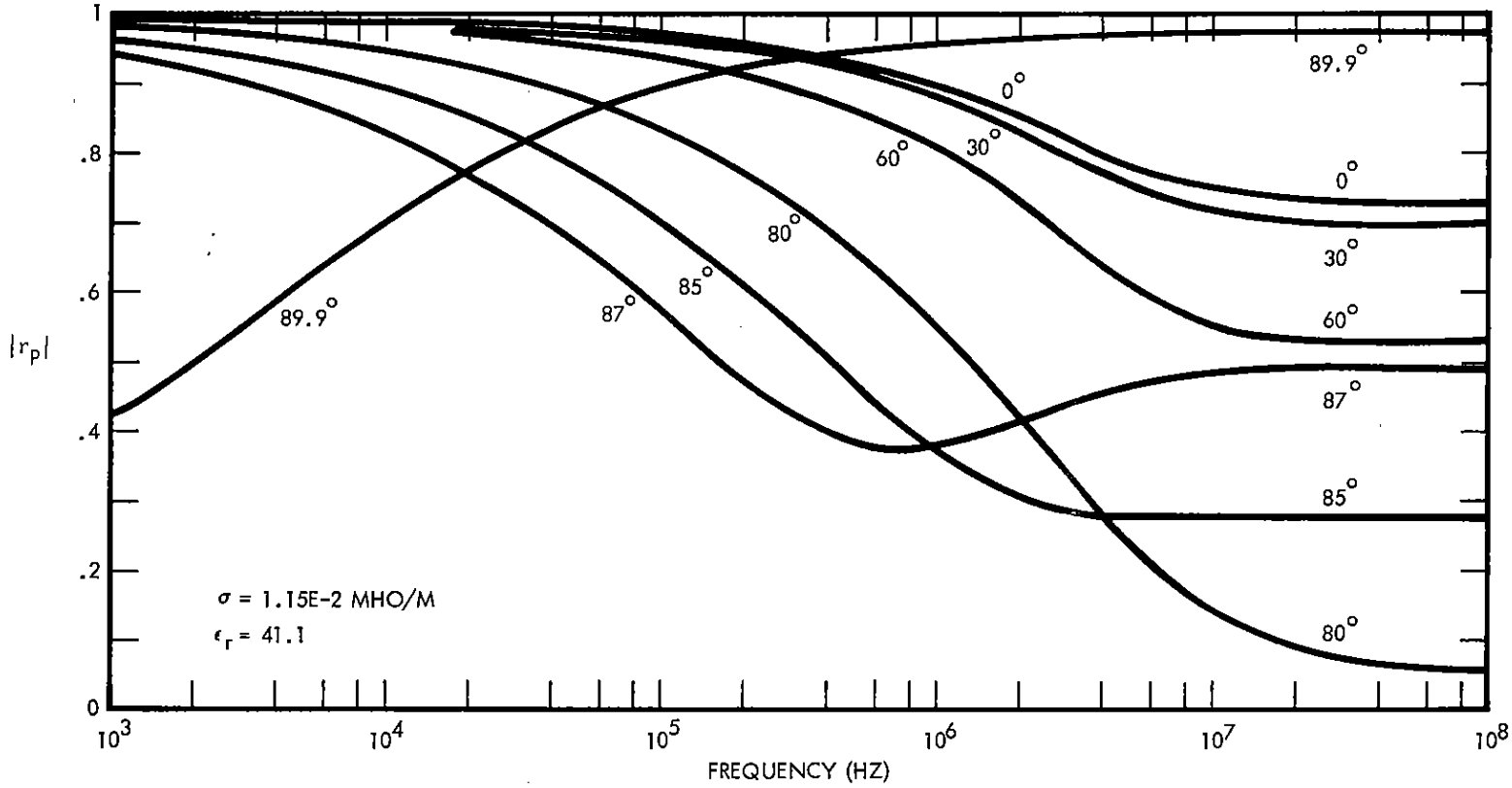

Figure 11. Amplitude of reflection coefficient for electrical field component parallel to plane of incidence (constant electrical parameters). Curves are for various incident angles.

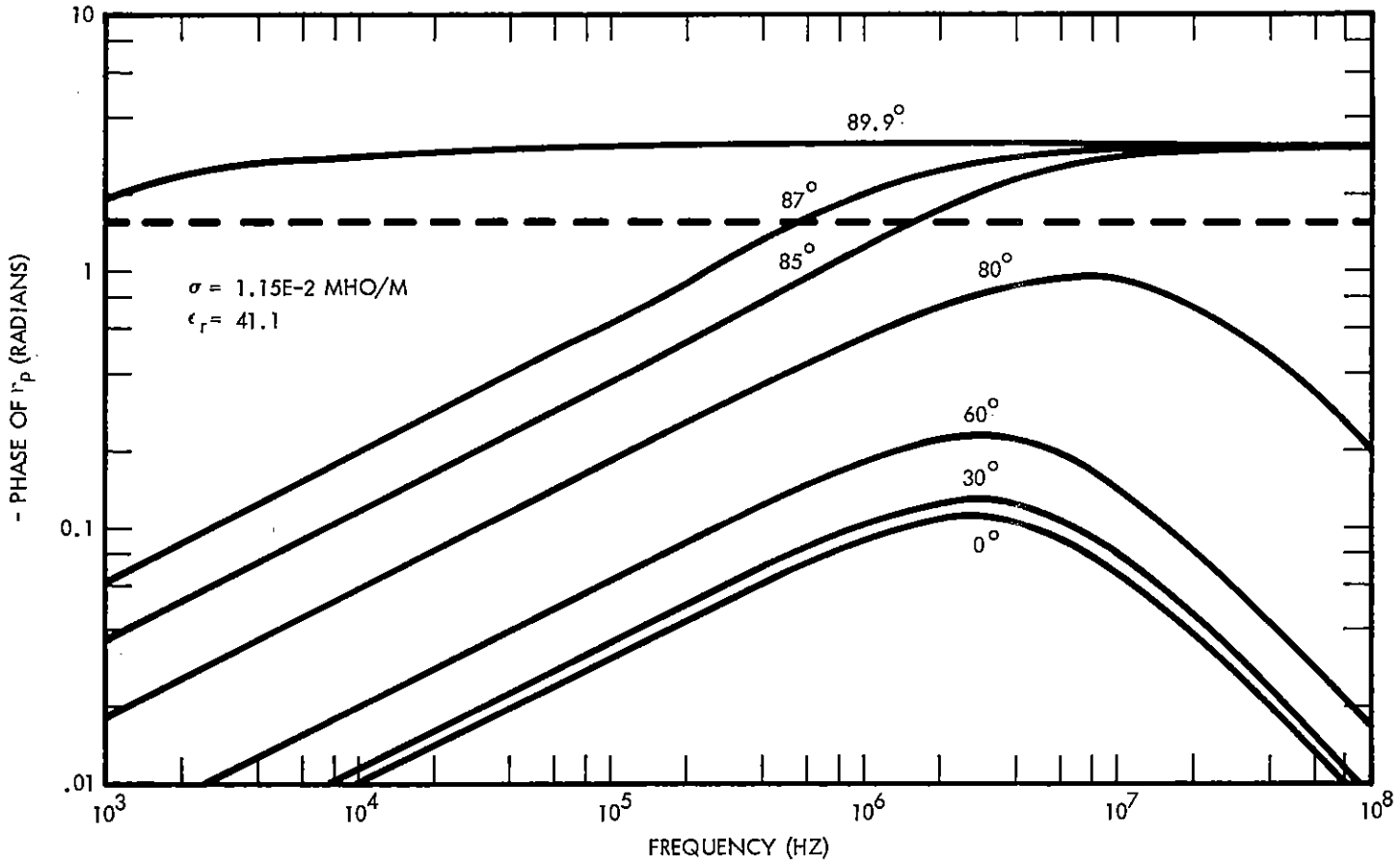

Figure 12. Phase of reflection coefficient for electric field component parallel to plane of incidence (constant electrical parameters). Curves are for various incident angles.

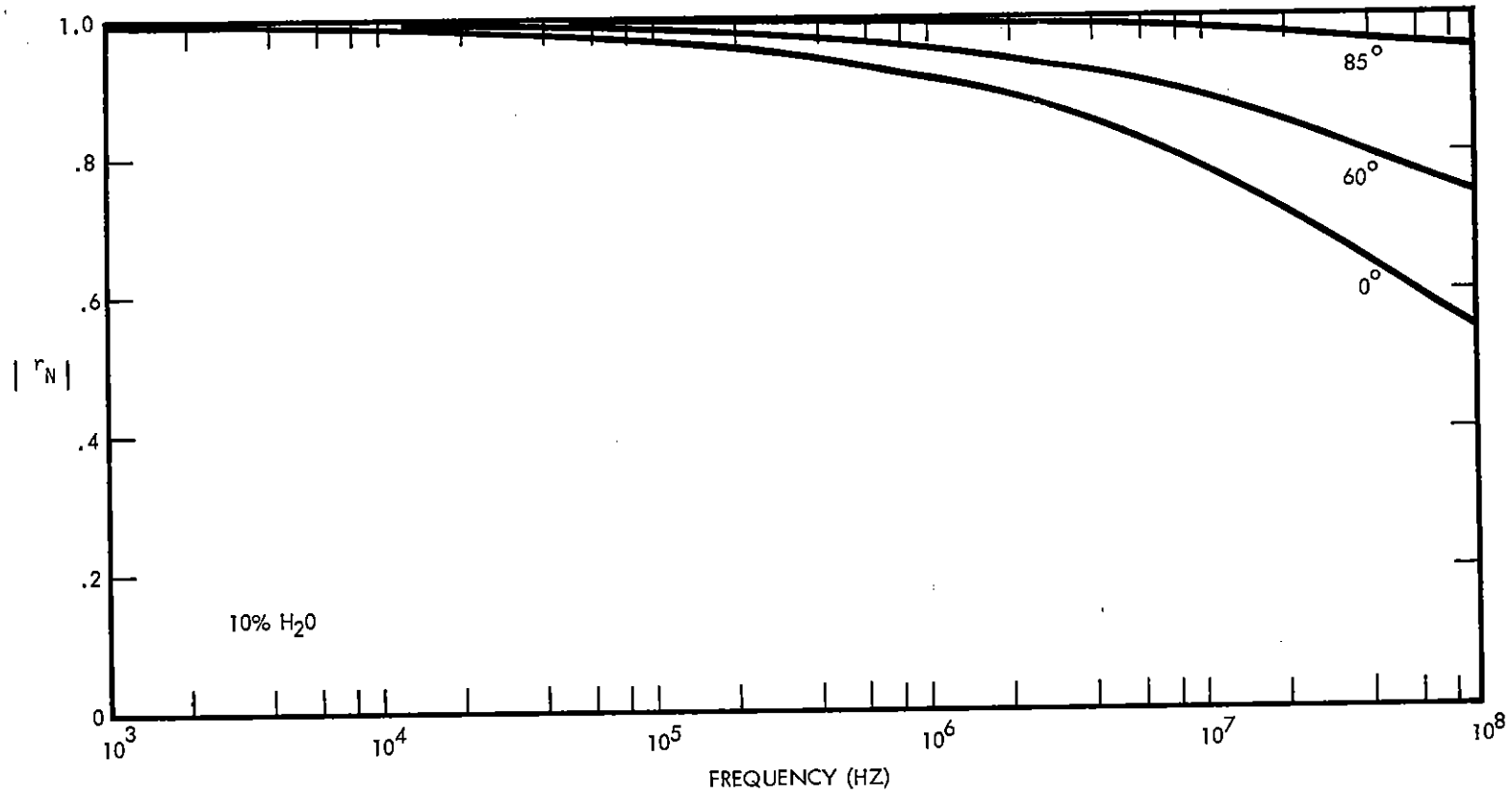

Figure 13. Amplitude of reflection coefficient for electric field component normal to plane of incidence (modified Scott's Curves). Curves are for various incident angles.

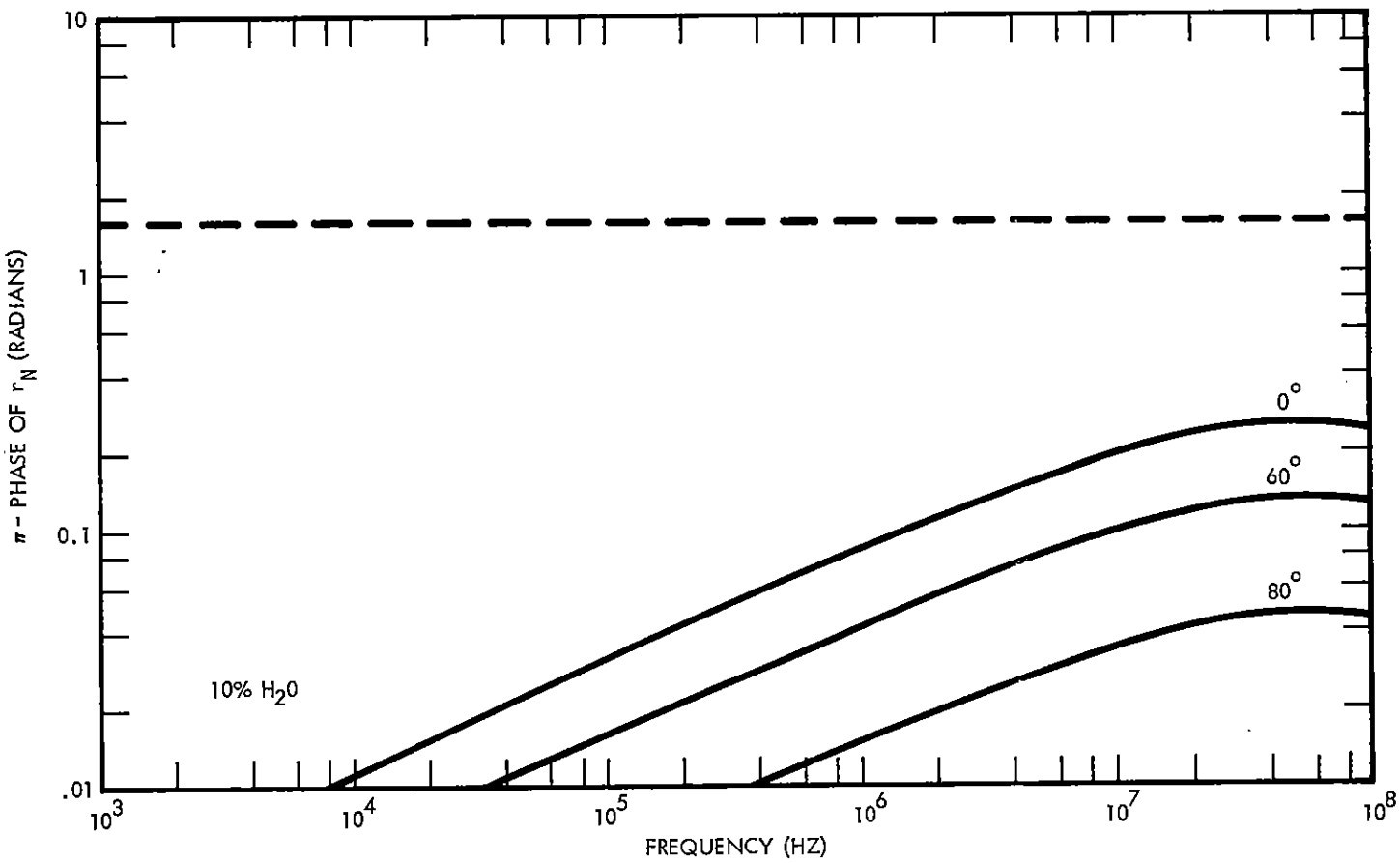

Figure 14. Phase of reflection coefficient for electric field component normal to plane of incidence (modified Scott's Curves). Curves are for various incident angles.

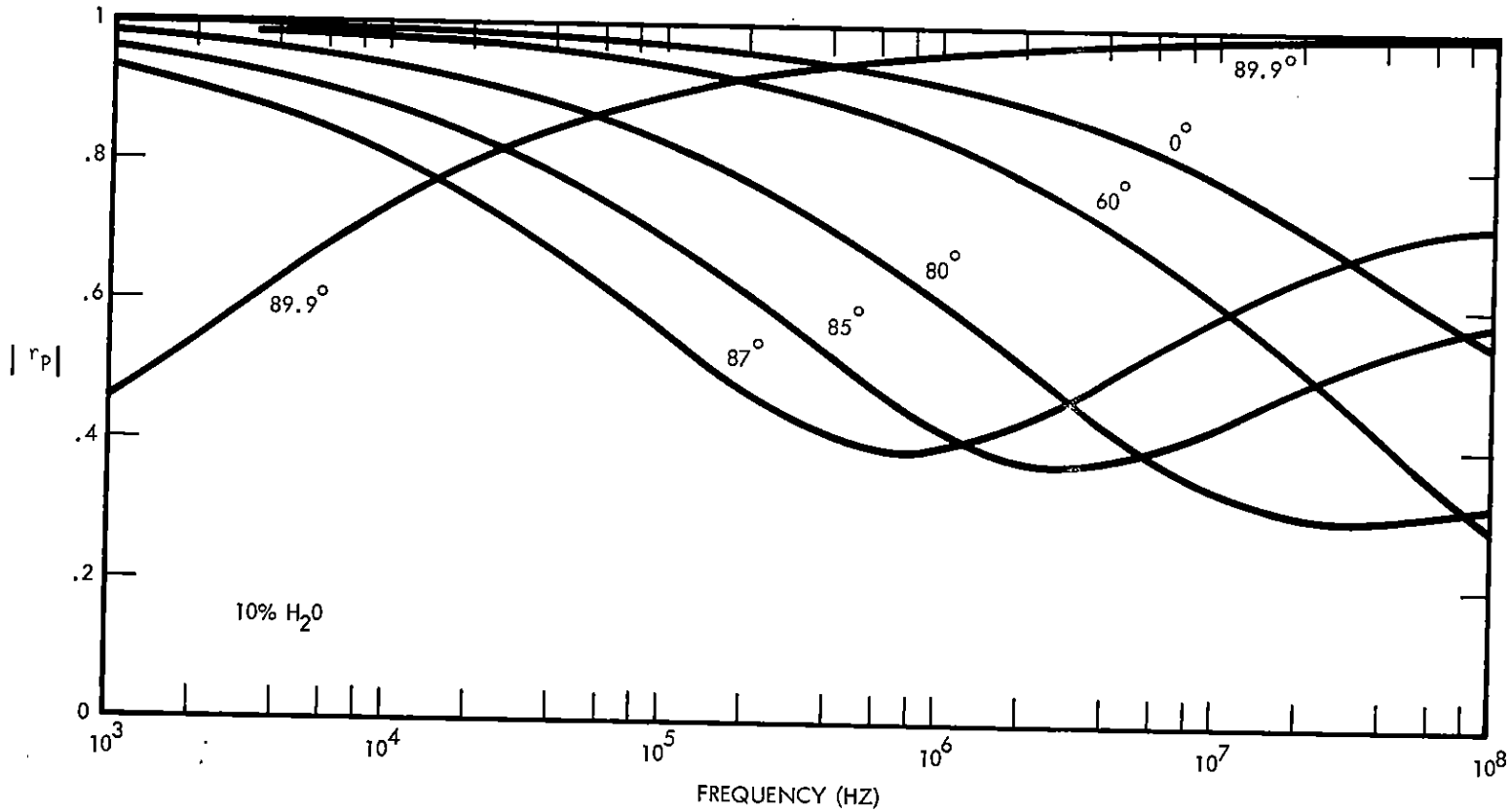

Figure 15. Amplitude of reflection coefficient for electric field component parallel to plane of incidence (modified Scott's Curves). Curves are for various incident angles.

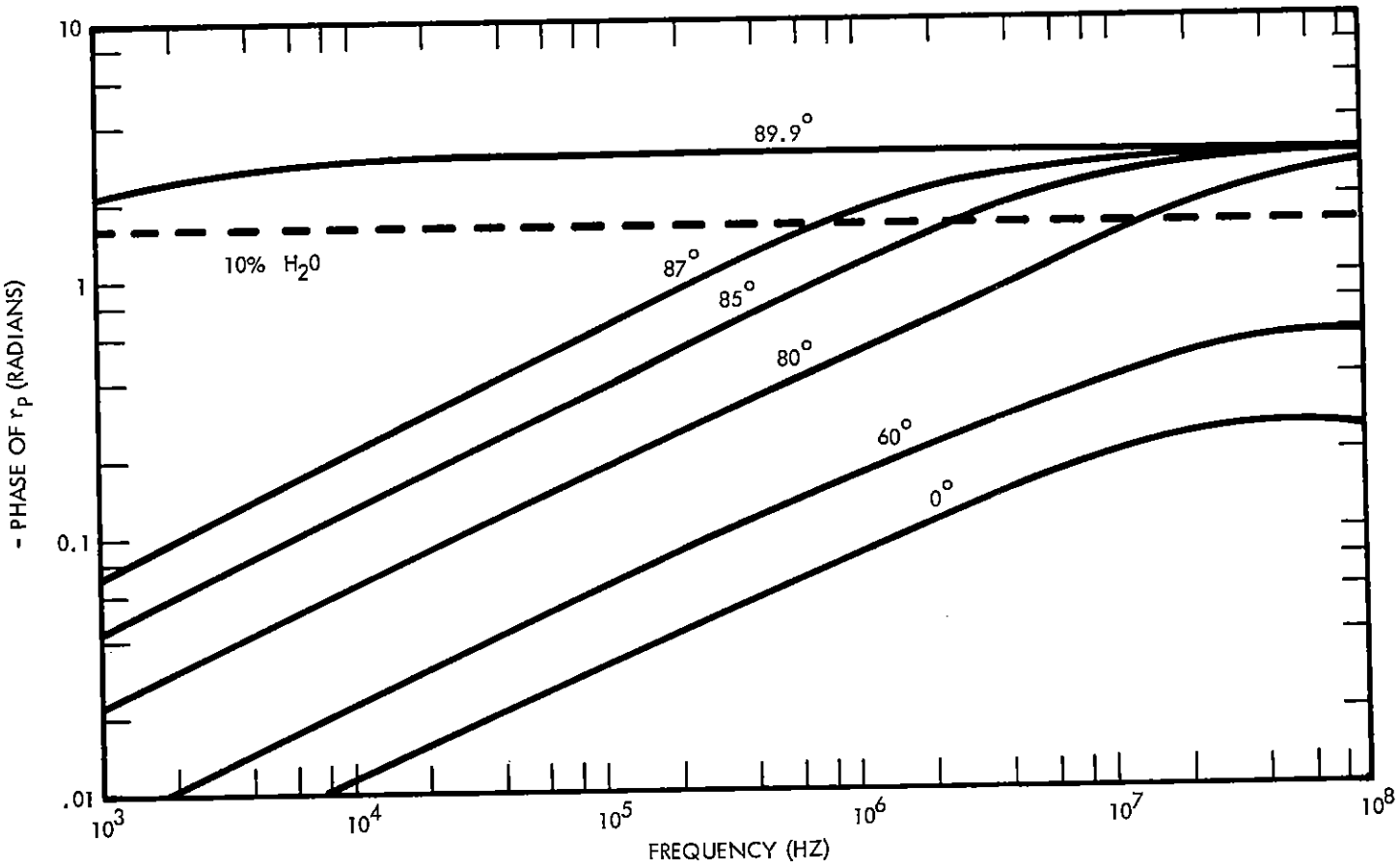

Figure 16. Phase of reflection coefficient for electric field component parallel to plane of incidence (modified Scott's Curves). Curves are for various incident angles.

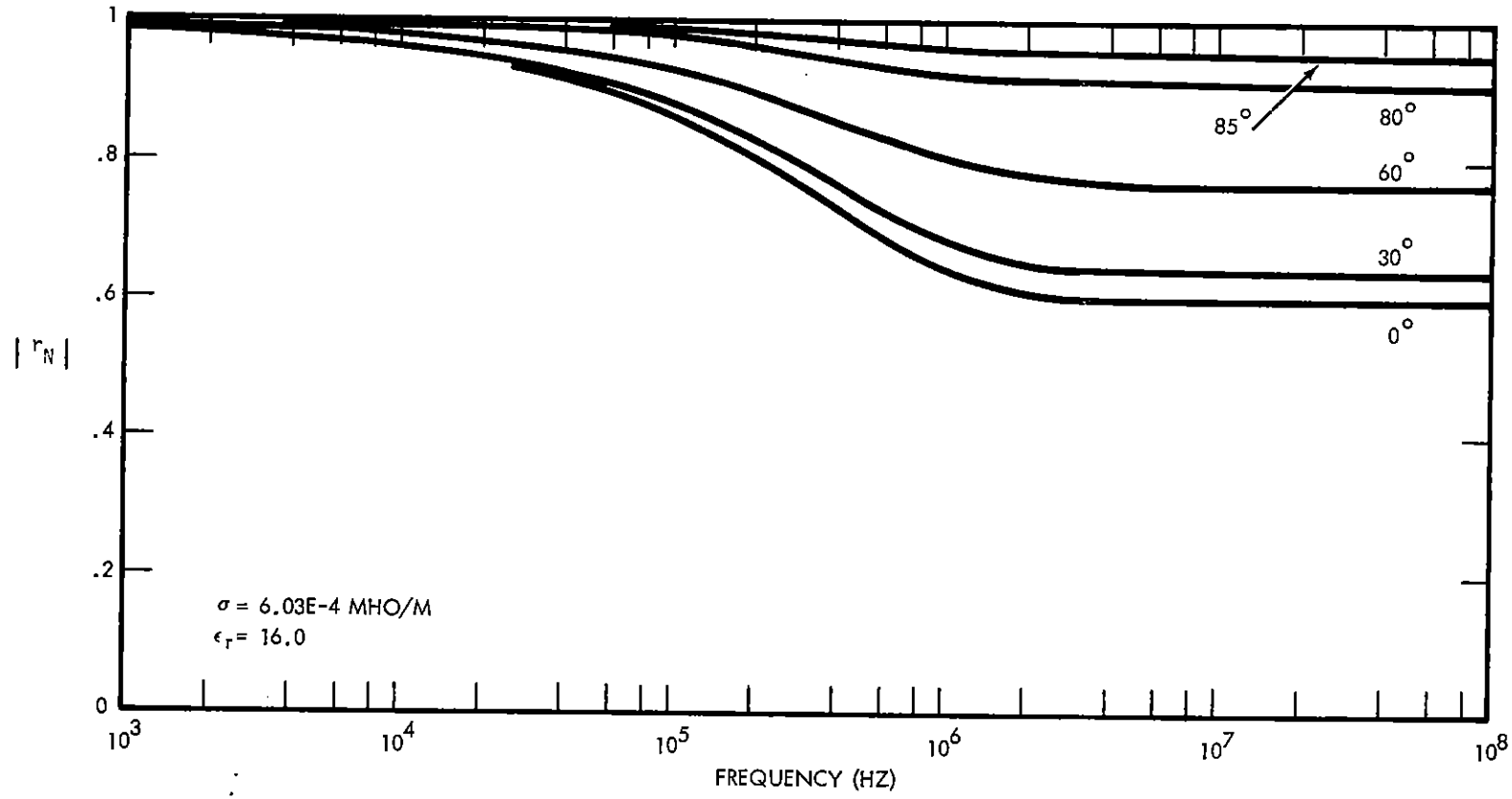

Figure 17. Amplitude of reflection coefficient for electric field component normal to plane of incidence (constant electrical parameters). Curves are for various incident angles.

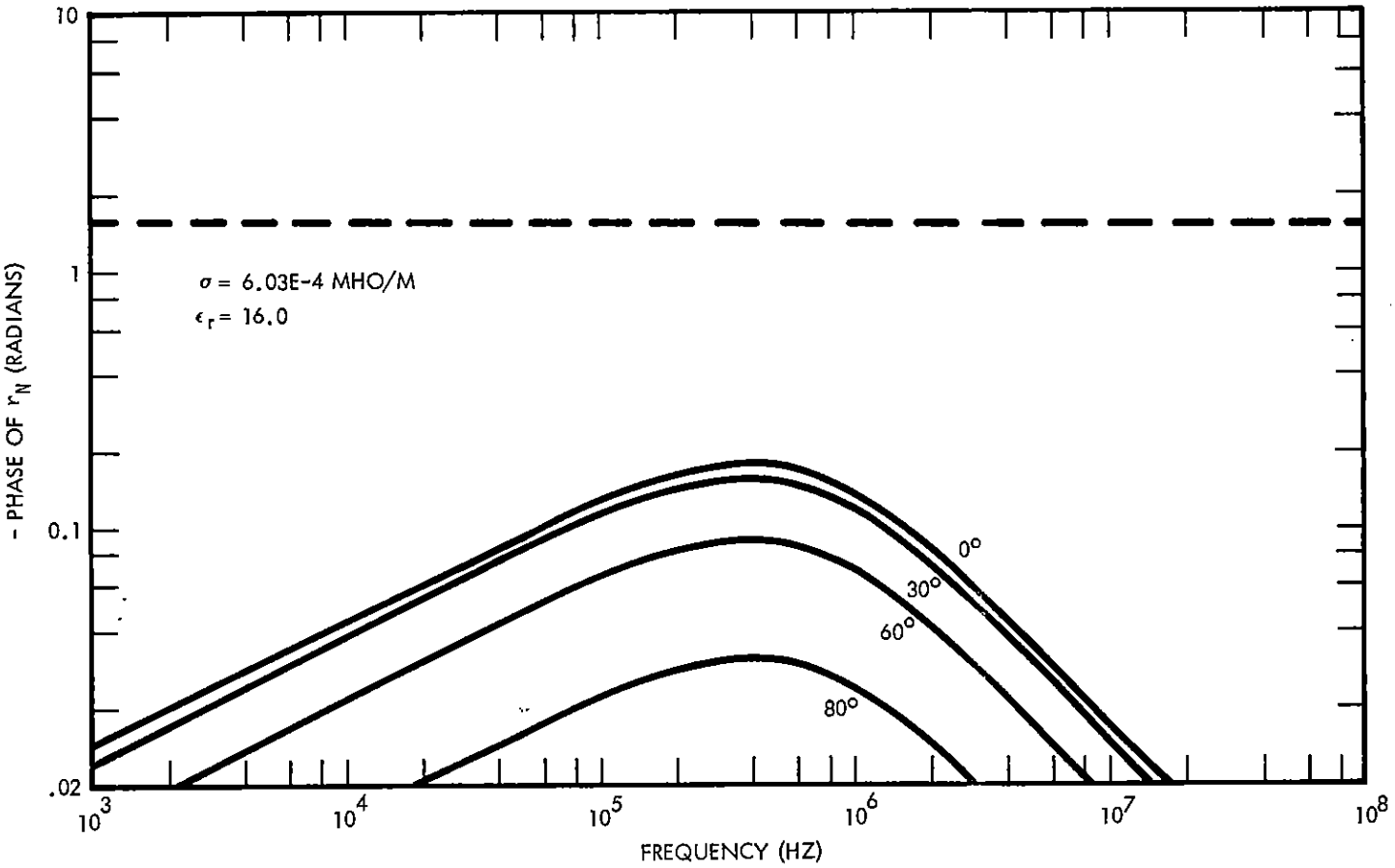

Figure 18. Phase of reflection coefficient for electric field component normal to plane of incidence (constant electrical parameters).

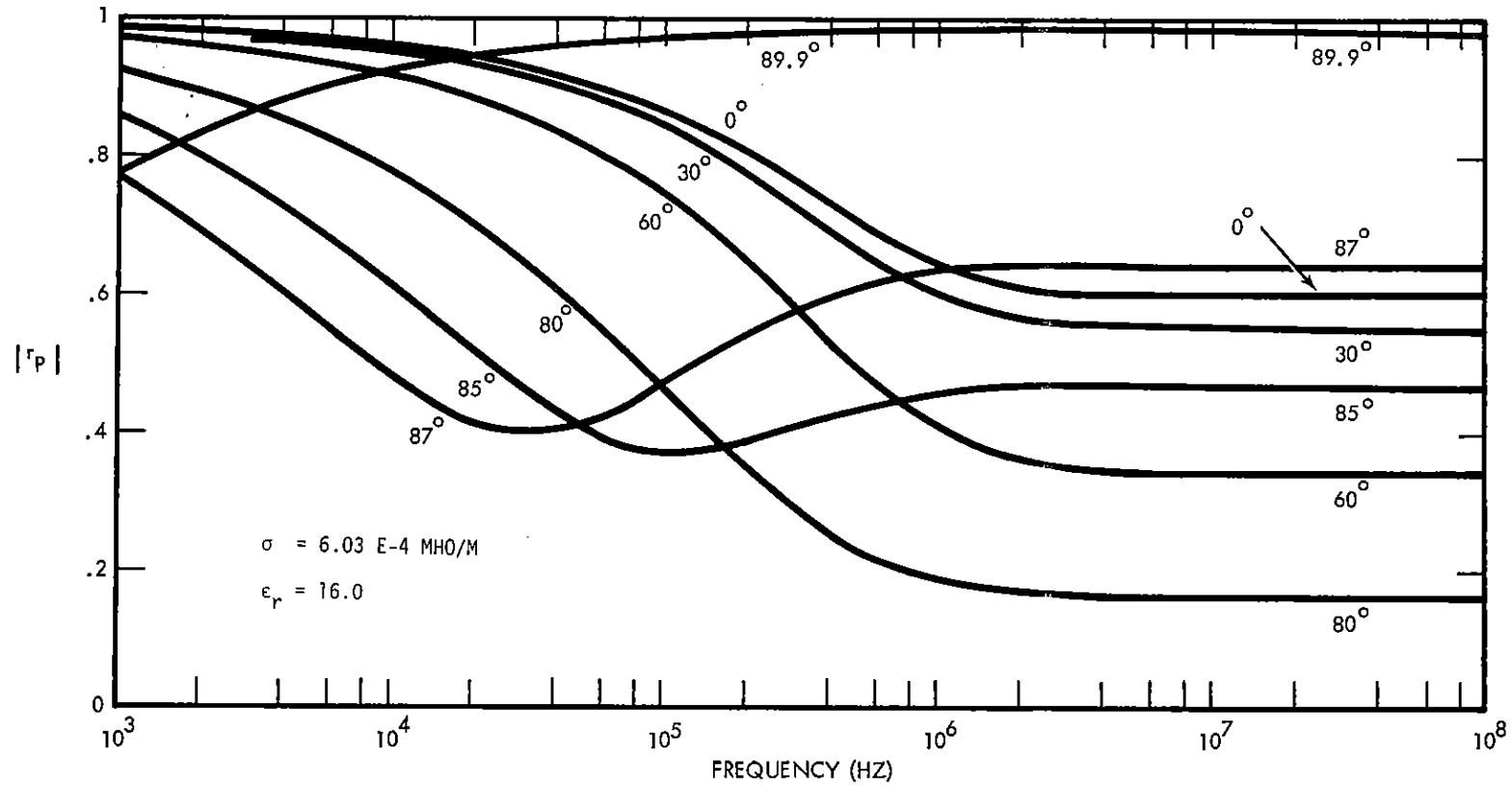

Figure 19. Amplitude of reflection coefficient for electric field component parallel to plane of incidence (constant electrical parameters). Curves are for various incident angles.

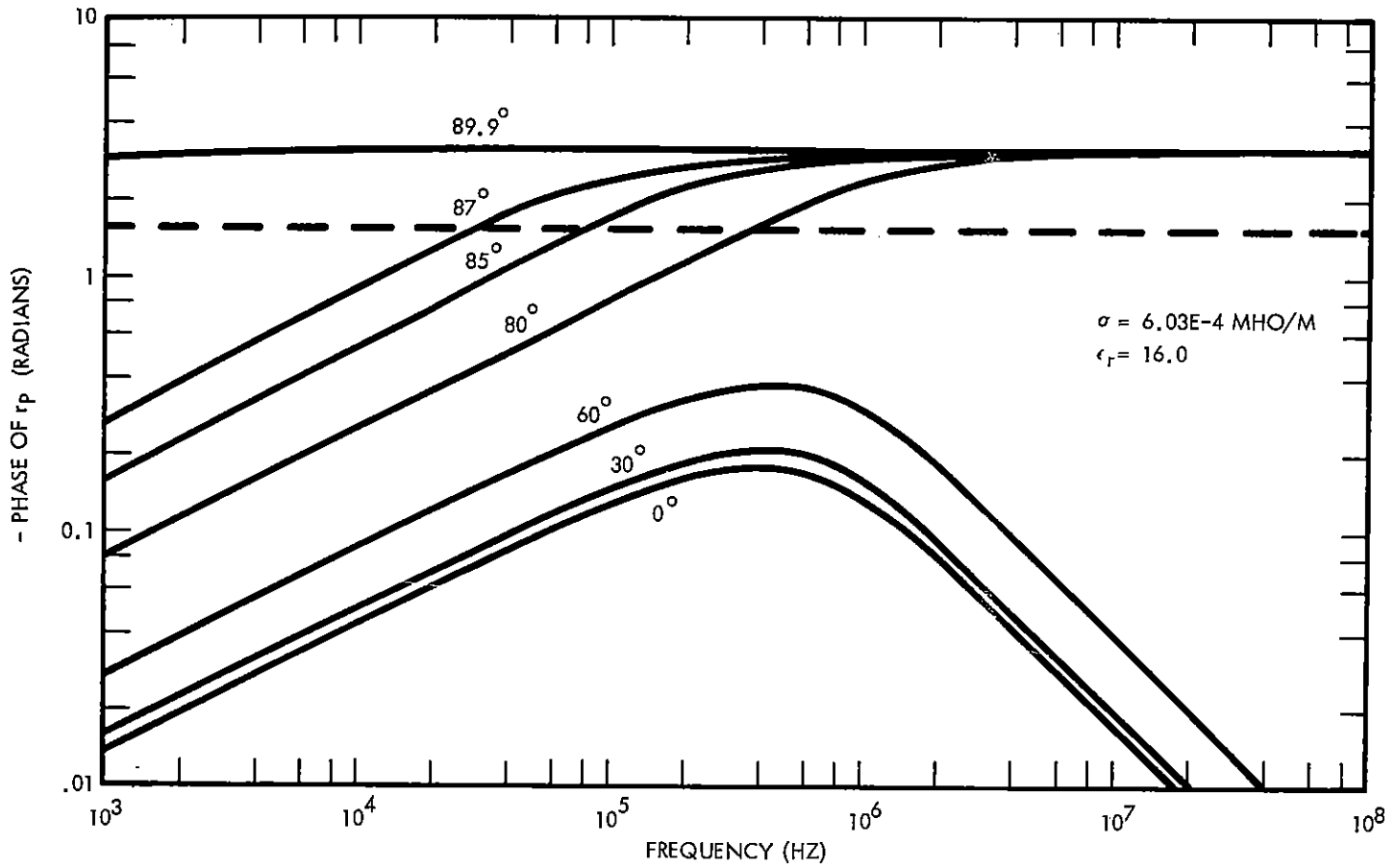

Figure 20. Phase of reflection coefficient for electric field component parallel to plane of incidence (constant electrical parameters). Curves are for various incident angles.

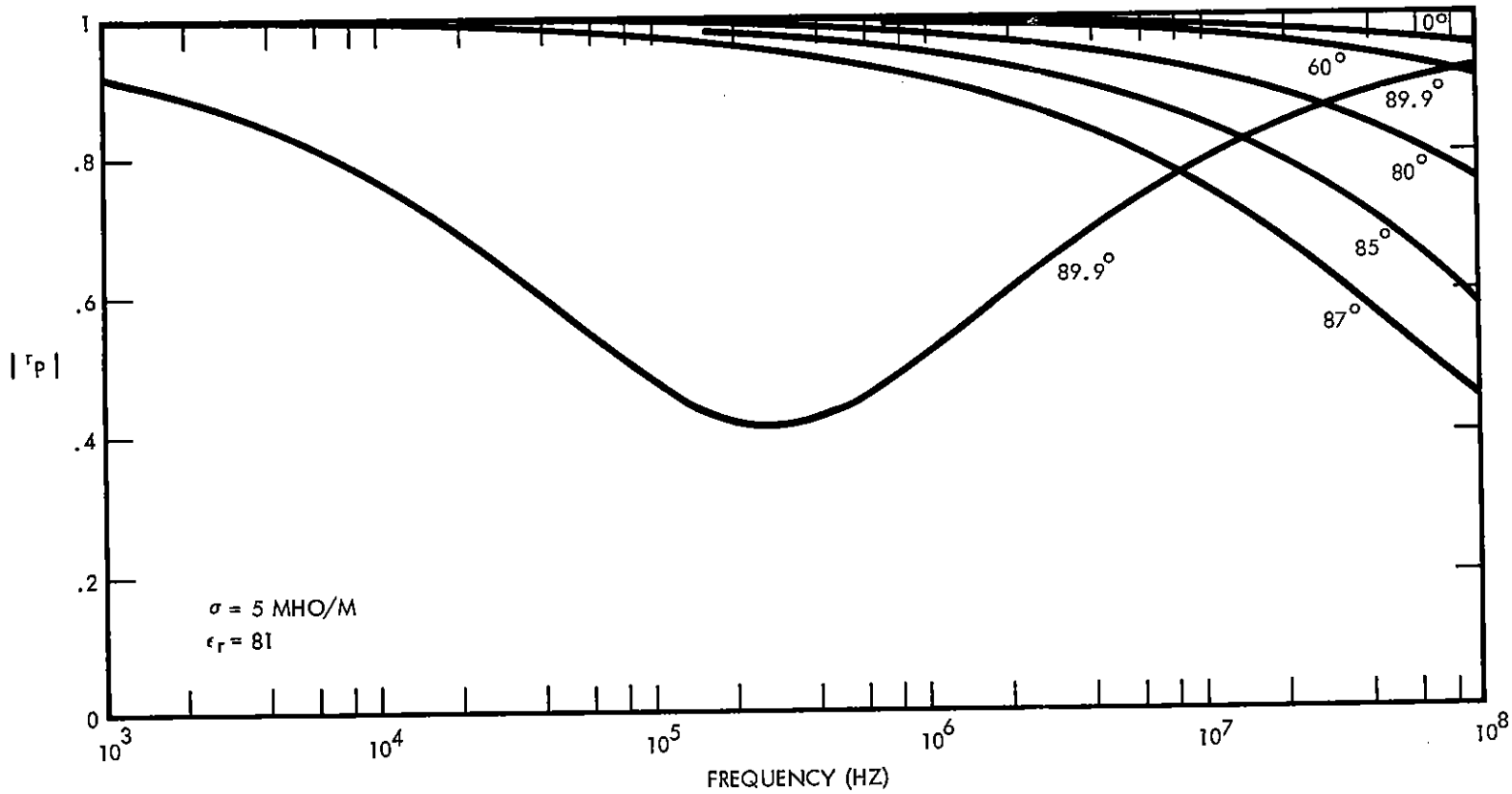

Figure 21. Amplitude of reflection coefficient for electric field component parallel to plane of incidence (constant parameter representation of sea water). Curves are for various incident angles.

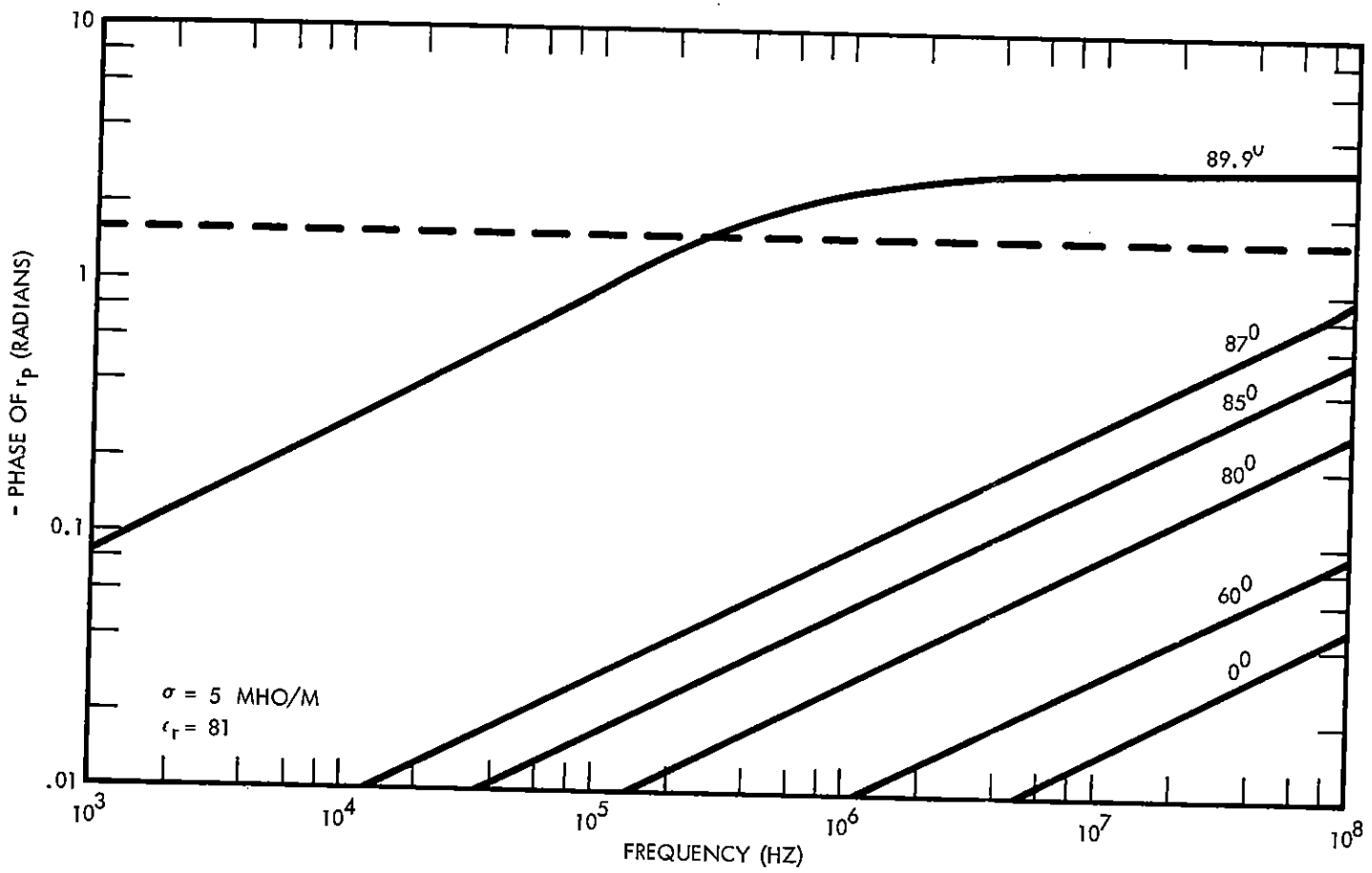

Figure 22. Phase of reflection coefficient for electric field component parallel to plane of incidence (constant parameter representation of sea water). Curves are for various angles of incidence.

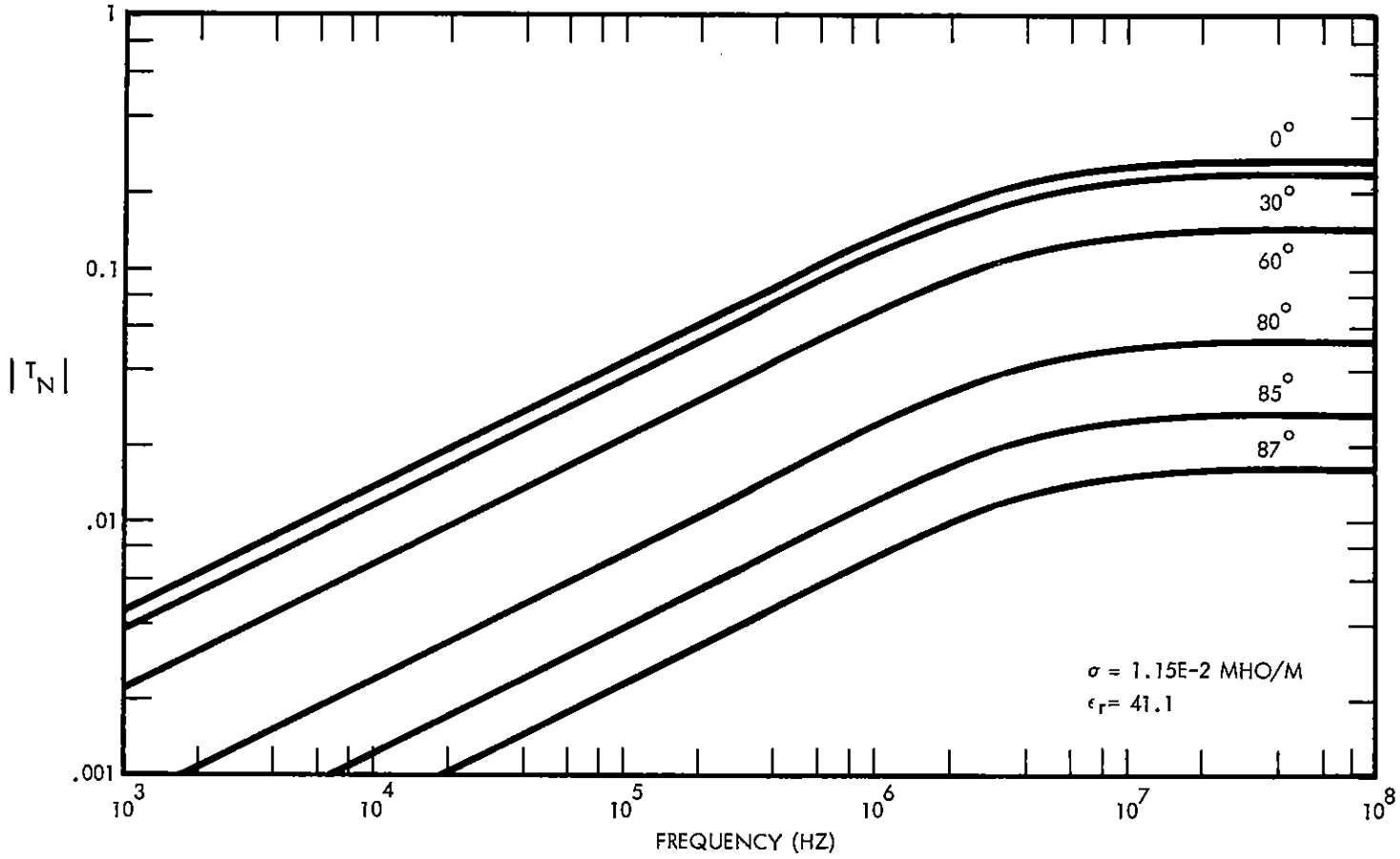

Figure 23. Transfer function amplitude for total electric field when field is normal to plane of incidence. Curves are for various angles of incidence.

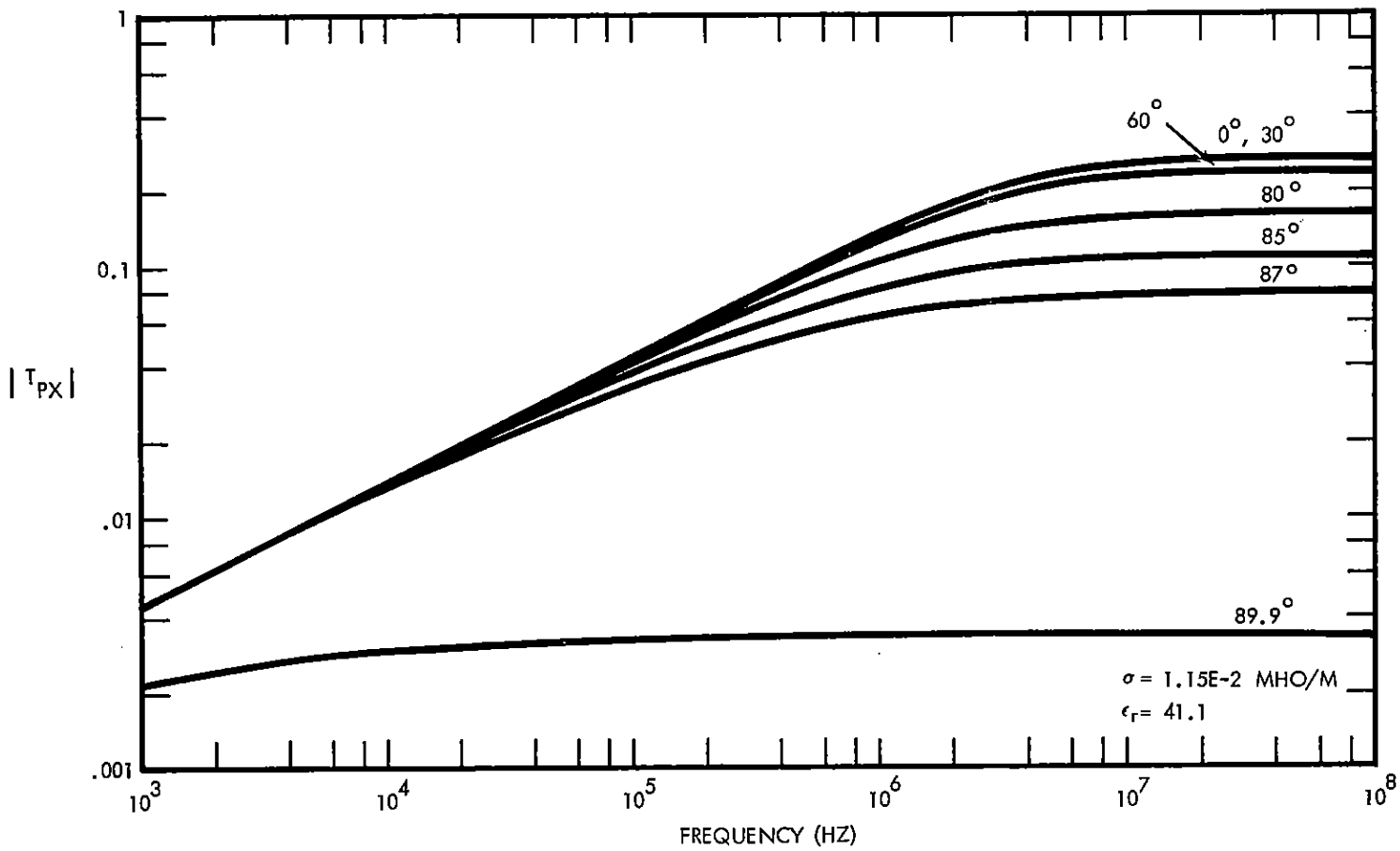

Figure 24. Transfer function amplitude for horizontal component of total electric field when field is parallel to plane of incidence. Curves are for various angles of incidence (constant electrical parameters).

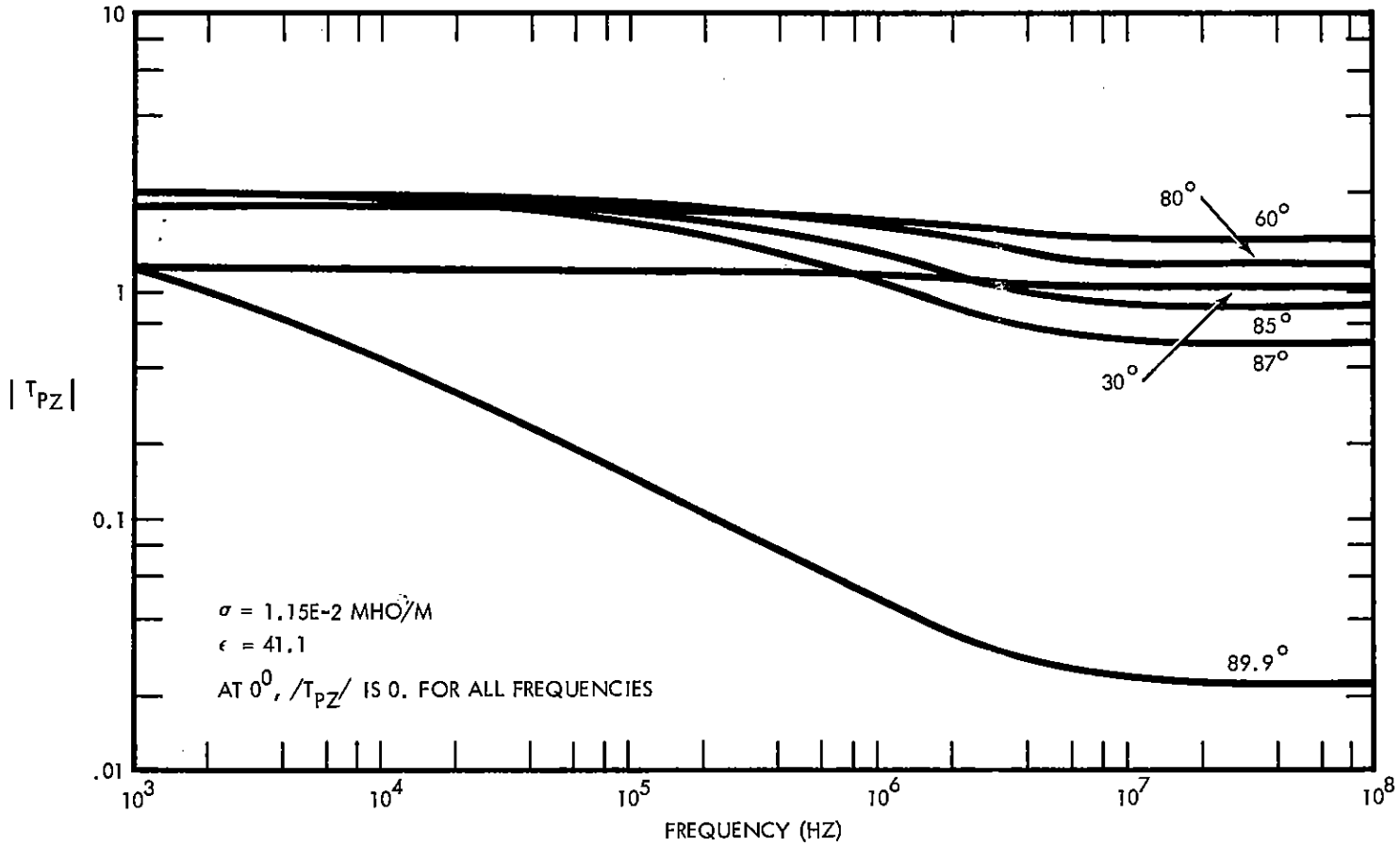

Figure 25. Transfer function amplitude for vertical component of total electric field when field is parallel to plane of incidence. Curves are for various angles of incidence (constant electrical parameters).

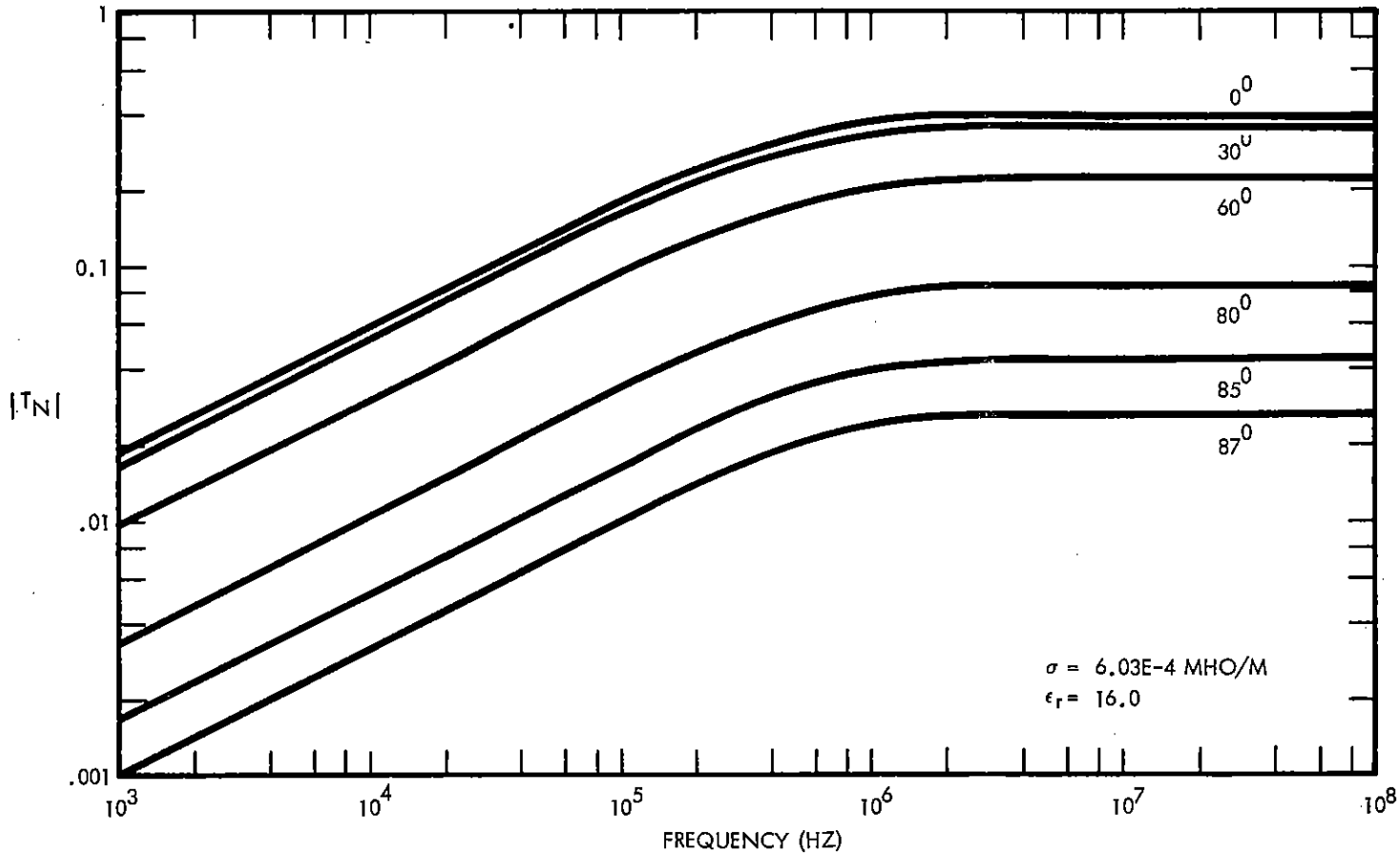

Figure 26. Transfer function amplitude for total electric field when field is normal to plane of incidence. Curves are for various angles of incidence (constant electrical parameters).

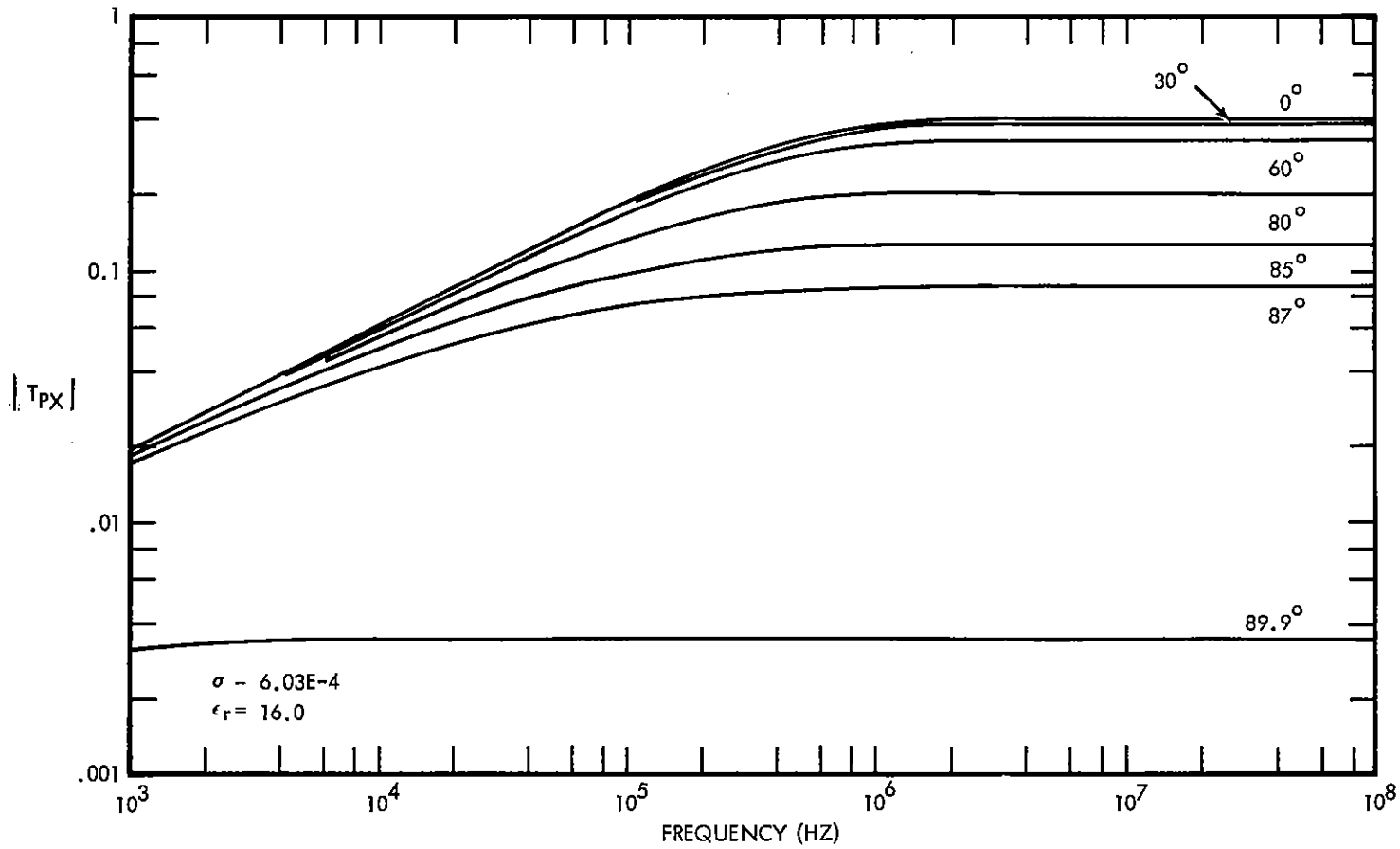

Figure 27. Transfer function amplitude for horizontal component of total electric field when field is parallel to plane of incidence. Curves are for various angles of incidence (constant electrical parameters).

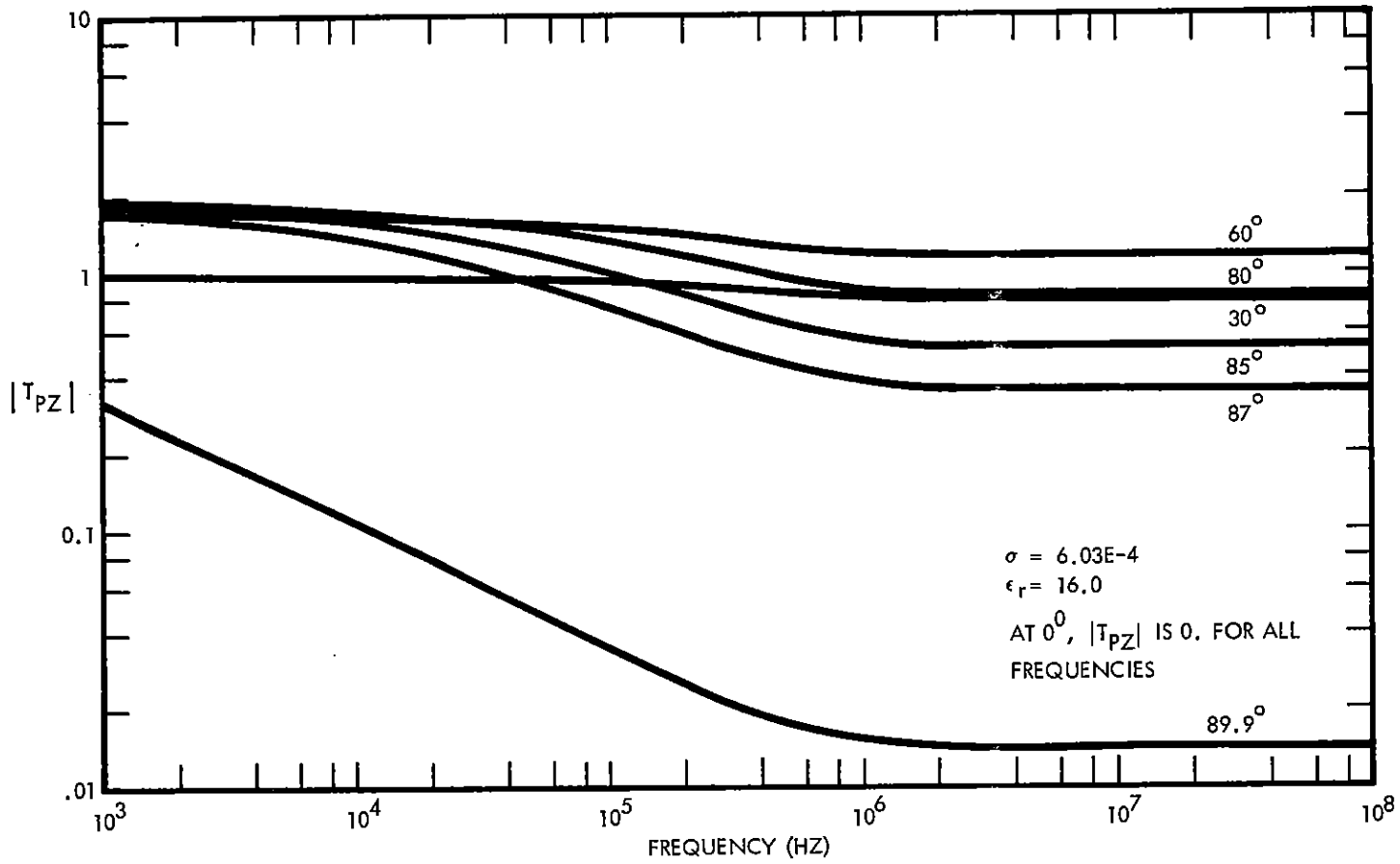

Figure 28. Transfer function amplitude for vertical component of total electric field when field is parallel to plane of incidence. Curves are for various angles of incidence (constant electrical parameters).

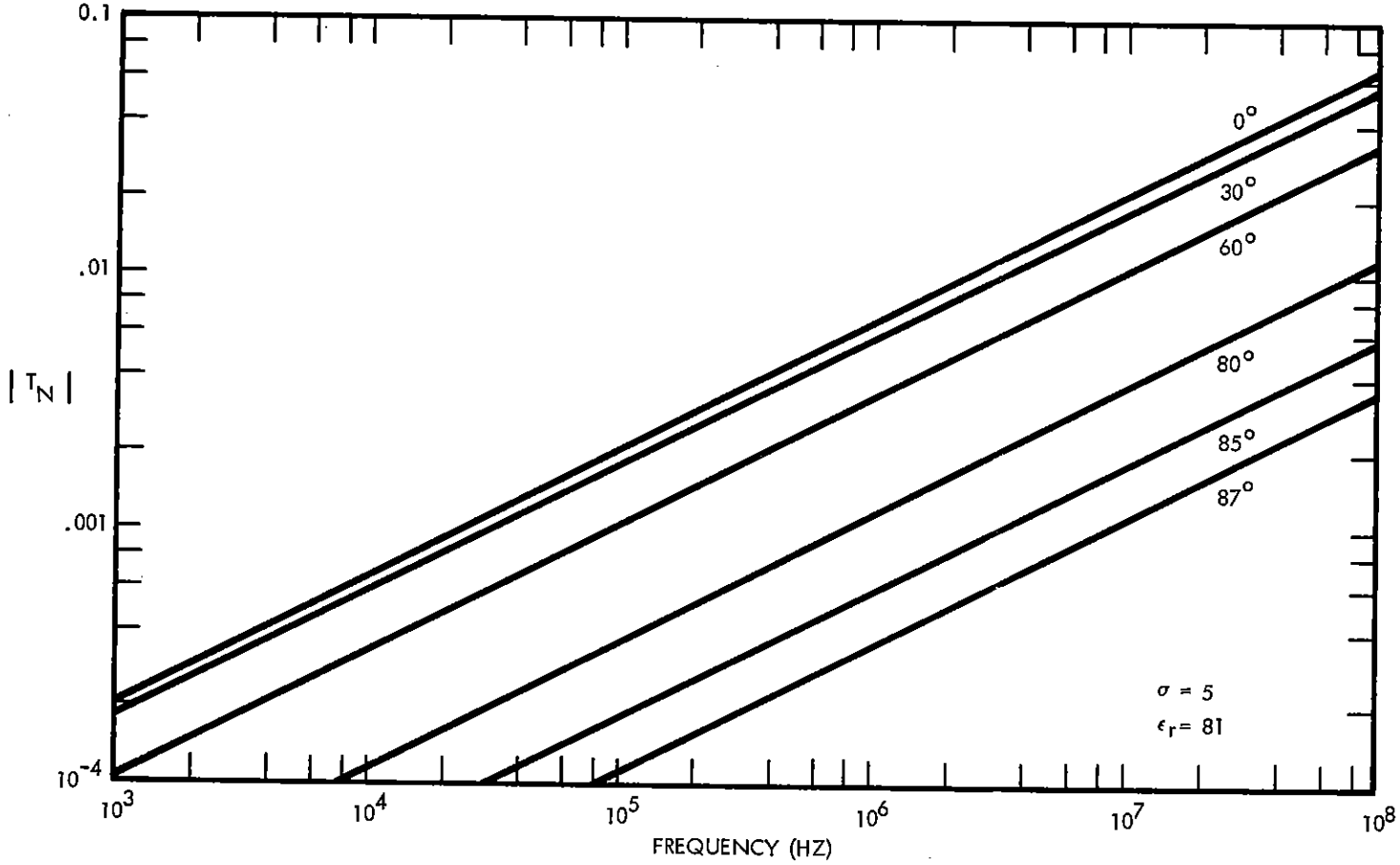

Figure 29. Transfer function amplitude for total electric field when field is normal to plane of incidence. Curves are for various angles of incidence (constant electrical parameters).

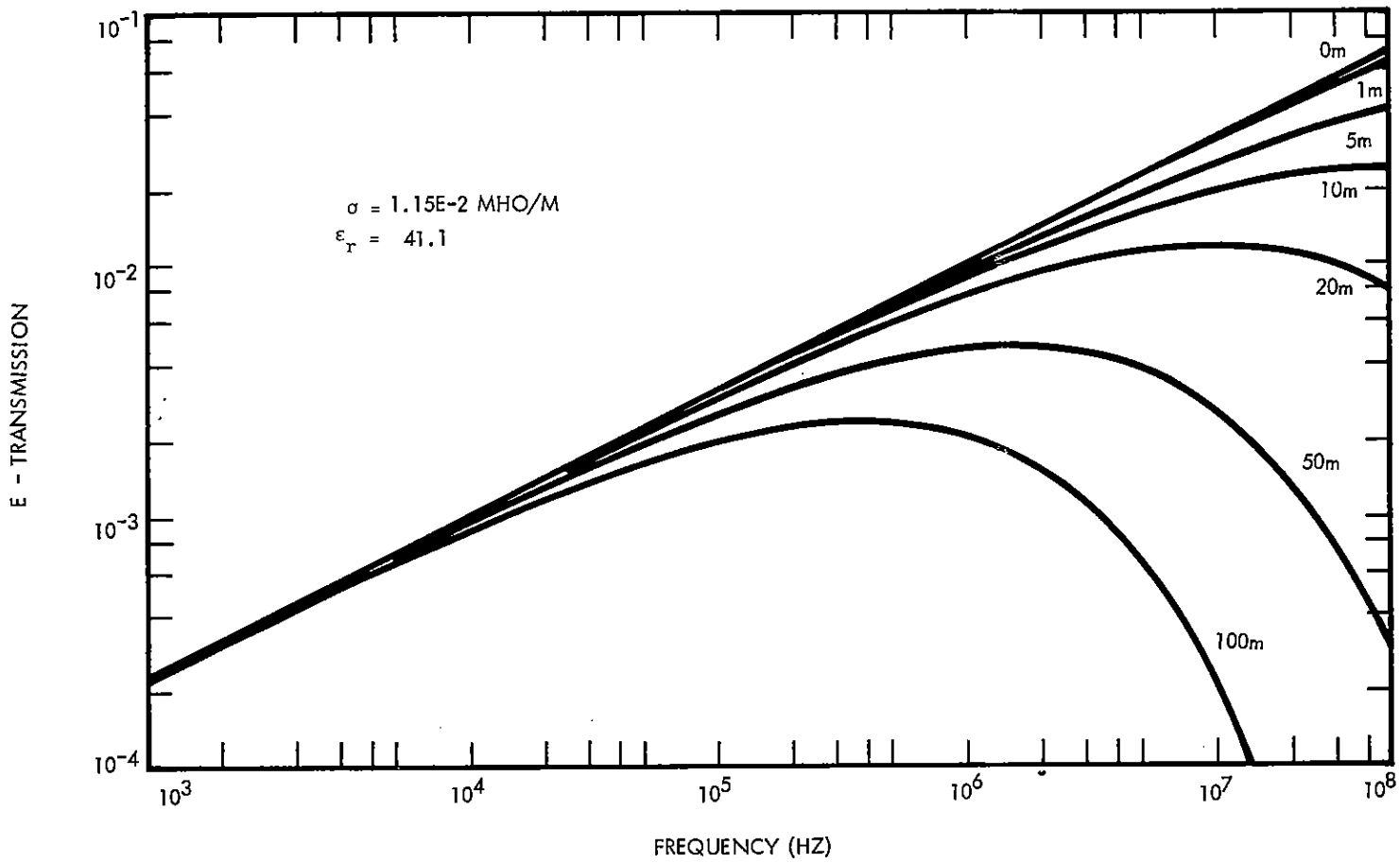

Figure 30. Electric field transfer function for various observer depths (vertical incidence).

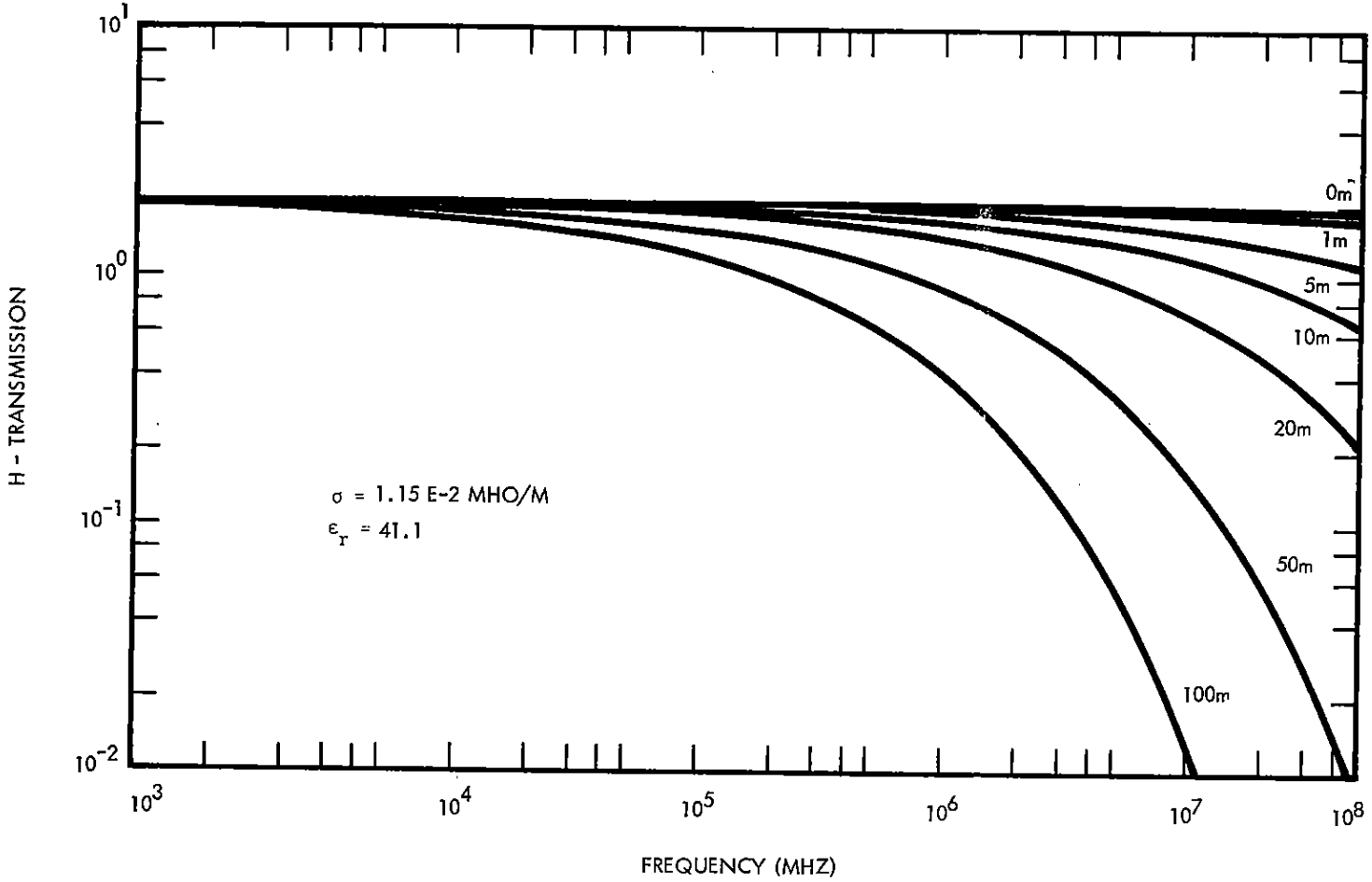

Figure 31. Magnetic field transfer function for various observer depths (vertical incidence).

are severely attenuated and the pulse diffuses downward with an exponential tail, sometimes called the "residue" (see Section 3).

4.2 Time Domain Calculations

In this section time domain calculations are presented which (1) show the effect of reflections for observers near the ground, (2) compare the results from several calculational methods, and (3) indicate the importance of representing the ground with frequency dependent electrical parameters. The geometry chosen was that of a 100 km burst in a geomagnetic field of about 70° dip angle. Observers at altitudes of 0m, 3m, and 10m were placed 100 tan 60° = 173 km to the magnetic west so that the component of the electric field parallel to the plane of incidence is taken to be 34% of the total magnitude (the normal component is 94%). An analytic function was used to represent the incident waveform:

$$E_i(t) = E_0 \left(e^{-\beta t} - e^{-\alpha t} \right)$$

where

$$\beta = 4.0 \times 10^6 \text{ sec.}$$
$$\alpha = 4.76 \times 10^8 \text{ sec.}$$
$$E_0 = 1.033$$

The function is normalized to a peak value of unity. Since the observers are so far away from the burst and close to each other, the change in geometric attenuation was ignored. The normalization to unity seems more useful than displaying actual field strengths since the quantitative changes become more obvious.

Four methods are used to calculate the reflected signal. The first method was the full Fourier transform method using a code

developed by John N. Wood and modified by Stephen J. Dalich* for the Air Force Weapons Laboratory and given to the author for purposes of this comparison. The code, Program RR, did not include reflection of the component of electric field normal to the plane of incidence (being developed primarily for air burst calculations) and assumed plane earth geometry. The code was again modified by the author and Robert M. Marks† to include all electric field components and a spherical earth approximation. The results of these calculations might be considered base-line calculations when comparing techniques. The second method used was the dielectric approximation and the third method was the perfect conductor approximation (see Section 2.5). The fourth method was a combination "large n" approximation and convolution approximation as discussed in Section II.

In the convolution approximation, the reflected field is equal to the incident field times the step function response of the ground (calculated with the "large n" approximation). At early times, the step function response looks like the dielectric approximation, while at late times, it approaches the perfect conductor approximation (which becomes valid at very late times). Therefore, even though the convolution approximation might not always be accurate, it has to be better than the other two approximations which are currently being used by some workers in the community. The additional time required to use this approximation will hardly make any difference in computer cost and the results are far superior.

All of the calculations assumed a plane earth geometry and an incidence angle of 60°, except the Fourier transform code which had spherical geometry build into it. At the observer, the angle of

* Science Applications, Inc., Albuquerque, New Mexico.

† Mission Research Corporation, Santa Barbara, California

the direct ray was also assumed to be 60° since the observers were close to the ground. The spherical geometry gives an actual incidence angle of 61.57°. Plane geometry gives delay times of 1.001 sh and 3.336 sh for the 3m and 10m observers, while spherical geometry calculations yield delays of 0.979 sh and 3.265 sh respectively. When used, the ground conductivity was assumed to be 1.15×10^{-2} mho/m and the dielectric coefficient was assumed to be 41.1. One comparison was made with frequency dependent parameters given by a modified Scott's curve-fit for 10 per cent water content. The modification is described in Section 4.1. The constant parameters correspond to the values of the curve-fits at 1 MHz.

Figure 32 shows the normal (to the plane of incidence) electric field component, calculated by Program RR for the three observers. The incident field is also plotted for comparison. The horizontal component of the parallel electric field is qualitatively similar but much smaller. Figure 33 shows the vertical components. Crosses (X) on the curves indicate negative values.

Figures 34 through 36 show comparisons of all three electric field components as calculated by the four techniques for a surface observer. The worst approximation is the perfect conductor approximation which predicts no horizontal field component. The dielectric approximation is good for a few shakes in predicting the horizontal components, but does not allow the reflected pulse to build up and become comparable to the incident pulse. At 12 sh, the dielectric approximation is too large by a factor of 5 for the normal component. The large n/convolution approximation, on the other hand, follows the general shape of the signal predicted by Program RR, but diverges slightly (by a factor of 1.7 at 12 sh for the normal component). The vertical component of the electric field is not too badly effected by any approximation, but the superiority of the large n/convolution approximation is obvious. Figure 37 compares the techniques for a 3m observer height and the normal component of the field.

In Figure 38, a comparison is shown between the horizontal field predicted under the assumption of constant ground parameters and that predicted with a modified Scott's curve-fit. The results are quite similar and, since the frequency dependence was fudged above 1 MHz anyway, it hardly seems worth the effort to use frequency dependent parameters for the high altitude burst signal at this time.

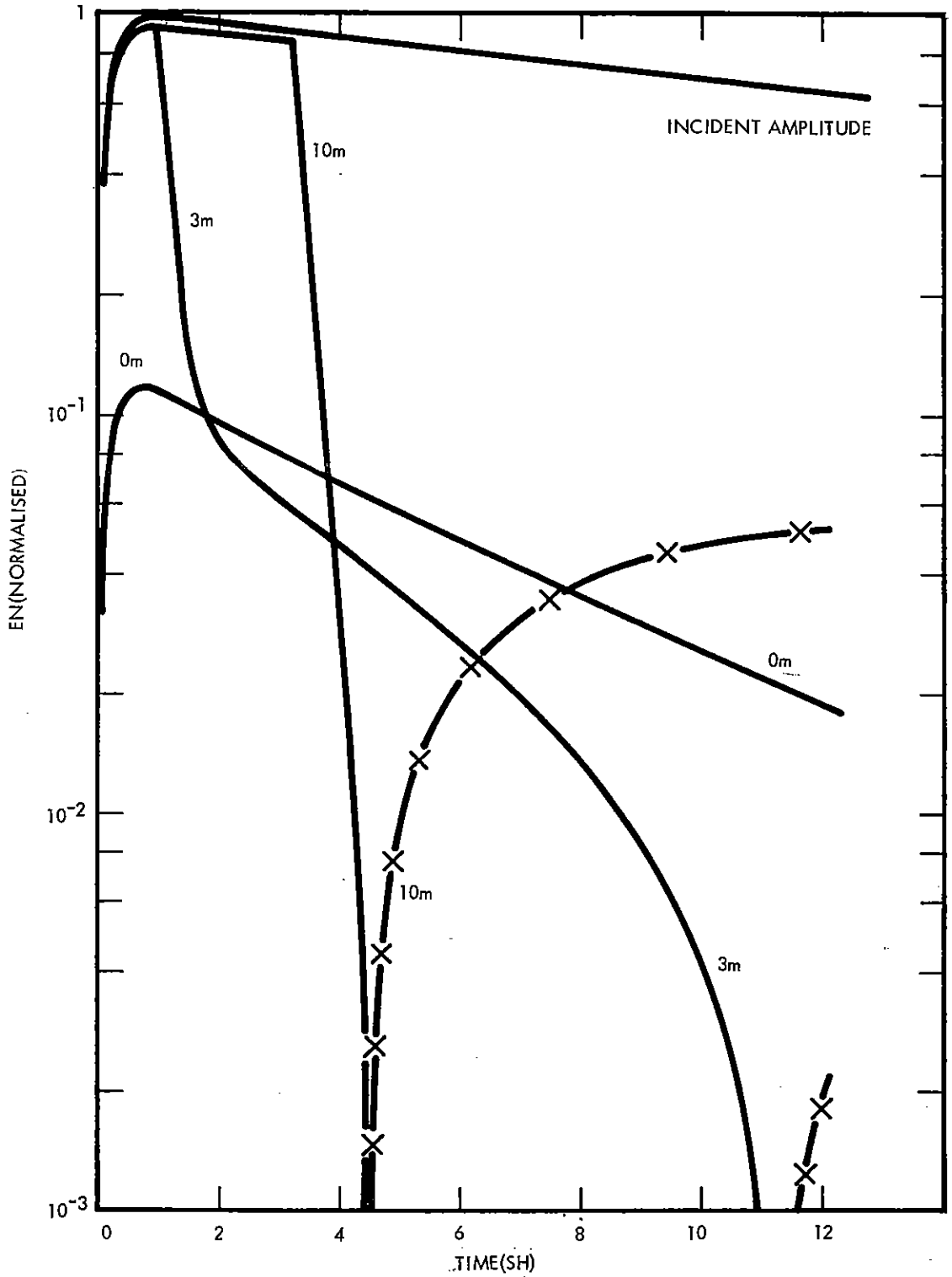

Figure 32. Horizontal component (normal to plane of incidence) of electric field to west of a high altitude burst with reflections predicted by program RR. Double exponential used as incident waveform. Observers at various altitudes, 173 km surface distance from 100 km burst.

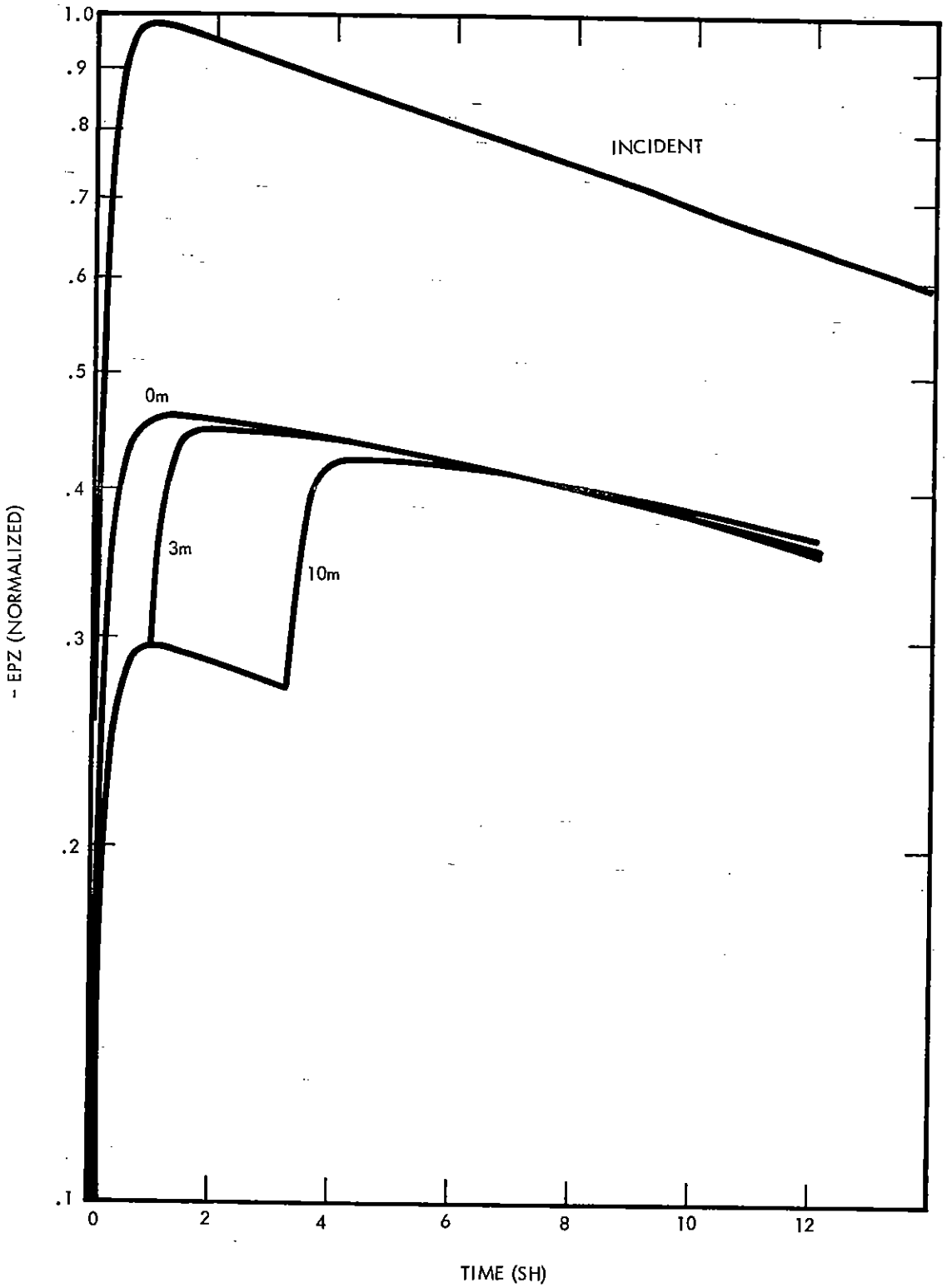

Figure 33. Vertical component of electric field to west of a high altitude burst with reflections predicted by program RR. Double exponential used as incident waveform. Observers at various altitudes, 173 km surface distance from 100 km burst.

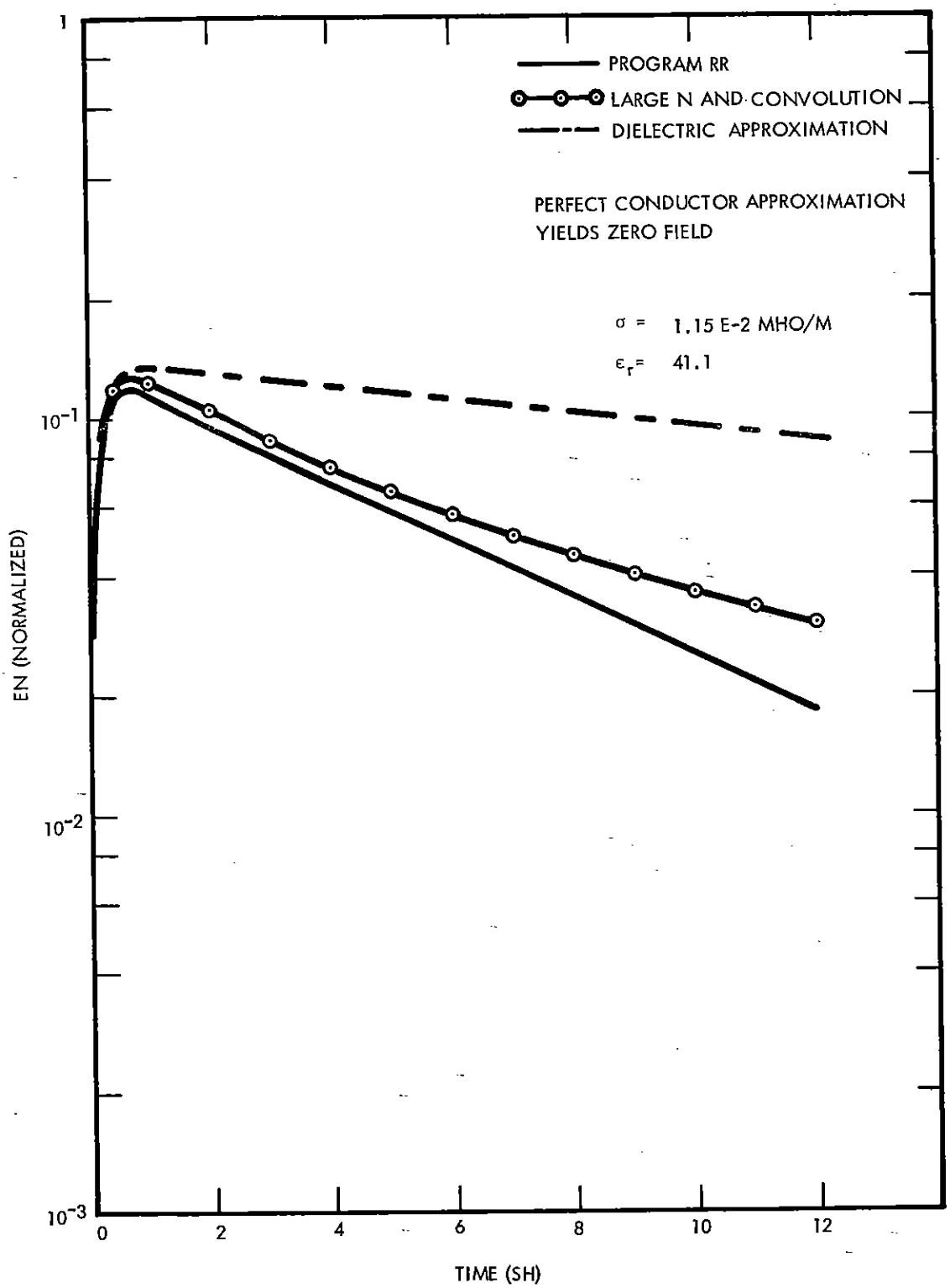

Figure 34. Comparison between horizontal components (normal to plane of incidence) predicted by various methods for a westward observer on the surface.

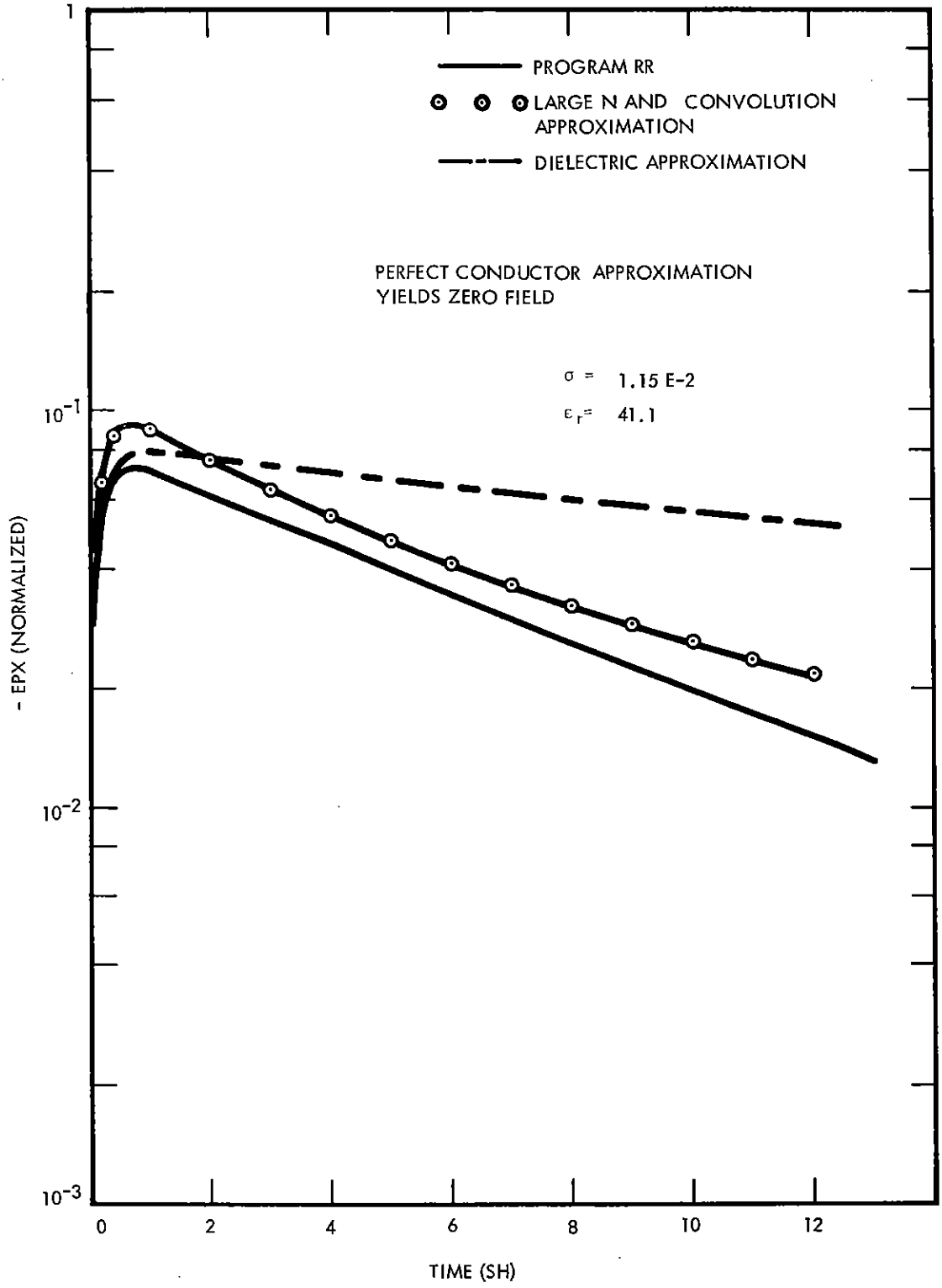

Figure 35. Comparison between horizontal components (parallel to plane of incidence) predicted by various methods for a westward observer on the surface.

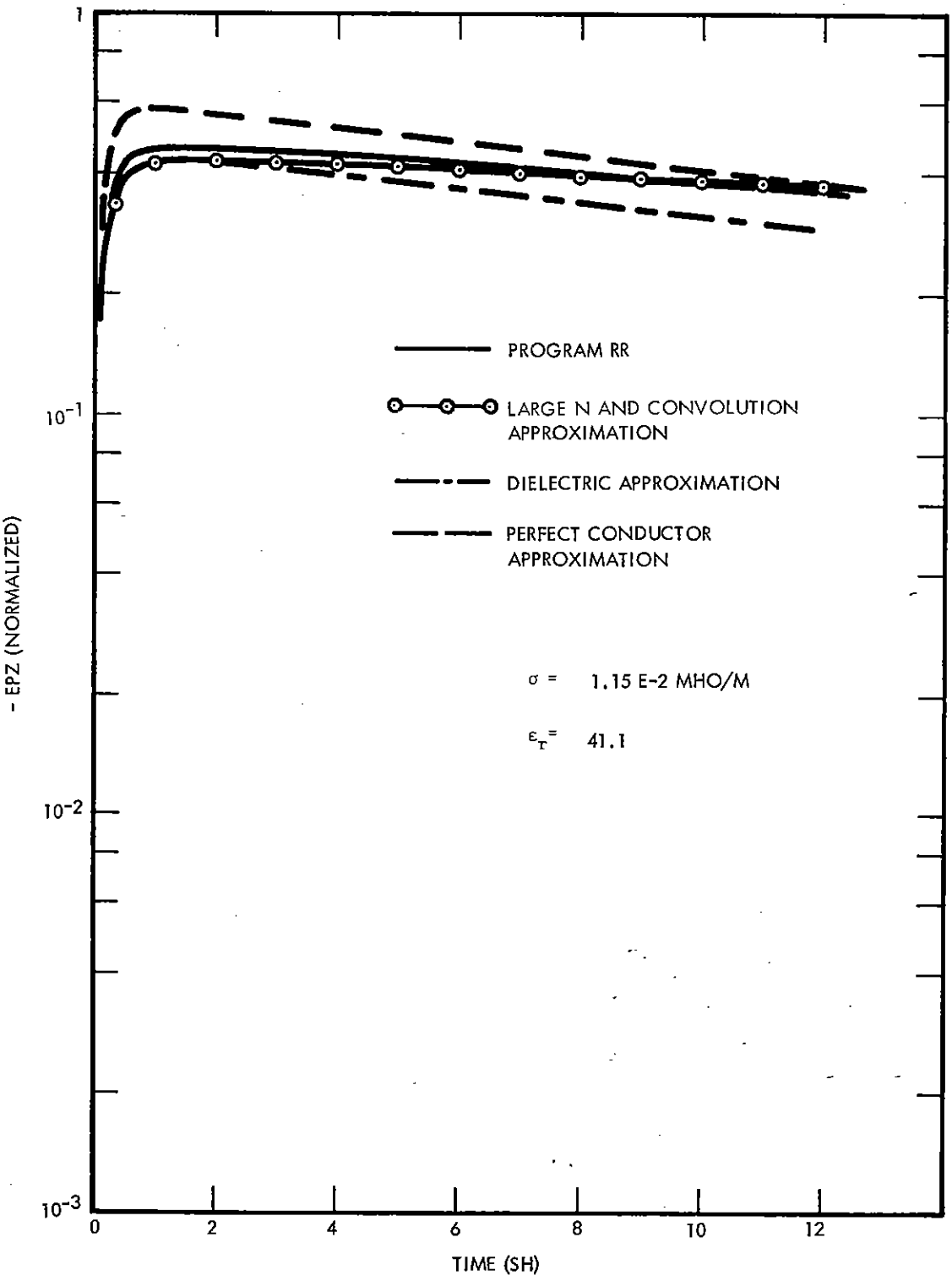

Figure 36. Comparison between vertical components predicted by various methods for a westward observer on the surface.

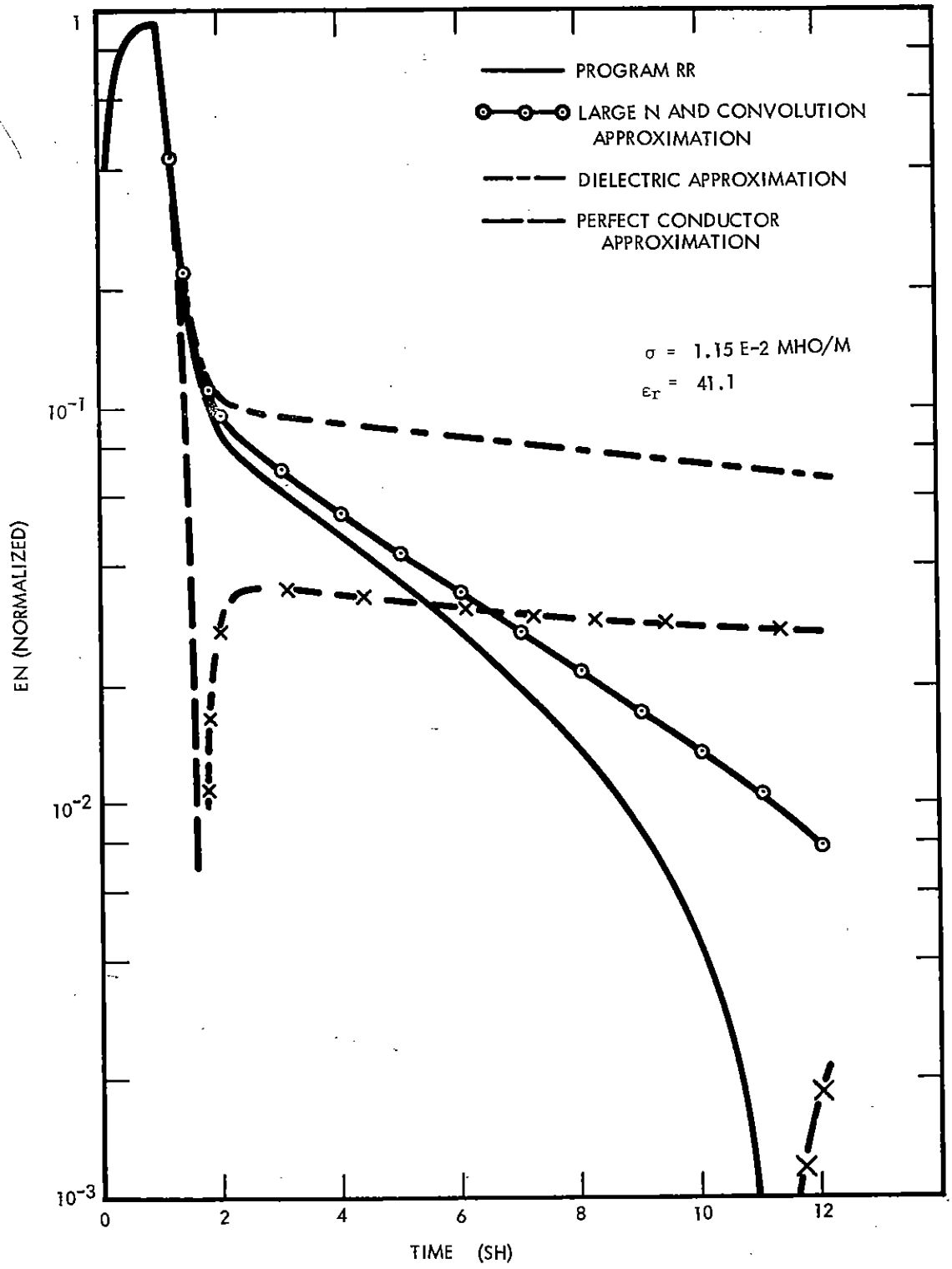

Figure 37. Comparison between horizontal components (normal to plane of incidence) predicted by various methods for a westward observer 3m above the surface.

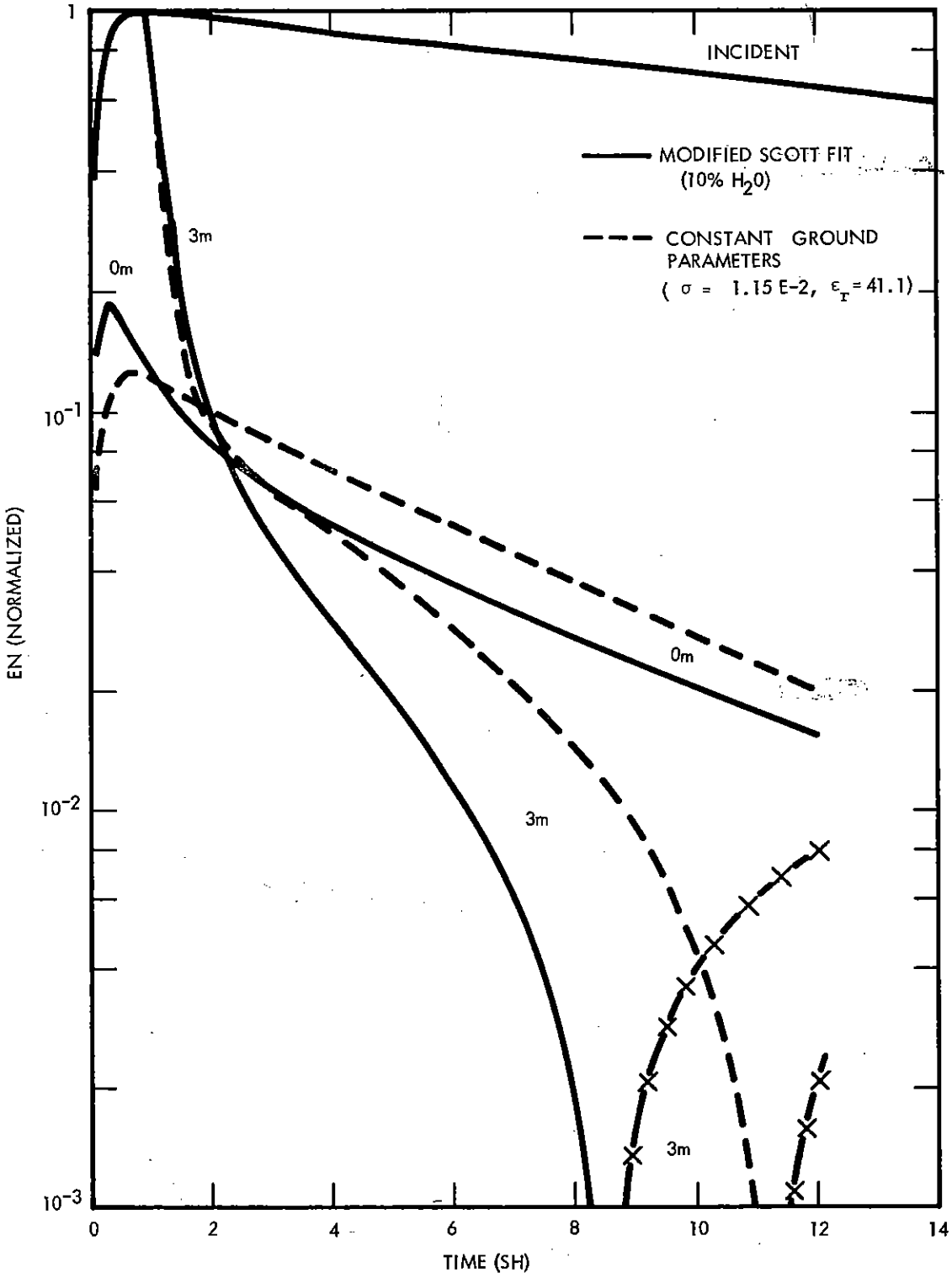

Figure 38. Comparison between horizontal electric field predicted by program RR using constant electrical parameters and that predicted using a modified version of Scott's curve-fit. Observers at 0m and 3m altitude, 173 km south of 100 km burst. Double exponential used as incident waveform.

REFERENCES

1. Jacobson, J.J., "1965 Conductivity Survey in Wisconsin (U)", DECO Report 30-P-13, DECO Electronics, Incorporated, 1966 (U).

2. Scott, J.H., "Electrical and Magnetic Properties of Rock and Soil (U)", United States Geological Survey, Technical Letter, Special Project 16, May 1966. Also appears as EMP Theoretical Note 18, Air Force Weapons Laboratory.

3. Judy, M.M., and W.R. Eberle, "A Laboratory Method for the Measurement of the Dielectric Constant of Rock and Soil Samples in the Frequency Range 10^2 - 10^8 Hertz (U)", EMP Sensor and Simulation Note 88, Air Force Weapons Laboratory, June 1969 (U).

4. Carrol, R.D., and W.R. Eberle, "Earth Impedance Measurements at Malstrom Minuteman Site I-6, Montana (U)", Special Project performed for the Air Force Weapons Laboratory by the United States Geological Survey under contract DO-F29601-68-F-0007.

5. Longmire, C.L., and H.J. Longley, "Time Domain Treatment of Media with Frequency-Dependent Electric Parameters (U)", MRC-N-1, Mission Research Corporation, March 1971.

6. Baum, C.E., "The Reflection of Pulsed Waves from the Surface of a Conducting Dielectric (U)", EMP Theoretical Note 25, Air Force Weapons Laboratory, February 1967 (U).

7. Henley, J., "Program Reflect (U)", DC-TN-2099-28, The Dikewood Corporation, June 1970 (U).

8. Goldman, S., Laplace Transform Theory and Electrical Transients, Dover Publications, Inc., New York, 1966.

References (continued)

9. Malik, J. S., "EM Pulse Fields in Dissipative Media (U)," EMP Theoretical Note 8, Air Force Weapons Laboratory, April 1965.

10. Stratton, J. A., Electromagnetic Theory, McGraw-Hill Book Company, New York, 1941.

11. Longley, H. J. and C. L. Longmire, Private Communication.

12. Kilb, R. W., and C. L. Longmire, Private Communication.

APPENDIX A

HIGH ALTITUDE BURST SIGNAL POLARIZATION

The high frequency radiated electric field will be polarized in the direction parallel to that in which a radially moving electron would be initially deflected by the geomagnetic field near the base of the gamma deposition region. Define the polarization vector

$$\vec{p} \equiv - \frac{1}{|B|} \hat{r} \times \vec{B} \qquad (A.1)$$

where $\vec{B}$ is the geomagnetic field vector and $\hat{r}$ is a unit radial vector. The polarization vector is oriented in the direction of the radiated electric field (early time) and has a magnitude equal to or less than unity, the value unity occurring in the directions where $\hat{r} \cdot \vec{B} = 0$. If the base of the deposition region was a flat surface over a flat earth (so that the geometric or R_o/R attenuation was constant as a function of position) and if the currents were constant over this surface area (assuming high enough conductivity to attenuate any fields generated within the deposition region), then the magnitude of $\vec{p}$ could be used to scale the early time fields as a function of position. These conditions are approximately met by a large, high altitude burst when the observer is not too close to the earth's tangent.

When calculating $\vec{p}$, the value of $\vec{B}$ must be chosen in the region where most of the radiated signal is generated. If the region is so large that there is a significant variation of $\vec{B}$ within it, the results of the polarization calculation will be inconclusive. This problem would be important in regions of low conductivity, e.g., near a tangent ray or in the upward direction.

For the purpose of making a useful approximation, we assume a two dimensional $\vec{B}$ such that it has a vertical (B_z) and one horizontal component (B_x). The coordinate system is shown in Figure A-1. Magnetic north is in the -x direction. In cartesian coordinates then,

$$\vec{p} = -\frac{1}{|B|}\left[\hat{i}(B_z \sin\theta \sin\phi) + \hat{j}(B_x \cos\theta - B_z \sin\theta \cos\phi) - \hat{k}(B_x \sin\theta \sin\phi)\right] \qquad (A.2)$$

With θ_B defined as the magnetic dip angle measured from the horizontal (downward and northward being positive), such as over the United States,

$$B_x = -|B| \cos\theta_B$$

$$B_z = -|B| \sin\theta_B$$

so that

$$\vec{p} = -\frac{1}{|B|}\left[\hat{i}(\sin\theta_B \sin\theta \sin\phi) + \hat{j}(\cos\theta_B \cos\theta - \sin\theta_B \sin\theta \cos\phi) - \hat{k}(\cos\theta_B \sin\theta \sin\phi)\right] \qquad (A.3)$$

One can see that $|p| = 1$ for $\theta = 180° - \theta_B$ and $\phi = 0$ corresponding to the line of sight normal to the magnetic field lines. When the polarization vector is resolved into its spherical polar components, the $\hat{r}$ component will be identically zero, the $\hat{\theta}$ component will be the component parallel to the plane of incidence, and the $\hat{\phi}$ component will be the component normal to the plane of incidence:

$$p_r = 0 \qquad (A.4)$$

$$p_\theta = \cos\theta_B \sin\phi \qquad (A.5)$$

$$p_\phi = -(\sin\theta_B \sin\theta - \cos\theta_B \cos\theta \cos\phi) \qquad (A.6)$$

It is clear upon inspection that p_θ (the component parallel to the plane of incidence) is identically zero along the magnetic north-south line passing through the burst, and it has maximum magnitude to the east and west. The magnitude of p_ϕ has a maximum, with respect to

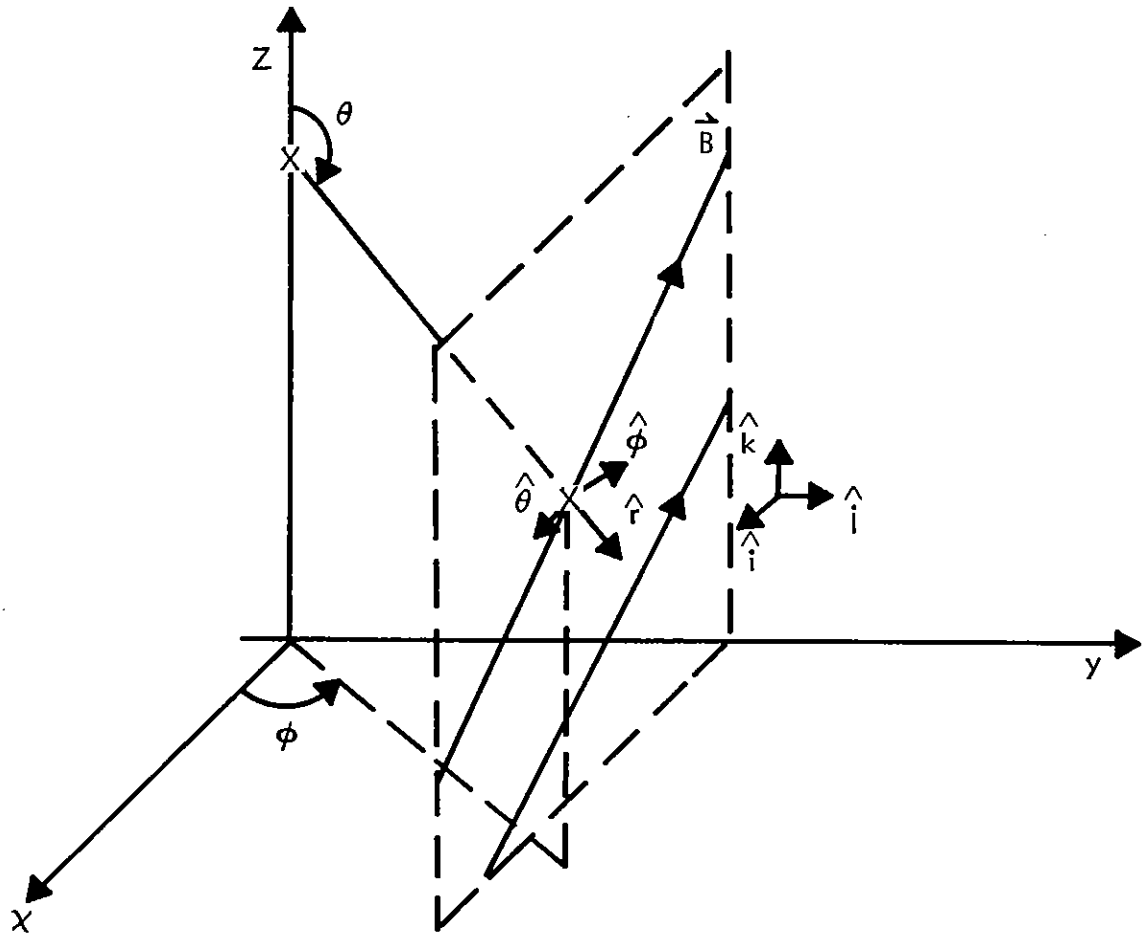

Figure A-1. Geometry for polarization calculation.

variations in ϕ, in the north-south direction. The absolute maximum occurs at $\theta = 180° - \theta_B$, $\phi = 0$ and $\theta = \theta_B$, $\phi = 180°$. One of these will be in the upward direction and of no interest in this problem. The magnitude of $\vec{p}$ is zero when $\hat{r}$ is parallel to $\vec{B}$, i.e., $\phi = 0$, $\theta = 90° + \theta_B$ and $\phi = 180°$, $\theta = 90° - \theta_B$.

The θ_B of interest is actually a function of position, but for many first order approximations, the value near the earth's surface directly below the burst can be used.

The maximum and minimum electric field magnitudes should correspond roughly to the maximum and minimum $|p|$. However, other factors influence the location of these fields and the polarization vector should not be relied upon too heavily for this information.

Since $|p|$ varies with position, the components p_θ and p_ϕ must be divided by $|p|$ at each position in order to determine the fraction of the total field with each polarization. One can define the relative polarization by

$$\vec{P} \equiv \frac{\vec{p}}{|p|} \tag{A.7}$$

where

$$\begin{aligned} |p|^2 &= p_\theta^2 + p_\phi^2 \\ &= \cos^2\theta_B(\sin^2\phi + \cos^2\theta \cos^2\phi) \\ &\quad + \sin^2\theta_B \sin^2\phi - \frac{1}{2} \sin 2\theta_B \sin 2\theta \cos\phi \end{aligned} \tag{A.8}$$

Each component of $\vec{P}$, i.e. P_θ and P_ϕ is the fraction of the total field magnitude oriented in that direction such that

$$1 = P_\theta^2 + P_\phi^2 \quad .$$

Before looking at the polarization predicted by an actual computer code, consider the case of a 100 km burst over the United States.

The magnetic dip angle is roughly 70°. The magnetic declination varies from about 15° W to 15° E, but we will use a coordinate system oriented along the magnetic north-south line through surface zero (below the burst), and stay close enough to that line to ignore significant variations. For a large enough burst, then, the maximum field strength will occur about 100 km • tan 70° or 275 km to the south ($\phi = 0$). The minimum will occur 100 km • tan 20° or 36 km to the north ($\phi = 180°$). The distance to the earth's tangent is about $110\sqrt{100}$ or 1100 km. The polarization will be in the $\hat{\phi}$ direction with the maximum P_θ being about ±0.34 in the magnetic east and west directions, i.e., at most, the component in the plane of incidence will be about 34 per cent of the total field. The sign of P_θ will be positive to the magnetic east (downward vertical component) and negative to the magnetic west (upward vertical component).

Figures A-2 and A-3 show the electric field polarization over the United States from a 100 km burst using equations A.5 through A.7. These contours use θ_B equal to 70°. Figure A-4 shows P_θ for a burst in which θ_B equals 30°, e.g., near Johnston Island in the Pacific. The last contours show a situation in which a large fraction of the electric field is oriented in the plane of incidence. In each case, only the contour lines in the magnetic east half-plane are shown. P_θ changes sign upon reflection across the north-south plane, while P_ϕ is symmetric upon reflection. The importance of Figure A-2 is mainly in showing that over the United States, most of the electric field is oriented normal to the plane of incidence and, hence, that the incident and reflected pulses tend to cancel. Thus, one can expect lower high altitude burst fields, after the reflected signal lag time, than one might expect from the incident field calculation alone.

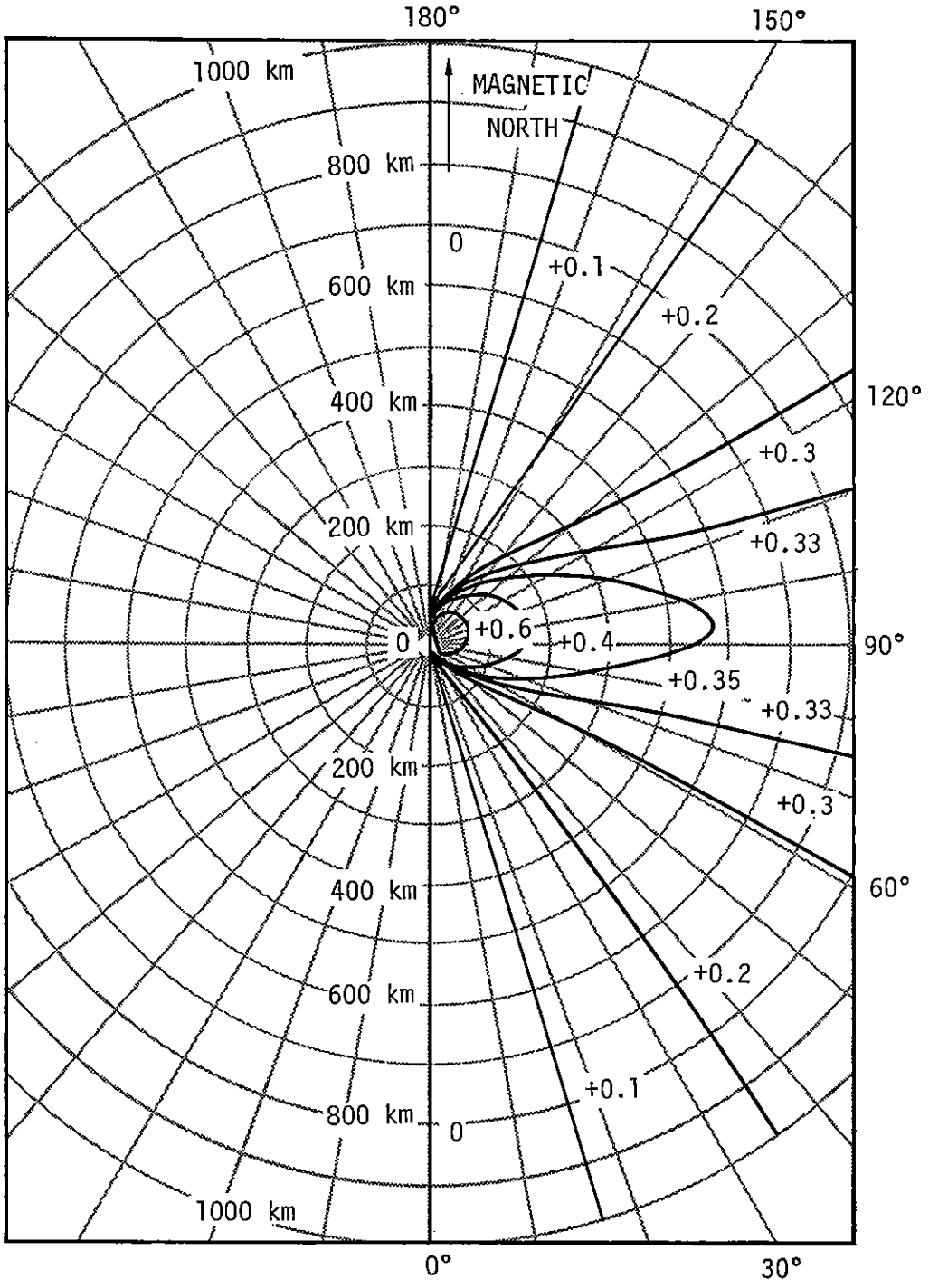

Figure A-2. Contours of P_θ for a 100 km burst and magnetic dip angle of 70°. Contours in magnetic west half-plane have opposite polarity.

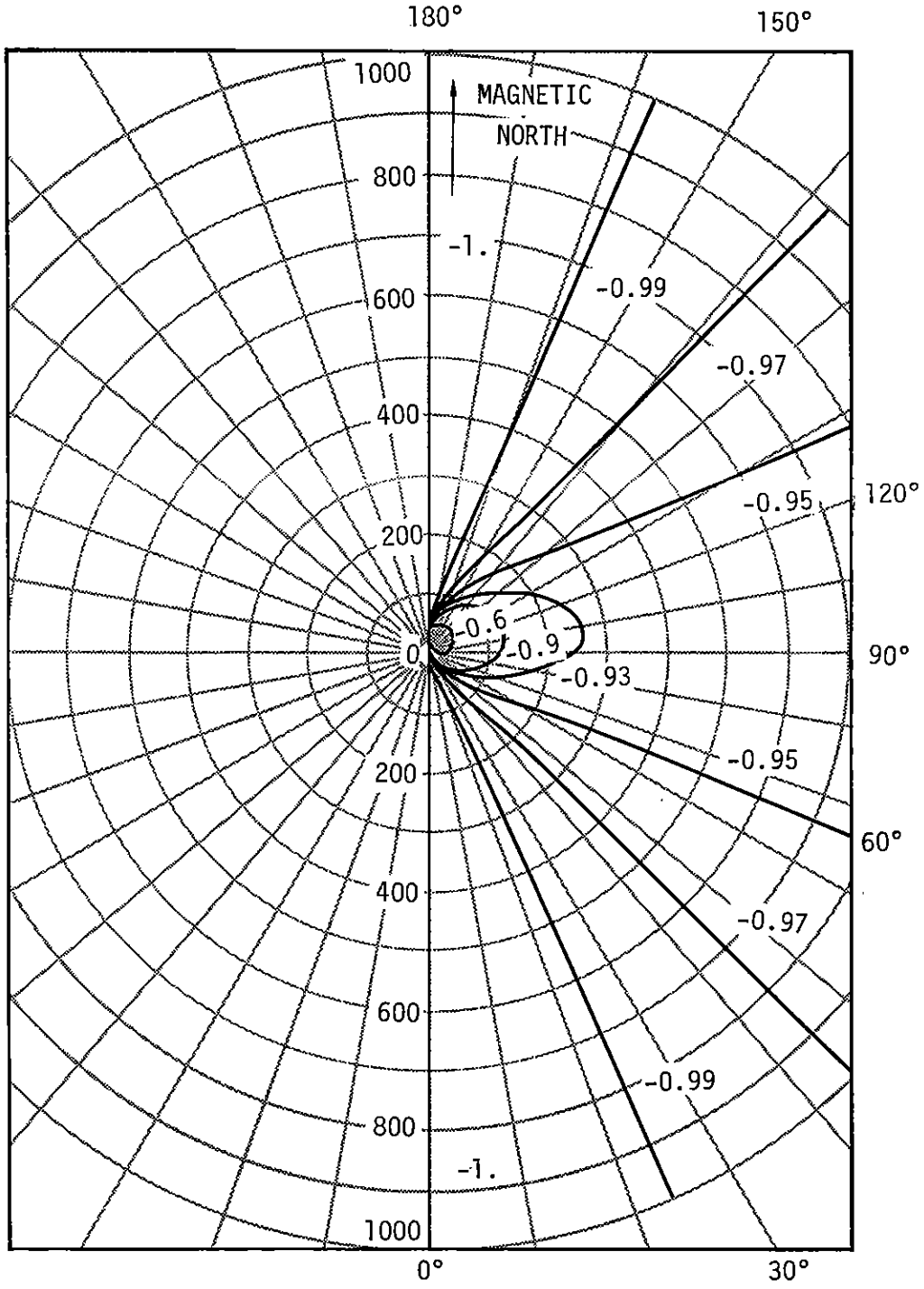

Figure A-3. Contours of P_ϕ for a 100 km burst and a magnetic dip angle of 70°. Contours in magnetic west half-plane have same polarity.

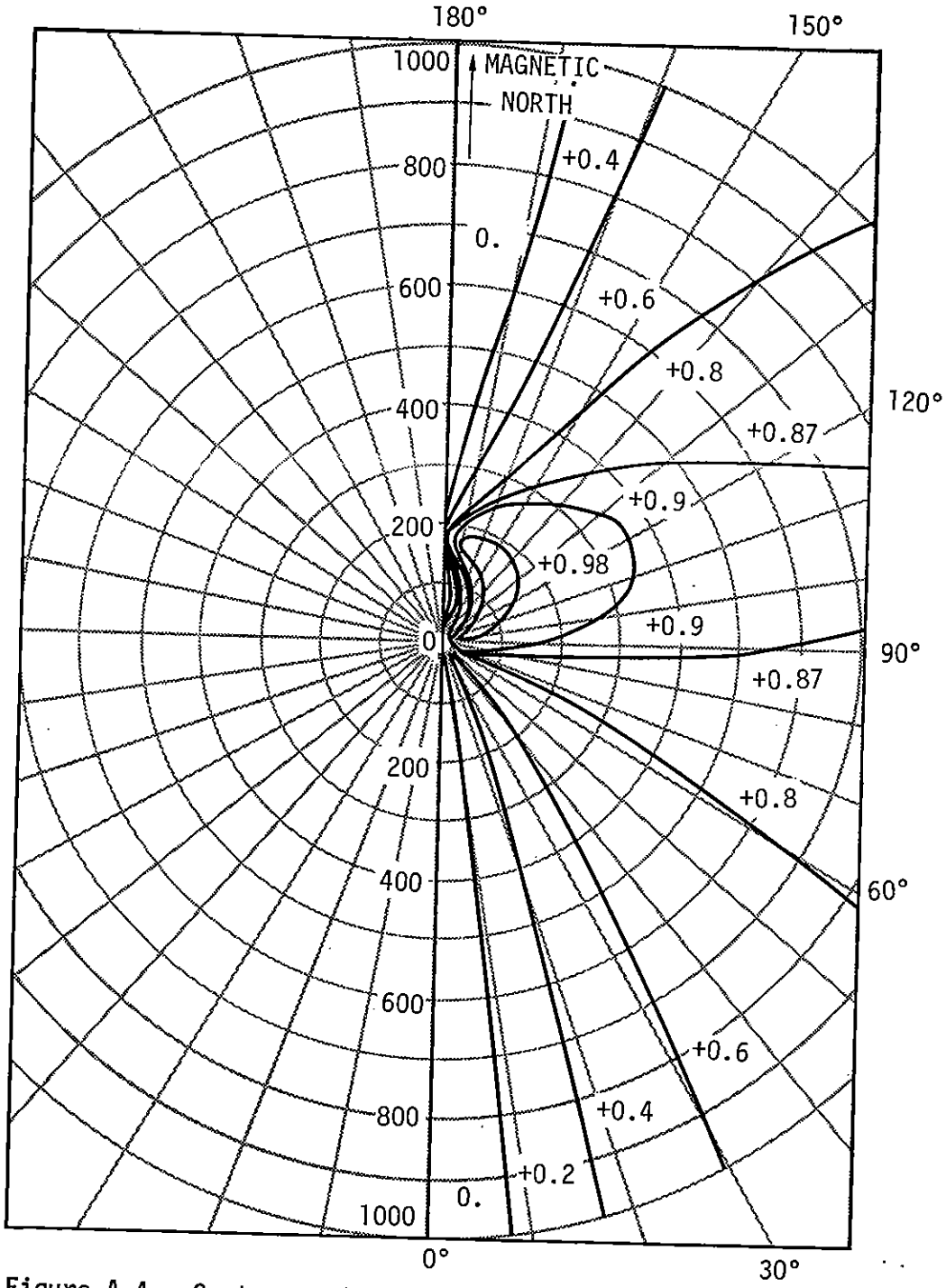

Figure A-4. Contours of P_θ for a 100 km burst and magnetic dip angle of 30°. Contours in magnetic west half-plane have opposite polarity.